

Rochester Institute of Technology

RIT Digital Institutional Repository

Theses

7-10-2020

Electrical Performance Retention of Doped Carbon Nanotube Conductors for High Current Applications

Karen J. Soule
kjs4859@rit.edu

Follow this and additional works at: <https://repository.rit.edu/theses>

Recommended Citation

Soule, Karen J., "Electrical Performance Retention of Doped Carbon Nanotube Conductors for High Current Applications" (2020). Thesis. Rochester Institute of Technology. Accessed from

This Dissertation is brought to you for free and open access by the RIT Libraries. For more information, please contact repository@rit.edu.

RIT

Electrical Performance Retention of Doped Carbon Nanotube Conductors for High Current Applications

by

Karen J. Soule

A Dissertation Submitted in Partial Fulfillment of the Requirements for the
Degree of Doctor of Philosophy in Engineering

Department of Engineering
Kate Gleason College of Engineering

Rochester Institute of Technology

Rochester, NY

July 10th, 2020

Electrical Performance Retention of Doped Carbon Nanotube Conductors for High Current Applications

by
Karen J. Soule

Committee Approval:

We, the undersigned committee members, certify that we have advised and/or supervised the candidate on the work described in this dissertation. We further certify that we have reviewed the dissertation manuscript and approve it in partial fulfillment of the requirements of the degree of Doctor of Philosophy in Engineering.

Dr. Brian J. Landi Date
Professor, Chemical Engineering

Dr. Steven J. Weinstein Date
Department Head and Professor, Chemical Engineering

Dr. Ivan Puchades Date
Assistant Professor, Electrical and Microelectronic Engineering

Dr. Cory D. Cress Date
Materials Research Engineer, U.S. Naval Research Laboratory

Certified by:

Dr. Edward Hensel Date
Department Head, Engineering Ph.D.

ABSTRACT

Kate Gleason College of Engineering
Rochester Institute of Technology

Degree: Doctor of Philosophy

Program: Engineering

Authors Name: Karen J. Soule

Advisors Name: Brian J. Landi

Dissertation Title: Electrical Performance Retention of Doped Carbon Nanotube Conductors for High Current Applications

Carbon nanotube (CNT) wires are light-weight and robust alternatives to conventional metal conductors. The weight savings, increased flexure tolerance, and corrosion resistance of CNT conductors make them a viable solution for a variety of space, defense, and power transmission applications. An individual CNT has orders of magnitude greater electrical conductivity than conventional metal conductors, but this has not been realized in bulk CNT networks. Recently, the use of chemical dopants has resulted in bulk CNT wire conductivities approaching 10 MS/m. As the electrical conductivity of CNT wires continues to approach that of conventional metals, deployment of CNT conductors will require an understanding of how doped CNT conductors behave during practical operation.

The initial dissertation research applied radial densification and KAuBr_4 chemical doping to commercially available CNT wires resulting in a 6x improvement in electrical conductivity and 67% increase in failure current density. Novel procedures were developed to probe the electrical performance retention as a function of increasing and sustained current application. KAuBr_4 -densified CNT wires can withstand current densities up to 32 MA/m² with no degradation in electrical conductivity, exceeding the as-received CNT material's degradation threshold by greater than 3x. The improved electrical conductivity of KAuBr_4 -densified CNT wires prevents the onset of Joule heating allowing for the doping benefits to be maintained at increased applied current densities.

Further analysis compared the resulting electrical performance retention of three commonly used chemical dopants: I_2 , IBr, and KAuBr_4 . The as-received and KAuBr_4 doped CNT wires can maintain σ_{Rest} until near wire failure, while the I_2 and IBr doped CNT wires experience degradation at current densities greater than 5 MA/m². With repeated low current cycling, KAuBr_4 was identified as the only dopant able to maintain its initial electrical conductivity over time. Thermal stability analysis determined that I_2 and IBr doped CNT wires undergo dopant desorption, while KAuBr_4 doped CNT wires result in dopant degradation into other viable dopants, thus maintaining improved electrical conductivity over greater applied current densities. KAuBr_4 doped CNT wires have emerged as lightweight conductors capable of retaining their improved electrical properties during long-term, high current applications. Thus, motivating the future adoption of stable KAuBr_4 doped CNT wires in a variety of space and defense technologies.

ACKNOWLEDGMENTS

My heart is full considering all of my friends, family, and colleagues that have been instrumental to my success. I am so grateful for your continued support.

I'd like to start with thanking my advisor, Dr. Brian Landi, for mentoring me not only in research but also professionalism, critical thinking, and making difficult decisions. Brian has fostered an incredible work environment that has been paramount to both my academic and personal growth. Without Brian's guidance, completion of my Ph.D. would have been impossible, he has always pushed me to be a better researcher and is solely responsible for my ability to write anything over 5 pages.

Throughout my 10 years at RIT I have been privileged with working with so many kind and intelligent people. It would be impossible to list everyone who has helped me along this path, but I will do my best to highlight a few who particularly embody the overwhelming support I have received throughout my academic career. My committee, Dr. Steven Weinstein, Dr. Cory Cress, and Dr. Ivan Puchades, asked tough questions and helped me to learn how to dig deeper. I am a better researcher as a direct result of their guidance. I could not be more grateful for everyone at the NanoPower Research Laboratories. My fellow Ph.D. students have helped me through the ups and downs, research grinds, and bouts of existential confusion that have made up this journey. In no particular order, I'd like to thank my colleagues and friends: Mohad Baboli, Anthony Leggiero, Nathanael Cox, Andrew Bucossi, Jason Staub, Jamie Rossi, Stephen Polly, Dylan McIntyre, Daniel Broderick, Alex Tomkiewicz, Martin Dann, Chris Schauerman, Matt Ganter, Paul Gregorious, Elaine Lewis, Julie Olney, Stephanie Hart, and Alyssa Owens. My time at RIT has been made better in countless ways by each of you, thank you for your friendship and help along the way.

Outside RIT, my life has been surrounded with loving, incredible people who I owe my success to. My mother, Ginette Soule, has pushed me to work hard and dream bigger, thank you for always believing in me. My father, Jim Soule, has been my rock. Thank you for always supporting me, from fielding three phone calls a day to always letting me know how much you care, I could not have done this without you. I'd also like to thank my Aunt Patti for helping me navigate life through too many talks over too many glasses of wine, your grace and humor are something I can only aspire to. I am also so lucky for the incredible young women in my life who have always supported me and have made my life so full of love and fun: Bridget Kearney, Mohad Baboli, Lindsey Parker, Jillian Heenan, Ana Nier, Amanda Sciacca, and Taylor Baker. I can't thank you enough. I'm also grateful for the friendship of Rick Houston, Mike Hardy, and Tom Meade, our late night chats have varied from insightful to hilarious, bringing much needed clarity or distraction. My success is shared with each of you, I love you all.

TABLE OF CONTENTS

LIST OF FIGURES.....	ix
1 Introduction.....	1
2 CNT Fundamentals	3
2.1 Carbon Nanotube Structure.....	3
2.2 CNT Synthesis	5
2.3 Wire Fabrication	6
2.4 Chemical Doping of CNTs	8
2.5 Current-Carrying Capacity of CNTs.....	13
2.6 Conductivity and CCC Stability	19
3 Dissertation Overview	23
4 Characterization of CNT Conductors	25
4.1 Physical Characterization of CNT Conductors.....	25
4.1.1 Surface Morphology & Analysis.....	25
4.1.2 Diameter & Cross-Sectional Area.....	25
4.1.3 Mass & Density.....	26
4.2 Electrical Characterization.....	26
4.2.1 Resistance per Length and Electrical Conductivity	26
4.2.2 Failure Current Density.....	27

4.3	Thermal Characterization.....	27
4.3.1	Thermogravimetric Analysis.....	27
4.3.2	Thermal Imaging.....	27
4.4	Elemental Analysis	28
4.4.1	Energy Dispersive X-Ray Spectroscopy.....	28
5	Sustaining Enhanced Electrical Conductivity in KAuBr ₄ -Doped Carbon Nanotube Wires at High Current Densities.....	29
5.1	Abstract.....	29
5.2	Introduction.....	30
5.3	Experimental.....	34
5.3.1	CNT Wire Preparation for Doping and Densification Study	34
5.3.2	Physical Characterization.....	34
5.3.3	Electrical Characterization.....	35
5.3.4	CNT Wire Preparation for Thermal Stability Study	37
5.3.5	Elemental Analysis of KAuBr ₄ -Doped CNT Wires.....	38
5.4	Results.....	38
5.4.1	Physical Characterization.....	38
5.4.2	Electrical Conductivity.....	40
5.4.3	Failure Current Density.....	42
5.4.4	Electrical Conductivity Retention.....	44

5.4.5	Thermal Stability and Enhancement	50
5.4.6	Elemental Analysis of KAuBr ₄ -Doped CNT Wires.....	54
5.5	Discussion	59
5.6	Conclusion	61
6	Halogen Doped CNT Wires: Doping Efficacy, Electrical Performance Retention, and Dopant Degradation	62
6.1	Abstract	62
6.2	Introduction.....	63
6.3	Results and Discussions.....	65
6.4	Experimental Section	82
6.5	Conclusions.....	84
7	Additional Considerations	84
7.1	Chemical Doping of Extruded CNT Wires.....	87
7.2	Chemical Doping of DexMat CNT Wires	89
7.3	Chemical Doping of Commercial CNT Wires with I ₂ Vapor.....	90
7.4	Stability as a Function of Doping Conditions.....	91
7.5	Low Current Stability: Ambient Doping	94
7.6	Temperature and Electrical Performance Retention	98
7.7	Forced Cooling to Demonstrate Current Carrying Capacity Possibilities	99
7.8	Power Analysis	101

7.9	Conclusions.....	102
8	Dissertation Conclusions	105
9	References.....	110

LIST OF FIGURES

Figure 1: Illustration of how the chiral vector determines the diameter and helical pitch of the hexagonal-bonded carbon atoms and the resulting electronic properties. ⁵	4
Figure 2: SEM images of NCTI sheet material (a) as-received, (b) after an initial thermal oxidation to remove amorphous carbon, (c) after a concentrated HCl soak to remove metal catalyst impurities and final thermal oxidation. Reproduced with permission from the NanoPower Research Laboratories. ¹⁶	6
Figure 3: Electrical conductivity of purified and doped NCTI sheet materials for 43 various dopants. Reproduced with permission from the NanoPower Research Laboratories. ¹⁶	9
Figure 4: Valence and conduction energy levels of SWCNTs compared to the electrochemical potential of each dopant species. Reproduced with permission from the NanoPower Research Laboratories. ¹⁶	10
Figure 5: The temperature dependent electrical conductivity measurements of low and high density wires from CNT sheet material with and without KAuBr ₄ -doping. Reproduced with permission from the NanoPower Research Laboratories. ³¹	11
Figure 6: (a) The resulting voltage measurements and calculated resistance as a function of applied current for KAuBr ₄ -doped wires densified from CNT sheet material. (b) The failure current as a function of diameter and the resulting failure current equation. The inset is an image of the CNT wires after failure. Reproduced with permission from the NanoPower Research Laboratories. ⁴³	15
Figure 7: The thermocouple temperature (blue line) of a KAuBr ₄ -doped CNT wire as a function of increasing applied current related to the applied temperature during TGA (red line). Reproduced with permission from the NanoPower Research Laboratories. ⁴³	16
Figure 8: Current-voltage profiles along with the measured temperature of to 1.5 mm diameter wires densified from CNT sheet material with and without KAuBr ₄ doping. The current was applied in increasing 0.1 A steps held for 30 seconds. Reproduced with permission from the NanoPower Research Laboratories. ⁴³	17
Figure 9: The maximum current before 100°C as a function of linear density was determined for various diameters of KAuBr ₄ CNT wires from densified sheet material. Reproduced with permission from the NanoPower Research Laboratories. ⁴³	18

Figure 10: The electrical conductivity as a function of time for CSA, I₂, IBr, and KAuBr₄-doped, electronic-type separated or mixed, SWCNT thin-films, compared to the purified SWCNT films. Reproduced with permission from the NanoPower Research Laboratories.¹⁶ 20

Figure 11: Representative diagram of the KAuBr₄ chemical doping and radial densification of CNT wires. 29

Figure 12. Overview of the representative procedure to determine the electrical conductivity retention of the CNT wires as a function of the applied current vs. time for the first few cycles using 30 second “on” and “rest” steps, detailing how the initial conductivity (σ_0), resting conductivities (σ_{Rest}), and working conductivities (σ_{Work}) are obtained..... 36

Figure 13: Overview of the initial I-V sweep and first cycle of the constant applied current procedure, detailing how the initial conductivity (σ_0) and resting conductivities (σ_{Rest}) are obtained..... 37

Figure 14: A schematic demonstrating the thermal oxidation and KAuBr₄ doping processes used to create the CNT wire samples for the thermal stability study..... 38

Figure 15. (a-c) SEM images of (a) as-received, (b) H₂O-densified, and (c) KAuBr₄-densified CNT wires. (d) Average diameter and electrical conductivity of five samples for each treatment. Error bars represent the standard deviation from the five measurements obtained via optical microscopy. 40

Figure 16: Cross-section SEMs of as-received, H₂O-densified, and KAuBr₄-densified CNT yarns..... 40

Figure 17: Resistance per length measurements taken at room temperature indicating the different charge transport properties of the CNT yarns, independent of changes in diameter. 42

Figure 18. (a) The voltage and current density profiles of the as-received, H₂O-densified, and KAuBr₄-densified CNT wires from Figure 15, obtained by increasing the current by 10 mA steps, then maintained a constant current for 30 seconds. (b-d) SEM images of the CNT wires after failure..... 44

Figure 19: Relative change in resting and working conductivities for as-received, H₂O-densified, and KAuBr₄-densified CNT yarns with varying current “on” step times. 46

Figure 20. The resting and working conductivities for the as-received, H₂O-densified, and KAuBr₄-densified CNT wires measured with 30 s, 10 mA steps until failure..... 48

Figure 21: The resting conductivities of the as-received, H₂O-densified, and KAuBr₄-densified CNT wires after each 1 hour cycle at 50% or 75% of the current density at failure for a total of 24 cycles..... 49

Figure 22: Thermogravimetric analysis of as-received and KAuBr ₄ -densified CNT yarns compared to neat KAuBr ₄ solids.....	51
Figure 23: Resistance per length of CNT yarn samples for thermal stability study taken at room temperature.	52
Figure 24. The (a) resting and (b) working conductivities normalized with respect to the initial conductivity of each CNT wire as a function of applied current density.....	54
Figure 25: SEMs of the CNT wires samples along with bromine and gold elemental analysis from EDX spectroscopy for KAuBr ₄ -doped CNT samples a) before (KAuBr ₄ - ■) and b) after thermal oxidation to 400 °C (KAuBr ₄ , 400 °C in air – □).	56
Figure 26: Elemental spatial analysis from EDX spectroscopy of potassium, carbon, iron, and oxygen for KAuBr ₄ -doped CNT samples a) before (KAuBr ₄ - ■) and b) after thermal oxidation to 400 °C (KAuBr ₄ , 400 °C in air – □).....	57
Figure 27: Diameter measurements of as-received and doped CNT wires.....	67
Figure 28: (a) Conductance for 2.5 cm CNT wire lengths and (b) electrical conductivity of as-received and doped CNT wires.....	68
Figure 29: (a) The current-voltage profiles of as-received and doped CNT wires brought to failure using 10 mA, 30 s applied current steps. The average (b) current at failure and (c) failure current density of the as-received and doped CNT wires.	70
Figure 30: (a) The resting conductivity as a function of applied current density for the as-received and doped CNT wires. (b) The resting conductivity as a function of cycles performed at 25% of the failure current density for the as-received and doped CNT wires.	72
Figure 31: (a) Normalized derivative weight as a function of increasing temperature of the as-received and doped CNT wires and the pure doping solids. (b) Thermogravimetric analysis of as-received and doped CNT wires along with the pure doping solids.	73
Figure 32: The average room temperature electrical conductivity of as-received and doped CNT wires with and without thermal oxidations to 200 and 400 °C calculated by 5 samples per treatment.....	74
Figure 33: SEM images of the as-doped and thermally oxidized I ₂ doped CNT wires along with the iodine elemental analysis from EDX spectroscopy.	76

Figure 34: SEM images of the as-doped and thermally oxidized IBr doped CNT wires along with the iodine and bromine elemental analysis from EDX spectroscopy..... 77

Figure 35: SEM images of the as-doped and thermally oxidized KAuBr₄ doped CNT wires along with the potassium, gold, and bromine elemental analysis from EDX spectroscopy. 78

Figure 36: The mass percentage of halogen remaining compared to the conductivity retention of the (a) I₂, (b) IBr, and (c) KAuBr₄, doped CNT wires with and without thermal oxidation to 200 and 400 °C. . 80

Figure 37: The remaining mass percent of (a) iodine and (b) iodine and bromine present compared to the electrical conductivity retention for the IBr doped CNT wires with and without thermal oxidation to 200 and 400 °C. 80

Figure 38: Representative graph relating temperature and electrical conductivity of halogen and KAuBr₄ doped CNT wires demonstrating the relationship between dopant degradation and electrical conductivity. 81

Figure 39: Resistance per length measurements of an extruded wire doped with KAuBr₄, I₂, and IBr. After 10 days of storage in ambient conditions, the resistance per length of the as-extruded wire was measured again and then doped with KAuBr₄ in organic solution..... 88

Figure 40: Scanning electron microscope images of (a) 20 μm DexMat wire and (b) 3-ply DexMat wire.. 89

Figure 41: Resistance per length of 20 μm DexMat CNT wire after exposure to a vacuum oven or IBr doping solution and the resulting change as a function of time. 90

Figure 42: The average room temperature electrical conductivity for as-received, IBr, and KAuBr₄ doped CNT wires. The doped CNT wires were exposed to the doping solutions for 1 or 3 hours..... 92

Figure 43: (a) The current-voltage profiles of as-received, IBr, and KAuBr₄ doped CNT wires during increasing 10 mA current steps held for 30 seconds until ultimate wire failure. The doped CNT wires were exposed to the doping solutions of 1 or 3 hours. (b) The resulting failure current densities for the as-received and doped CNT wires. 93

Figure 44: Resting conductivity as a function of increasing applied current density for as-received, IBr, and KAuBr₄ doped CNT wires. The doped CNT wires were exposed to the doping solutions for 1 or 3 hours. 94

Figure 45: The current and voltage profiles of as-received CNT wires exposed to constant applied current cycles corresponding to a) 25, (b) 50, and (c) 75% of the failure current density (FCD) with intermittent rest and I-V sweeps.....	95
Figure 46: The relative (a) resting and (b) working electrical conductivities of the as-received CNT wires exposed to 25, 50, and 75% of the failure current density (FCD).	96
Figure 47: The resting conductivity as a function of time for constant current cycling of as-received CNT wires at an applied current density corresponding to 25% of the failure current density.	97
Figure 48: The resting conductivity of as-received CNT wires exposed to 25% of their failure current density in air or argon environments.....	98
Figure 49: The relative changes in resting and working resistances for 1mm diameter (a) H ₂ O-densified and (b) KAuBr ₄ -densified CNT wires as a function of increasing applied current and the corresponding temperature measurements.	99
Figure 50: (a) Resulting current densities as a function of applied voltage for 10 tex, 3-ply DexMat, and 20 μm DexMat CNT wires in 0 °C polypropylene. (b) The current density at failure for the 10 tex, 3-ply DexMat, and 20 μm DexMat CNT wires in room temperature air and 0 °C polypropylene. The improvement in current density at failure for the samples in 0 °C propylene glycol compared to the samples tested in air are listed.	100
Figure 51: Power dissipation and resulting normalized resistances of as-received and KAuBr ₄ doped 10 tex CNT wires, 20 μm DexMat CNT wires, and 127 μm copper wires.	102

1 Introduction

Carbon Nanotube (CNT) conductors have emerged as a viable lightweight, strong, and conductive alternative to traditional metals. CNTs have a density approximately 89% less than that of copper, thus replacing conventional copper wiring with CNT conductors would allow for greater payloads and reduced fuel costs for a variety of aerospace applications. Individual CNTs have been demonstrated to have electrical conductivities and current carrying capacities greater than copper, but this has not been realized in bulk CNT wires due to resistance between the individual CNTs. Recent work has used chemical dopants to improve the electrical conductivity of bulk CNT wires resulting in values approaching 10 MS/m, corresponding to a mass-normalized electrical conductivity greater than copper. Beyond improvements in electrical conductivity, the adoption of CNT conductors requires a thorough understanding of how operating conditions affect performance and long-term stability.

The following dissertation begins with a review of the literature focused on the improvement in electrical conductivity of CNT wires via chemical doping, the state of current-carrying capacity testing for these doped CNT wires, and recent work probing the stability of these dopants as a function of time, temperature, and applied current density. Chapter 3 sets out to summarize the state of the field, drawing attention to the various research opportunities, and outlines the objectives of this dissertation. Chapter 4 outlines the standard procedures by which the physical, electrical, thermal, and elemental analyses are performed. Chapter 5 discusses the improvements in electrical conductivity brought about via potassium tetrabromoaurate (KAuBr_4) chemical doping coupled with physical densification. The work outlines the developed procedures by which electrical performance

retention as a function of increasing applied current density and constant current cycling are determined. Chapter 6 directly compares the effect of iodine (I_2), iodine monobromide (IBr), and $KAuBr_4$ chemical doping on improving the electrical conductivity and current-carrying capacity of CNT wires. Electrical performance retention testing demonstrates the varied stability of the doped CNT conductors. Controlled thermal oxidation procedures are coupled with elemental analysis via energy dispersive X-ray spectroscopy allowing for the relationship between dopant thermal stability and electrical performance retention to be understood. The degradation mechanisms of the doped CNT wires are proposed. Chapter 7 reviews a variety of additional considerations including an analysis of varied doping procedures on electrical performance, chemical doping of novel CNT materials, ambient doping as a result of low current exposure, forced cooling for improved current-carrying capacity, and analyses regarding the temperature of the conductors during operation and the resulting power. This dissertation concludes with a summary of the presented work and considerations regarding the adoption of doped CNT conductors.

2 CNT Fundamentals

In the fall of 1991 Iijima announced his discovery of “Helical Microtubules of Graphitic Carbon.” The work discovered that arc-discharge evaporation of carbon in argon resulted in what was referred to as graphitic carbon needles with diameters from 4-30 nm and up to 1 μm .¹ The graphitic carbon needles were determined to have 2-50 concentric tubes and each tube consists of carbon-atom hexagons with varying helical pitch around the needle axis.¹ In the years to follow, carbon nanotubes (CNTs) would be realized for their unique electrical and physical properties. Between 2000 and 2010, the number of journal articles published annually about carbon nanotubes increased from less than 1,000 per year to almost 9,000.² The progression of work has led to advancements and optimization of CNT synthesis and bulk wire fabrication. The electrical transport of individual CNTs has been studied rigorously and the difficulties in realizing these properties within bulk CNT networks has been well documented. Chemical dopants have been identified to improve the conductivity of bulk CNT conductors with recent advances claiming electrical conductivities of $\sim 8.5 \text{ MS/m}$ and specific conductivities greater than copper and aluminum.^{3,4} As the gap between the electrical conductivity of conventional metals and doped-CNT conductors continues to close, further considerations of how doped-CNT conductors behave during operation must be explored.

2.1 Carbon Nanotube Structure

Carbon nanotubes (CNT) are tubules of hexagonally bonded carbon with diameters on the nanoscale. The carbon nanotube structure is closely related to graphene, where the carbon atoms are sp^2 hybridized and form a honey comb structure. A CNT can be best understood as a graphene sheet rolled into seamless cylinder seen in Figure 1.⁵ The CNT is “rolled”

based on a chiral vector ($\vec{C} = n\vec{a}_1 + m\vec{a}_2$), the magnitude of the vector directly relates to the CNTs diameter and the direction of the vector determines the helical pitch of the honeycomb structure about the nanotube axis.⁶ This pitch directly relates to the CNT electronic properties. When $n = m$ or $n - m = 3l$, where l is an integer, the electronic-type of the CNTs is metallic.⁷ When $n - m \neq 3l$, the CNTs are semiconducting.⁷ These properties dominate when there is just one graphene-like cylinder, referred to as a single wall carbon nanotube (SWCNT). Synthesis techniques can also result in several concentric graphene-like cylinders which is referred to a multi-walled carbon nanotube (MWCNT). The van der Waals interactions between adjacent CNTs result in the nanotubes forming bundles. The theoretical density of SWCNTs within a bundle can be approximated assuming a hexagonally close packed geometry and appropriate van der Waals spacing. For SWCNTs with a diameter of ~ 1.2 - 1.4 nm, the upper limit of the bundle density is ~ 1 g/cm³.⁸

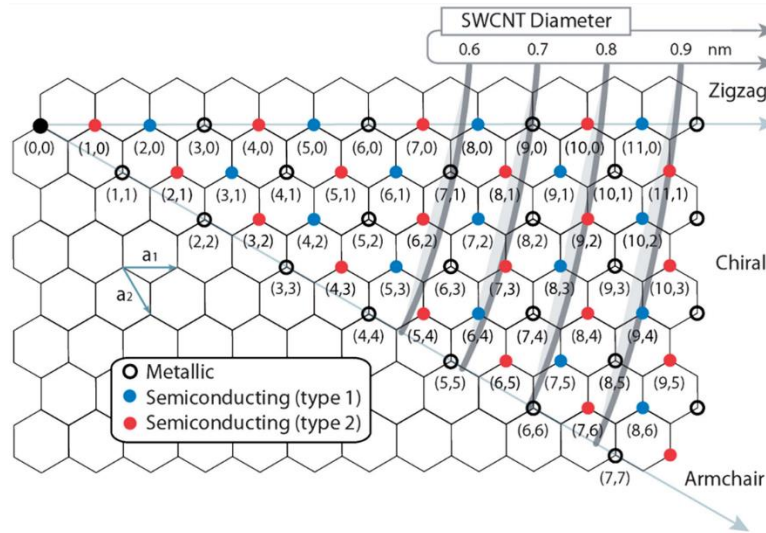


Figure 1: Illustration of how the chiral vector determines the diameter and helical pitch of the hexagonal-bonded carbon atoms and the resulting electronic properties.⁵

2.2 CNT Synthesis

Carbon nanotubes are commonly produced via three main techniques: i) arc discharge, ii) laser ablation, iii) chemical vapor deposition.⁹⁻¹¹ Arc discharge and laser vaporization involve vaporizing graphitic carbon and condensing that carbon into CNTs. For both techniques, the addition of metal catalyst particles results in the production of SWCNTs, while pure carbon sources produce MWCNTs. Arc-discharge was the technique used by Iijima in the discovery of CNTs in 1991.¹ Arc-discharge requires high temperatures of 1,700 °C or more, but has the potential for scale up, moderate cost, and is capable of producing both SWCNTs and MWCNTs.^{10,11} Laser ablation operates at ~900-1200 °C and is one of the superior methods for producing high quality and high purity SWCNTs with electronic and physical properties that are tunable via the buffer gas properties, temperature, and other parameters.^{10,12} Laser ablation is relatively high cost and limited to in scale compared to the other synthesis techniques because of the energy required to power the laser and the cost of the laser system.^{11,13} Chemical vapor deposition (CVD) involves hydrocarbon gases breaking down at a catalyst to form CNTs. The process results in high purity CNTs and does not require high temperatures. CVD processes can produce vertically aligned forests of CNTs, aerogels, and CNT soot.¹⁰

During the synthesis of CNTs amorphous carbon and metal catalyst impurities are formed in conjunction with the CNT material. Acid reflux and thermal oxidation processes can result in high purity SWCNTs from CNT soot.¹⁴ Bulk CNT papers can be purified via thermal oxidation to 520 °C which removes amorphous carbon, thus allowing the following hydrochloric acid treatment to better infiltrate the CNT network to dissolve catalyst impurities, followed by a final 500 °C thermal oxidation to remove trace acid and carbon

impurities.¹⁵ Scanning electron microscope images in Figure 2 show the effects of purification on commercially available CNT sheets.¹⁶

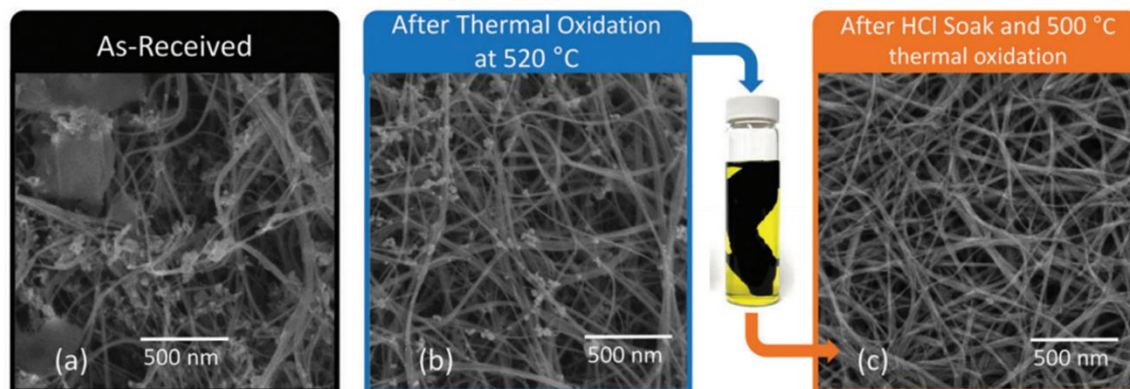


Figure 2: SEM images of NCTI sheet material (a) as-received, (b) after an initial thermal oxidation to remove amorphous carbon, (c) after a concentrated HCl soak to remove metal catalyst impurities and final thermal oxidation. Reproduced with permission from the NanoPower Research Laboratories.¹⁶

SWCNTs can be separated into their electronic-types (metallic and semiconducting) using processes such as column chromatography, density gradient ultracentrifugation, and electrophoresis.^{17–19} Isolating electronic-type and diameter SWCNTs could prove useful for electronic applications where specific bandgap materials are required. NanoIntegris has commercialized electronic-type separated SWCNTs with purities greater than 98%.²⁰

2.3 Wire Fabrication

Currently there are three distinct techniques for the production of CNT wires: (i) wet-spinning, (ii) dry-spinning, and (3) densification of CNT sheet material. The production of CNT wires directly effects the network properties (e.g., alignment, extent of bundling, impurities from CNT synthesis) as well as the CNT properties (e.g., amount of walls, electronic type, defects, etc.).

Wet-spinning involves dissolving CNTs in superacids which are subsequently extruded into a coagulant bath. A similar process has been developed for the production of Kevlar fibers and scale-up has been successful achieved. Superacids, such as chlorosulfonic acid, extract electrons from SWCNTs causing a slight positive charge at the carbon atoms, this charge transfer overcomes the van der Waal interactions and allows for dispersion of the CNTs.²¹⁻²³ Increasing SWCNT concentration causes anion-mediated attractions and eventual spatial constraints to produce a liquid-crystalline phase. The alignment of SWCNTs within this liquid-crystalline dispersion allows for the extrusion of highly aligned CNT wires.^{3,4,24} The extrusion process allows for a variety of SWCNT starting materials to be used. Therefore, synthesis and subsequent processing can be tuned so that CNT conductors can be produced with specific SWCNT properties (e.g., electronic-type, CNT diameter, high purity and quality, etc.). Optimization of extrusion parameters (e.g., coagulation bath solvent, extrusion speed, CNT material, etc.) has resulted in CNT wires with electrical conductivities up to ~ 8.5 MS/m.^{3,24}

Dry-spinning involves either fibers being drawn from aligned CNT forests^{25,26} or directly from an aerogel²⁷⁻²⁹. Drawing fibers from aligned CNT forests depends on the van der Waal forces of the highly aligned forests creating bundles; the highest reported conductivity is 0.03 MS/m.^{25,26} Directly spinning from an aerogel allows for a continuous production of CNT wires²⁹. Winding these CNT fibers after exposure to acetone can be used to densify the CNTs as a result of capillary-induced densification.^{28,30} This CVD and subsequent winding process has been scaled by Nanocomp Technologies, Inc. (NCTI)²⁸; recent measurements of these commercially-available CNT wires have determined an average electrical conductivity of 0.18 MS/m.

CNT wires can also be produced via densification of commercially-available, Nanocomp Technologies Inc. (NCTI), CNT sheet materials. The areal density of the CNT sheet material, the desired final wire diameter, and desired final wire density are used to determine the width of the strip of material which is used to produce a wire. The wire is then rolled by hand and densified through sufficiently smaller diameter radial drawing dies to the final desired diameter. The effect of CNT wire density was explored by preparing equivalent widths of NCTI CNT sheet material and densifying to various final drawing die diameters. The wires ranged in density from $\sim 500\text{-}1800\text{ kg/m}^3$ and the resulting conductivities ranged from $0.05\text{-}0.2\text{ MS/m}$.³¹ The final density values of the CNT wires were higher than that of theoretical density of close-packed CNTs due to the presence of iron catalyst.

2.4 Chemical Doping of CNTs

Puchades et al. explored the effect of alkali noble metal halides, gold halides, metal nitrates, metal halides, bases, acids, halides and ionic liquids, totaling 43 dopants, on purified NCTI CNT sheet materials.¹⁶ The conductivities post-purification and after chemical doping are displayed in Figure 3. KAuBr_4 , I_2 , and IBr were down selected based on their high electrical conductivity and interest from recent publications.^{4,31-35} Chlorosulfonic acid (CSA), which was not used in this preliminary experiment due to its propensity to disperse CNT sheet materials, was also included due to its ability to dope CNTs and its use in fabrication of CNT conductors. Thin-films of mixed and separated electronic-type SWCNTs were prepared from CSA dispersions and left as-produced (CSA), purified of CSA (purified), or purified then doped for 1 hour in $10\text{ mM KAuBr}_4(\text{aq})$, $100\text{ }^\circ\text{C I}_2$ vapor, or 0.36 M IBr in ethanol. IBr and KAuBr_4 were rinsed with their doping solvent then dried at room

temperature for 30 minutes. The electrical conductivities after purification for semiconducting, mixed, and metallic SWCNTs are 0.07, 0.05, and 0.09 MS/m, respectively. Semiconducting SWCNTs show the greatest improvement in electrical conductivity with an $\sim 3x$ improvement with CSA, IBr, and I_2 , while $KAuBr_4$ shows a factor of 6 improvement to 0.43 MS/m. For metallic SWCNTs, CSA results in a 3.6x increase in conductivity, compared to 2.6x for $KAuBr_4$, demonstrating the importance of specific electronic interactions.¹⁶

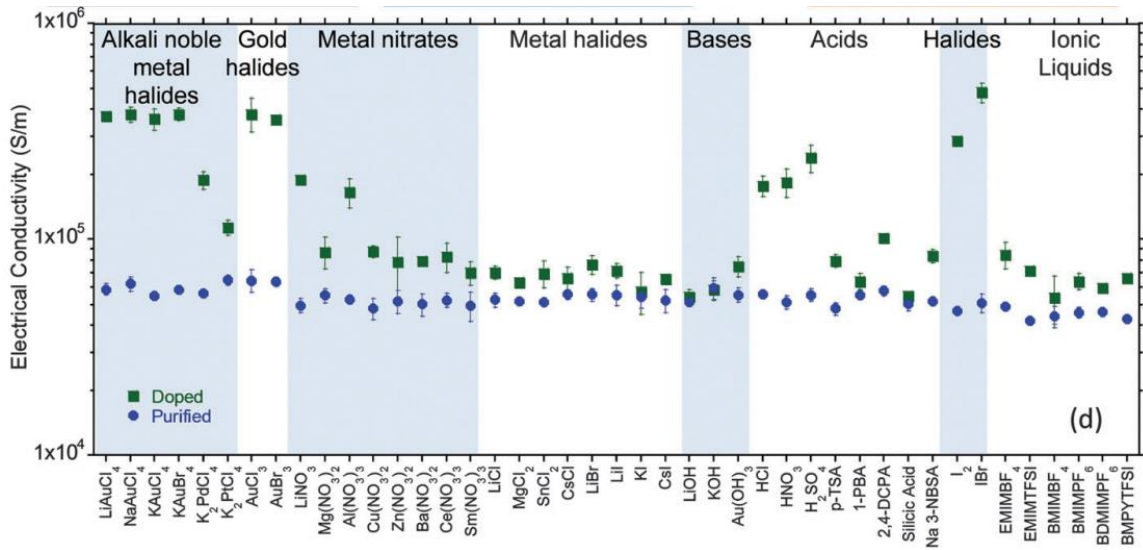


Figure 3: Electrical conductivity of purified and doped NCTI sheet materials for 43 various dopants. Reproduced with permission from the NanoPower Research Laboratories.¹⁶

The work went on to relate the valence and conduction energy levels of the SWCNTs to the redox potential of the four dopants, presented in Figure 4.¹⁶ Each of the dopants have a greater electrochemical potential than the first semiconducting valence energy level. The increased doping efficacy of $KAuBr_4$, compared to the other dopants, for semiconducting SWCNT is likely due to S_{33} being depleted by $KAuBr_4$, but not by the other dopants¹⁶

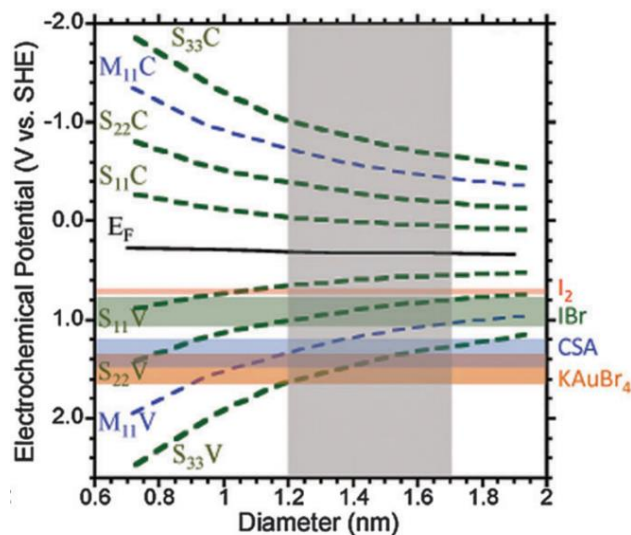


Figure 4: Valence and conduction energy levels of SWCNTs compared to the electrochemical potential of each dopant species. Reproduced with permission from the NanoPower Research Laboratories.¹⁶

Previously, the effect of increasing densification on the resulting conductivity for CNT wires produced from densified sheet material was discussed. The work determined that without chemical doping, the conductivity ranged from 0.05-0.2 MS/m based on densities between 500-1800 kg/m³. Chemical doping with KAuBr₄ (aq) increases the electrical conductivity by ~6x to 0.2-1.3 MS/m, for wires drawn to similar final drawing die diameters.³¹ Temperature dependent electrical measurements over the range of 100-400 K were used to investigate the conduction mechanisms of the densified CNT wires as a function of density and chemical doping. The results shown in Figure 5 demonstrate that the as-produced CNT wires have an increase in electrical conductivity with increasing temperature, while the KAuBr₄-doped CNTs have a decrease in electrical conductivity with increasing temperature.³¹ The positive temperature coefficient of resistance (TCR) seen in the KAuBr₄-doped samples is consistent with conventional metal conductors.

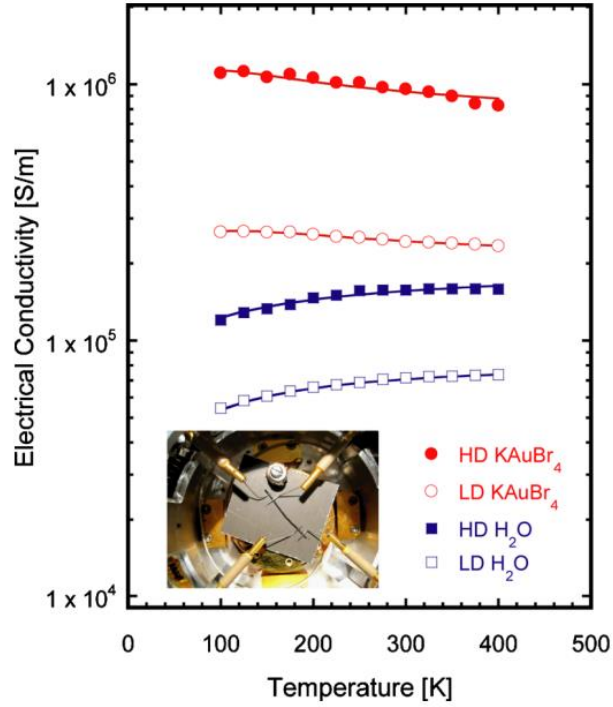


Figure 5: The temperature dependent electrical conductivity measurements of low and high density wires from CNT sheet material with and without KAuBr₄-doping. Reproduced with permission from the NanoPower Research Laboratories.³¹

Previous work by Kaiser et al. developed Equation 1, relating metallic conduction and tunneling to model the temperature-dependent conductivity of CNTs. Coefficients A and B determine the relative contribution of both conduction mechanisms, respectively. T_b is related to the magnitude of the tunneling barrier energy. T_s is the temperature at which thermally activated electrical conduction over the barrier occurs. T_m is related to the energy of backscattering zone boundary phonons for CNTs and is referred to as the metallic parameter.

$$\sigma(T) = \left[B \exp\left(\frac{T_b}{T_s + T}\right) + A \exp\left(-\frac{T_m}{T}\right) \right]^{-1} \quad \text{Equation 1}$$

Alvarenga et al. used the temperature dependent data and Equation 1 to determine the changes in the magnitude of the tunneling barrier energy, the metallic behavior of the

CNTs, and the temperature at which thermally activated electrical conduction occurs over the barrier.³¹ The results are presented in Table 1. Chemical doping results in increasing the metallic parameter and reducing the turning point temperature, which is favorable for increased electrical conductivity. Considering these parameters are intrinsic to the individual nanotubes, densification does not affect the metallic parameter or turning point temperature. The tunneling barrier parameter decreases with chemical doping as well as with densification due to the increased proximity of the CNTs. A and B decrease with densification and doping indicating overall greater conductivity.

Table 1: Resulting parameters from Equation 1 based on temperature dependent resistivity measurements of low and high density wires from CNT sheet material with and without KAuBr_4 -doping. Reproduced with permission from the NanoPower Research Laboratories.³¹

Sample	A ($\Omega \mu\text{m}$)	B ($\Omega \mu\text{m}$)	T_m (K)	T_s (K)	T_b (K)	E_b (meV)
LD H_2O	8.01	4.01	133	166	377	32.4
HD H_2O	2.68	2.51	133	166	276	23.8
LD KAuBr_4	3.18	2.00	226	93	104	9.0
HD KAuBr_4	0.96	0.49	226	93	90	7.8

Solution based IBr doping of NCTI CNT wires was optimized to increase electrical conductivity to 0.85 MS/m, compared to the starting material with an electrical conductivity of 0.1 MS/m.³² Low dipole moment organic solvents were most effective in doping CNTs with IBr, this was attributed to the weak solvent interactions with the dopant and CNTs, thus resulting in equilibrium favoring the dopant intercalation into the CNT network.³² The optimized procedure for IBr doping of CNTs was 1 hour of exposure to 100 mM IBr dissolved in hexanes.³² HAuCl_4 doping of SWCNT thin-films did not find a direct correlation between electrical conductivity and polarity, indicating that a complex relationship between solvent effects and dopant efficacy exists. {Formatting Citation} The

doping efficacy of IBr and ICl on CNT films were directly compared. The procedure involved exposing CNT films to 1 M solutions of IBr or ICl dissolved in dichloromethane for 15 minutes and resulted in 42% and 67% reductions in resistance, respectively.³³ The improved doping efficacy of ICl results from its stronger electron affinity compared to IBr.³⁷

Zhao et al. doped purified double-walled carbon nanotube (DWCNT) cables in I₂ vapor at 200°C for 12 hours. The conductivity increases from 2 MS/m for the raw DWCNT cables to 6.7 MS/m for the I₂ doped samples.³⁴ The specific conductivity of the I₂ doped DWCNT sample is $19.6 \cdot 10^3 \text{ S} \cdot \text{m}^2/\text{kg}$, approximately 2x greater than copper ($6.5 \cdot 10^3 \text{ S} \cdot \text{m}^2/\text{kg}$) and ~30% greater than aluminum ($13.9 \cdot 10^3 \text{ S} \cdot \text{m}^2/\text{kg}$).³⁴ A similar I₂ doping procedure on extruded CNTs containing residual CSA had only a 1.7x improvement in electrical conductivity from the starting 2.9 MS/m to 5 MS/m.⁴ Zhang et al. doped NCTI CNT sheet material with I₂ vapor at 70 °C for 3-24 hours. The electrical conductivity increased by ~5x to 1.2 MS/m; improvement in electrical doping plateaued after three hours.³⁵ Energy dispersive x-ray spectroscopy showed a homogenous distribution of I₂ throughout the CNT network.

2.5 Current-Carrying Capacity of CNTs

Current-carrying capacity refers to the amount of current a conductor can pass as defined by a specific metric (e.g., failure, operating temperature, etc.). The failure current density (FCD) is often defined as the maximum current density prior to wire failure or complete breakage. The continuous current rating (CCR) refers to the current density a conductor can carry resulting in a particular operating temperature (T_o). These operating temperatures

are often related to the temperature ratings of particular insulators. In copper conductors, the CCR for various diameters and various insulators are well understood.^{38,39}

CNT conductor failure results from Joule heating increasing temperatures until eventual oxidation or vaporization of the conductor occurs. Joule heating occurs at increasing current densities and is directly related to electrical conductivity. The failure current density of CNTs is dependent upon the rate of heat being generated by a CNT conductor and heat being dissipated from the system. Individual CNTs in air can withstand current densities of 10^{10} - 10^{13} A/m² without degradation, which is approximately three orders of magnitude greater than copper.^{40,41} The high current-carrying capacity of individual CNTs is due to the high electrical conductivity and relative ease of heat dissipation. Copper conductors fail due to melting or electromigration. In 1884 William H. Preece determined that equating the heat generated ($H_D \propto \frac{I^2}{d^2}$) to the heat dissipated ($H_D \propto d$) of a copper wire at failure allows for a relationship between the failure current (FC) and diameter, presented in Equation 2, where μ represents a material-dependent fitting parameter 3.⁴²

$$FC = \mu * d^{3/2} \qquad \text{Equation 2}$$

Cress et al. prepared CNT wires from KAuBr₄-doped NCTI densified sheet material and determined the failure current for wires with diameters of 0.9 and 6 mm.⁴³ The current was applied using increasing 0.1 A steps held for 30 s each until wire failure. The resulting voltage and calculated resistance as a function of applied current are shown in Figure 6a. The maximum current at failure from Figure 6a is then plotted as a function of the diameter in Figure 6b and the material-dependent fitting parameter from Equation 2 was determined to be $3 \text{ A/mm}^{3/2}$.⁴³

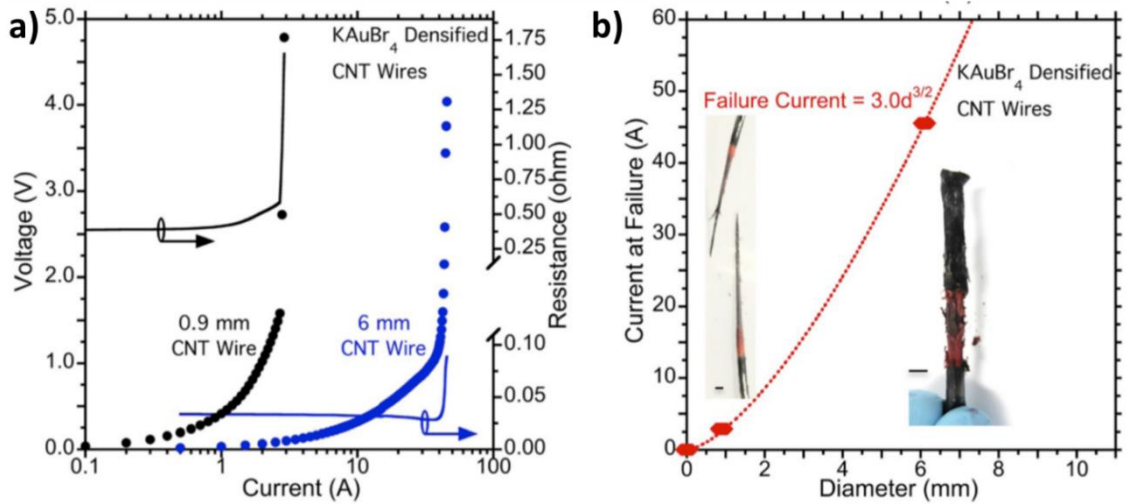


Figure 6: (a) The resulting voltage measurements and calculated resistance as a function of applied current for KAuBr_4 -doped wires densified from CNT sheet material. (b) The failure current as a function of diameter and the resulting failure current equation. The inset is an image of the CNT wires after failure. Reproduced with permission from the NanoPower Research Laboratories.⁴³

The failure current densities for the 0.9 and 6 mm wires are 4.6 and 1.6 MA/m^2 , respectively.⁴³ A thermocouple was used to measure the temperature of the 6 mm wire as it approaches failure, the temperature measured by the thermocouple was then related to the temperature taken during thermogravimetric analysis, presented in Figure 7. Relating these temperatures allowed for the realization that the temperature of the CNT wire at failure correlates to the first derivative thermogravimetric analysis (TGA) weight loss peak. Therefore, CNT failure due to applied current is the result of the temperature reaching that which the CNT material degrades. Quantifying the onset of doped-CNT conductor degradation will be a useful metric to identify CNT dopants for high current applications.

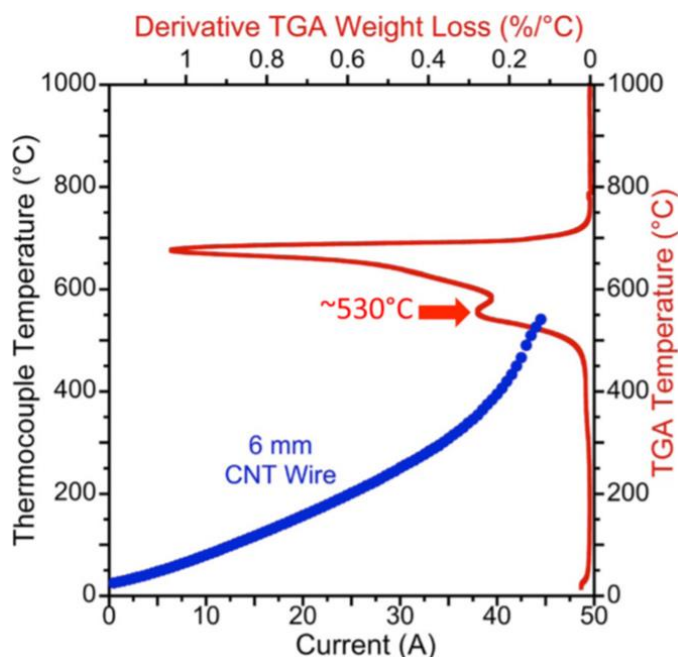


Figure 7: The thermocouple temperature (blue line) of a KAuBr_4 -doped CNT wire as a function of increasing applied current related to the applied temperature during TGA (red line). Reproduced with permission from the NanoPower Research Laboratories.⁴³

This work went on to determine the CCR(100°C) for CNT wires from densified CNT wires with and without chemical doping.⁴³ A thermocouple was used to measure the temperature caused by applying increasing 0.1 A steps held for 30 s to 1.5 mm diameter wires densified from CNT sheet material with and without KAuBr_4 doping. In Figure 8, the water densified sample has a linear increase in both temperature and voltage with increasing current, the current at 100°C was determined to be 3.6 A.⁴³ The KAuBr_4 densified sample increases linearly in voltage and temperature with increasing current until about ~ 6 A, where afterwards the temperature and voltage increase at a greater rate, indicating an increase in resistance. The authors attributed this increase in resistance with desorption of water as the temperature approaches 100°C and note that this may have an effect on the long-term stability.

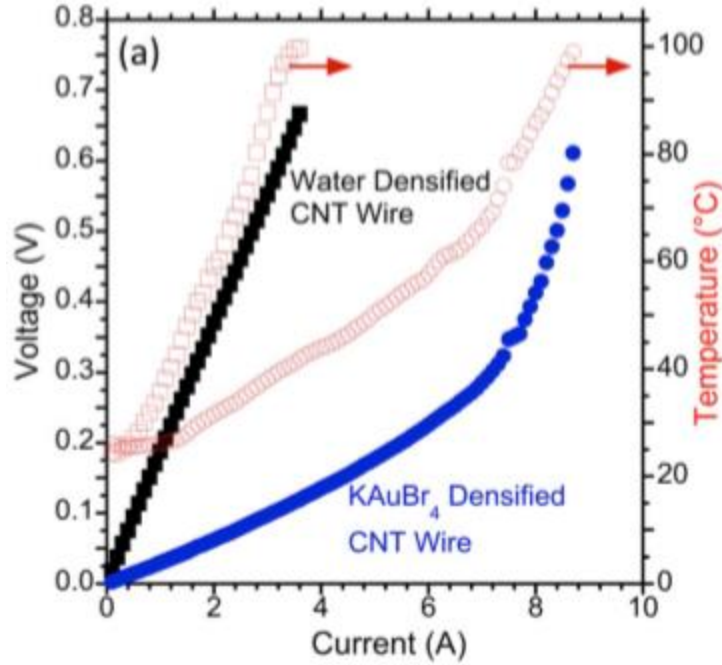


Figure 8: Current-voltage profiles along with the measured temperature of to 1.5 mm diameter wires densified from CNT sheet material with and without KAuBr₄ doping. The current was applied in increasing 0.1 A steps held for 30 seconds. Reproduced with permission from the NanoPower Research Laboratories.⁴³

The authors determined the current required to reach an operating temperature of 100°C for various diameters of KAuBr₄ CNT wires from densified sheet material. Using Equation 2 along with the understanding that $d \propto \sqrt{\rho_L}$, Equation 3 was developed to relate the linear density and the continuous current rating.⁴³ It is useful to consider the linear mass density of larger CNT conductors as it eliminates the need for accurate diameter measurements. Figure 9 includes the measured values of CCR(100 °C) and the resulting equation with a fitting parameter of $A = 2.16 A(m/g)^{3/4}$.⁴³ The author also demonstrated that forced convection via a fan causes an increase in CCR(100°C) from 38.5 A to 53.5 A for the 11.2 mm diameter KAuBr₄ CNT wire from densified sheet material.⁴³

$$CCR = A\rho_L^{\frac{3}{4}} \quad \text{Equation 3}$$

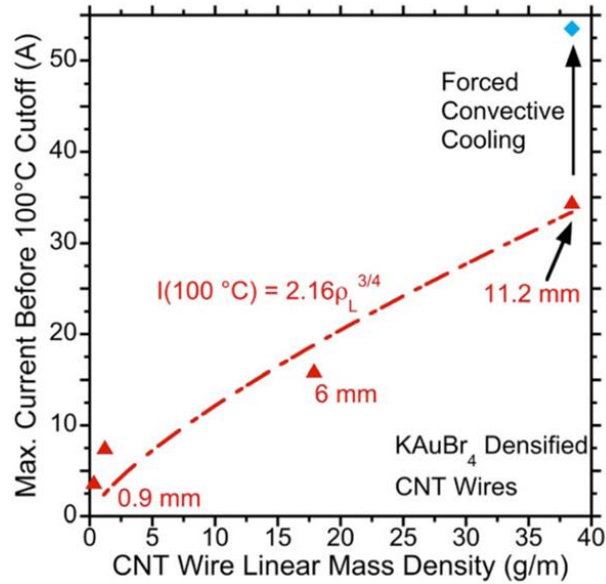


Figure 9: The maximum current before 100°C as a function of linear density was determined for various diameters of KAuBr₄ CNT wires from densified sheet material. Reproduced with permission from the NanoPower Research Laboratories.⁴³

Wang et al. determined the failure current density for 20.5 μm diameter CSA-extruded wires in varying ambient environments.⁴⁴ The test used increasing applied current densities which are held for 30 seconds then swept the current to 1 mA and back to the next increased current density until ultimate wire failure. The work referred to the failure current density as the maximum current density before breaking and did not state the magnitude of the increasing current density steps or the rate of the current sweeps. The tests were performed in vacuum, air, argon, and nitrogen resulting in failure current densities of 136, 211, 303, and 455 MA/m², respectively.⁴⁴ Vacuum was expected to have the lowest failure current density because the absence of gas molecules results in black-body radiation being the only means of heat dissipation. The presence of oxygen in the air environment results in oxidation at 211 MA/m². The increased current density in nitrogen environment compared to argon is a result of improved conductance between the CNT conductor and the surroundings.

The work by Zhao et al. which claimed to produce an I₂-doped DWCNT wire with a specific conductivity greater than copper and aluminum, went on to perform failure current density measurements.³⁴ The authors state that the current was increased step-wise but do not include information regarding the magnitude of the step increase, the resulting voltage or resistance measurements, or why the duration of the time steps were varied. The authors claim the failure current density of their I₂-doped 4.2 μm diameter wire was 1620 MA/m² in air.³⁴ They use Equation 2 to calculate a failure current density of 1570 MA/m² for copper with a 4.2 μm diameter wire. An I₂-doped extruded wire with residual CSA had a failure current density of 58 MA/m², two orders of magnitude less than the I₂-doped DWCNT wire.⁴

The failure current density of purified and IBr-doped NCTI CNT wires resulted in a failure current density of 26.6 MA/m², a 36% increase in failure current density compared to the starting material. The failure current density was tested by increasing 10 mA steps held for 30 seconds each with a separation of 2.5 cm between the voltage probes.

2.6 Conductivity and CCC Stability

The stability of CSA, I₂, IBr, and KAuBr₄ doped, electronic-type separated and mixed, SWCNT thin films was measured as a function of time in ambient conditions.¹⁶ There is no appreciable difference in stability based on electronic type, but dopant type did play a significant role. The halogen dopants, I₂ and IBr, were consistently the least stable. For all cases the conductivity decreases with time and is relatively stable after thirty days. Iodine doping results in a conductivity less than that of the purified CNTs within ten days, this is attributed to I₂ intercalation and removal from the CNT bundles resulting in residual disorder.⁴⁵ This theory is supported by the authors Raman analysis of the I₂ doped films

showing a ~50% increase in the D/G ratio after forty days, compared to the purified CNTs.¹⁶ For the mixed CNT samples, CSA maintains a conductivity ~1.7x greater than the purified after 70 days, while KAuBr₄ maintains a conductivity ~3.8x greater than the purified SWCNTs.¹⁶

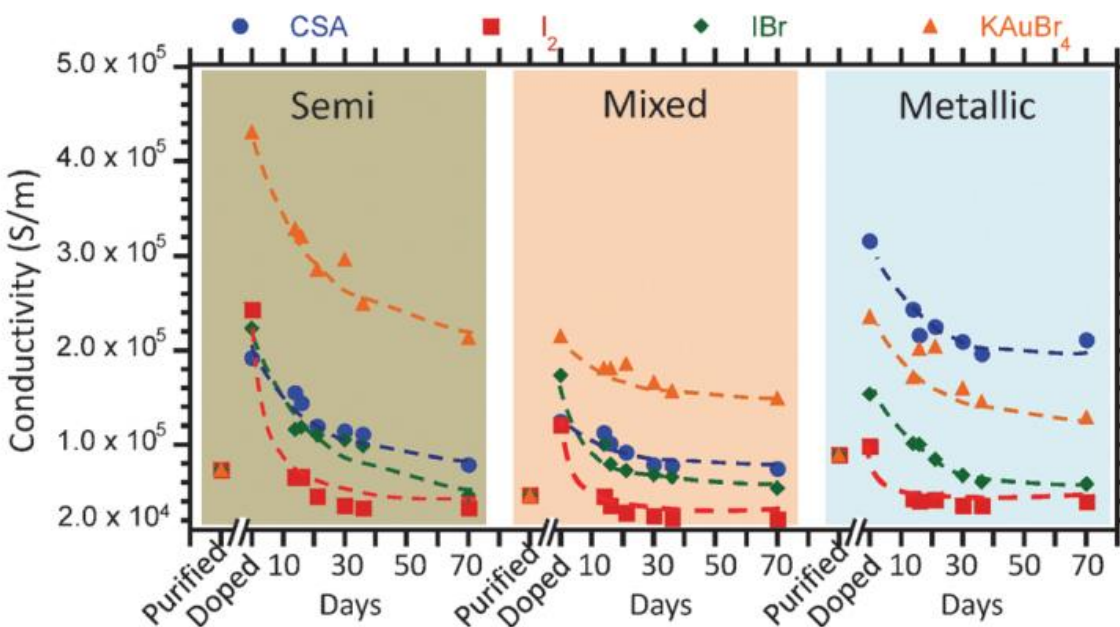


Figure 10: The electrical conductivity as a function of time for CSA, I₂, IBr, and KAuBr₄-doped, electronic-type separated or mixed, SWCNT thin-films, compared to the purified SWCNT films. Reproduced with permission from the NanoPower Research Laboratories.¹⁶

The resistance and temperature of a 11.2 mm diameter KAuBr₄-doped CNT wires from densified sheet material was measured as a function of time at an applied current resulting in an operating temperature of 100°C.⁴³ The results determined that the CNT wire was able to continuously carry 20 A for 24 hours with no significant change in resistance or temperature.

Jarosz et al. studied the effects of temperature cycling on the resistance of wires made from densified CNT sheet material, with and without the presence of KAuBr₄ doping.⁴⁶ Cycling

between -100 °C and 60 °C for 10 hours in a vacuum environment resulted in no appreciable change in resistance (<1%) for the CNT wires, independent of the presence of KAuBr₄ doping. This behavior is unlike copper materials, which experience a doubling in resistivity over the applied temperature range.⁴⁶

The work by Zhao et al. which claimed to produce an I₂-doped DWCNT wire with a specific conductivity greater than copper and aluminum claimed no change in electrical conductivity in seven days.³⁴ The similar work I₂-doping of an extruded CNT wire with residual CSA also claimed no change in electrical conductivity the 1 year. This is in stark contrast to the work by Puchades et al. which measured a decrease in conductivity to approximately that of the starting material within seven days.¹⁶ The different results are likely due to the doping procedure. Zhao and Behabtu doped the CNT wires in 200°C I₂ vapor for twelve hours, while Puchades doped the CNT wires in 100°C I₂ vapor for 1 hour. This might indicate that 12 hours of deposition results in saturation of I₂ on the CNT wires and that within the first seven days, the I₂ which is desorbing from the doped-CNT wire does not contribute to improved electrical conductivity. Zhang also found that iodine doped CNT materials have an ~30% reduction in conductivity within two weeks. The study which compared the doping efficacy of IBr and ICl also claimed no changes in electrical conductivity as a function of time.

The procedure performed by Wang et al. using current sweeps to increasing applied current densities which are held for 30 seconds then sweeping the current back to 1 mA until ultimate wire failure was performed so that the resistance at 1 mA could be determined.⁴⁴ This work can be thought of as attempting to measure the change in low-current resistivity of the doped CNT materials which should not be affected by Joule heating and the resulting

temperature depend changes in resistivity. The work falls short in doing so because it does not describe the time allotted for the sweep to 1 mA and if this is sufficient time for the material to reach room temperature. The low-current resistivity was plotted as function of the peak current density that the CNT wires had been exposed to.⁴⁴ The work identified 4 main regimes. Regime 1 is reversible, any applied current within this regime does not result in a change in low-current resistivity. Regime 2 is irreversible; increasing applied current results in an increase in resistivity. The authors relate this to the de-doping of CSA, stating that the boundary between regime 1 and regime 2 indicates a temperature greater than the boiling point of CSA. Regime 3 is another reversible regime; the material has been purified of CSA and has different electrical properties than the material in Regime 1. Regime 4 is irreversible, with increasing applied current material degradation occurs resulting in increasing resistivity. The authors claim that any current density within Regime 4 would result in eventual wire failure, but this is not substantiated.

3 Dissertation Overview

I₂, IBr, and KA_uBr₄ have emerged as premier dopants for enhancing the electrical conductivity of CNT conductors. Although the improvements in electrical conductivity of CNT conductors has been well documented, little is known regarding the current-carrying capacity and electrical conductivity retention of these doped-CNT conductors. As advances in electrical conductivity continue to improve, the field is poised to understand how these materials will behave during practical operation. Variations between CNT materials and ambiguity in testing conditions have resulted in substantial gaps in understanding how chemical dopants compare in their ability to improve the current-carrying capacity of carbon nanotube conductors. There are inconsistencies in the reported electrical conductivity stability of doped-CNT conductors. This dissertation sets out to systematically quantify current-carrying capacity and electrical conductivity retention of doped-CNT conductors as to identify chemical dopants that are stable for current-carrying applications.

This dissertation consists of two main bodies of work followed by additional considerations regarding the electrical performance retention of doped CNT conductors. The following list outlines the primary research focus areas:

1. Understanding the electrical performance retention of densified and KA_uBr₄ doped CNT wires via an analysis of thermal stability.
2. Direct comparison of the electrical performance retention of I₂, IBr, and KA_uBr₄ doped CNT wires and development of a degradation mechanism.

3. Additional considerations: varied doping procedures, doping of novel CNT materials, ambient doping, direct temperature measurements, and power calculations.

4 Characterization of CNT Conductors

4.1 Physical Characterization of CNT Conductors

4.1.1 Surface Morphology & Analysis

Scanning electron microscopy (SEM) images are used to gain insight into the surface morphology along the length of CNT conductors. The morphology and diameter of bulk CNT conductors can be analyzed at lower magnifications. The presence of void spaces, surface variations, and large metal deposits can be readily observed at $< 1,000\times$. Higher magnifications ($>5,000\times$) allow for qualitative analysis of CNT alignment, metal particles, and other nanoscale CNT network properties. SEM imaging of CNT wires near the point of failure allows for analysis of metal deposits that accumulate during electrical testing. An SEM equipped for energy-dispersive x-ray spectroscopy can be used to determine chemical composition of various metal particles within the samples.

4.1.2 Diameter & Cross-Sectional Area

Accurate cross-sectional area measurements of CNT conductors are needed for calculating electrical conductivity and current density. SEM images can be used to measure the cross-sectional area of CNT conductors that have been cut perpendicular to the axis of the conductor. Cross-sectioned samples are prepared using a VersaLaser VLS2.30 laser cutter from Universal Laser Systems in order to prevent physical deformation of the conductor's radial geometry. If cross-sectional SEM analysis determines that the geometry of a conductor is cylindrical, optical microscope images along the length of the conductor can be used to determine the diameter and the cross-sectional area can be calculated. Using optical microscope images is advantageous as it allows for the non-destructive and rapid measurement of conductor diameter.

4.1.3 Mass & Density

Mass measurements are collected using a Mettler-Toledo XP2U microbalance. Accurate measurements of mass are critical as the strength and electrical conductivity of CNT conductors is often compared to other conventional materials by mass-normalized metrics. The volumetric density of the CNT wires is determined by the cross-sectional area, mass, and length, measured with calipers. “Tex” is a unit of measure for the linear mass density and is defined as the mass in grams per kilometer. The NCTI CNT wires are typically described based on the tex of the material.

4.2 Electrical Characterization

4.2.1 Resistance per Length and Electrical Conductivity

The resistance per length of CNT conductors is determined using a National Instruments NI PXI-5652 source/measure unit and an NI PXI-4071 digital multimeter with a four terminal configuration. A four terminal configuration is used to determine the resistance per length of the conductor independent of contact resistance. The electrical conductivity of the conductor is calculated according to Equation 4. Where R/L is the resistance per length and A is the cross-sectional area.

$$\sigma = \frac{1}{\left(\frac{R}{L}\right) \cdot A} \quad \text{Equation 4}$$

The calculated electrical conductivity of a CNT conductor is considered an engineering conductivity due to its dependency on the density of the material. Reducing the cross-sectional area through densification increases the engineering conductivity via increasing the amount of conductive CNTs per unit area, but no change has occurred in the materials ability to conduct electricity. Normalizing the electrical conductivity to its volumetric

density, defined as the specific conductivity, eliminates the need for accurate diameter measurements and allows for accurate comparisons of electrical conductivity independent of diameter and density.

4.2.2 Failure Current Density

The maximum current at failure is determined by using an Arbin BT-2000 power supply in a four-terminal configuration, with a minimum critical length between voltage sensing probes and <1 cm between source and sense probes. Current is applied in increasing 10 mA steps and maintained for 30 s at each step until wire failure to determine the failure current density in air. The current density at failure is determined for each sample using the average diameter specific to the sample.

4.3 Thermal Characterization

4.3.1 Thermogravimetric Analysis

Thermogravimetric analysis (TGA) is performed using a TA Instruments TGA Q5000 (Balance Purge: N₂(g) 20 mL/min, Sample Purge: Air 20 mL/min, Ramp Rate: 10 °C/min). TGA analysis will provide information of the decomposition of CNT conductors with and without chemical doping as a function of temperature. The comparison of thermal stability of doped-CNT conductors is essential to identifying dopants for high current applications.

4.3.2 Thermal Imaging

Thermal imaging with a FLIR A35 infrared camera provides a non-contact means of measuring temperature. Non-contact temperature measurements circumvent possible issues due to conduction to a thermocouple. ASTM Standard E 1933-99a is used to determine the emissivity specific to each material to ensure accurate temperature measurements.

4.4 Elemental Analysis

4.4.1 Energy Dispersive X-Ray Spectroscopy

A Tescan Mira3 SEM equipped with a Bruker energy dispersive X-ray (EDX) spectrometer is used to determine the elemental composition of the surface of as-received and doped CNT wires. Understanding the atomic weight and mole composition of the doped CNT wires provides information about the amount of dopant adsorbed and how that dopant degrades after temperature and current exposure.

5 Sustaining Enhanced Electrical Conductivity in KAuBr_4 -Doped Carbon Nanotube Wires at High Current Densities

This chapter summarizes the use of physical densification and KAuBr_4 chemical doping of commercially available CNT wires to improve electrical conductivity and outlines the processes by which electrical performance retention as a function of increasing applied current density and constant current cycling are obtained. The work concludes with an analysis relating the thermal stability of the KAuBr_4 dopant and the resulting improvements in electrical performance retention. This excerpt is reprinted with permission from (Soule et al., Sustaining Enhanced Electrical Conductivity in KAuBr_4 -Doped Carbon Nanotube Wires at High Current Densities, *ACS Applied Nano Materials*, **2019**, 2, 11, 7340-7349).

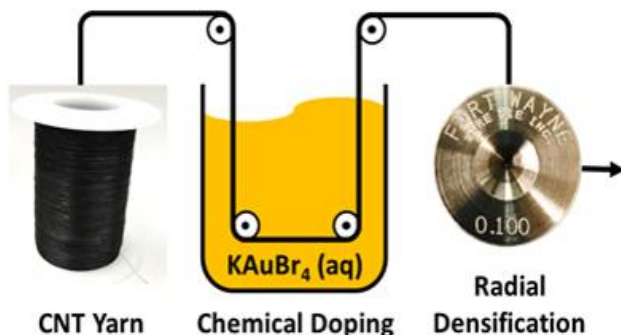


Figure 11: Representative diagram of the KAuBr_4 chemical doping and radial densification of CNT wires.

5.1 Abstract

Densification and chemical doping with KAuBr_4 is shown to improve the electrical conductivity of commercially-scaled CNT wires by a factor of 6 to values greater than 1 MS/m, while increasing the failure current density by 67% to $35 \pm 3 \text{ MA/m}^2$. The electrical conductivity retention is quantified via measuring changes in the conductivity during increasing applied current densities (working conductivity) and at room temperature after

current exposure (resting conductivity). CNT wires doped with KAuBr_4 exhibit no change in resting conductivity after application of current densities up to 32 MA/m^2 , which exceeds that of the as-received material by more than three times. The mechanism by which KAuBr_4 doping improves the electrical stability of CNT conductors at higher current densities was probed via analysis of CNT wires treated with various thermal oxidation and doping procedures. Energy dispersive X-ray spectroscopy was used to determine the elemental composition of KAuBr_4 -doped CNT wires after thermal oxidation to $400 \text{ }^\circ\text{C}$, demonstrating the presence of residual chemical dopants near the onset temperature of CNT conductor failure. Therefore, enhanced KAuBr_4 -doped and densified CNT wire performance is attributed to the inherent thermal stability of KAuBr_4 and its decomposition cascade into other chemically active dopants. Overall, the thermal stability of the chemical dopant is a critical factor for high current CNT conductor applications.

5.2 Introduction

Carbon nanotube (CNT)-based conductors are lightweight and robust candidate alternatives to conventional metal conductors for a variety of space, defense, and power transmission applications.^{4,47,48} Compared to conventional copper conductors, CNT conductors have approximately an order of magnitude lower physical density, have improved flexure tolerance, and are able to withstand corrosive environments.^{46,47} In a variety of mobile applications, these advantages allow for greater payloads, reduced fuel consumption, and reduced transportation costs, while allowing CNT conductors to operate under greater mechanical load and in chemically harsh environments.

Previous work has produced CNT conductors via dry spinning, extrusions of CNT-acid dispersions, and densification of commercially available CNT sheet material through radial

drawing dies.^{3,4,24,44,49,50} Initial work with commercial CNT sheet densification techniques found that optimization of the density could result in materials with an electrical conductivity of 0.12 MS/m.⁴⁹ The work demonstrated that chemically doping the material with aqueous potassium tetrabromoaurate (KAuBr₄) solution resulted in an order of magnitude increase in electrical conductivity.⁴⁹ More recently, the dopant efficacies of KAuBr₄, I₂, IBr, and chlorosulfonic acid (CSA) were compared and it was determined that KAuBr₄ results in the greatest improvement in electrical conductivity for semiconducting and mixed electronic-type single wall CNTs (SWCNTs).¹⁶ Results supported the mechanism that chemical doping occurs when the redox potential of the chemical species is more positive than the SWCNT electronic transitions versus a standard reference electrode.¹⁶ Raman analysis of the D/G ratio of CNTs before and after interhalogen doping has indicated that this doping is caused by physisorption which does not disrupt the highly-conductive sp² structure of the CNTs.³³ Of the chemical dopants analyzed, KAuBr₄ exhibited one of the greatest electrochemical redox potentials resulting in enhanced doping.¹⁶ The improved electrical conductivity of CNT conductors chemically doped with KAuBr₄ has also been attributed to the reduction of the tunneling barrier between individual CNTs and their bundles along with an increase in the number of charge carriers for intra-tube transport.⁴⁹ Therefore, both experimental and theoretical calculations⁵¹ support the strong electrochemical interaction between CNTs and KAuBr₄ leading to significant enhancement in bulk electrical conductivity through ex-situ doping.

In addition to electrical conductivity enhancement, power transmission applications require stability of the electrical conductivity during operation as a function of time, temperature, and applied current density. Jarosz et al. studied the effects of temperature cycling on the

resistance of wires made from densified CNT sheet material, with and without the presence of KAuBr_4 doping.⁴⁶ Cycling between $-100\text{ }^\circ\text{C}$ and $60\text{ }^\circ\text{C}$ for 10 hours in a vacuum environment resulted in no appreciable change in resistance ($<1\%$) for the CNT wires, independent of the presence of KAuBr_4 doping. This behavior is unlike copper materials, which double in resistivity over the applied temperature range.⁴⁶ Puchades et al. measured the electrical conductivity as a function of time in ambient, room temperature storage conditions for CNT samples doped with KAuBr_4 , I_2 , IBr , and CSA, demonstrating that the KAuBr_4 -doped CNT conductors maintained a conductivity ~ 3.8 times greater than the control sample over 70 days, while the CSA-doped samples only maintained a conductivity ~ 0.7 times greater than the control sample over the same time.¹⁶ These works provide an initial understanding of electrical conductivity retention with time and temperature cycling, but do not expose the CNT samples to elevated current densities and the resulting higher temperatures from Joule heating.

Recent work on chemically doped-CNT conductors has measured the current density at failure, long-term effects of applied current load, and the material degradation caused by increasing current.^{43,44} The failure current density of KAuBr_4 -doped and densified CNT sheet material conductors of various diameters allowed for a fuse law equation specific to this KAuBr_4 -doped material to be determined.⁴³ Fifty percent of the current at failure was applied to a KAuBr_4 -doped CNT conductor for over a month; after an initial conditioning period the CNT conductor was relatively stable, demonstrating that KAuBr_4 has the potential to be a stable dopant under continuous applied current.⁴³ The electrical stability as a function of current density has also been analyzed for CSA-doped, extruded CNT wires via increasing current steps held for 30 seconds with current sweeps between each

step, allowing for resistance to be determined as a function of the current to which the wires were previously exposed.⁴⁴ The work attributed the initial increase in resistance with dedoping of CNTs due to CSA removal because the step occurred at a temperature higher than the boiling point of CSA.⁴⁴ Therefore, the recent study would suggest that a relationship between dopant thermal stability and electrical conductivity retention exists.

The present work extends the progress of using KAuBr_4 chemical doping and densification to enhance the electrical transport properties of kilometer-scaled CNT wires. Following characterization of as-received, densified, and chemically doped and densified CNT samples, a thorough analysis of electrical conductivity retention is performed. The present work analyzes the difference between resistance during current application and the resting resistance at room temperature after current application. KAuBr_4 -doped CNT conductors exhibit very stable electrical performance retention with increasing current density, unlike the as-received material. The ability to withstand multiple cycles of increased current is explored via application of 50% and 75% of the failure current density, specific to each treatment, for 24 1-hour cycles. A low current I-V sweep after each cycle is used to determine the degradation of the CNT conductors. Thus, providing insights into how long-term high current density exposure effects as-received and doped CNT materials. Thermal oxidation and chemical doping studies are used to investigate the relationship between thermal stability of the dopant and electrical conductivity retention, thus illustrating the role dopant thermal stability has on high current applications.

5.3 Experimental

5.3.1 CNT Wire Preparation for Doping and Densification Study

CNT yarns were purchased from Nanocomp Technologies Inc. (8-12 Tex, Lot # 60023) and will be used as CNT conductive wire throughout this work. Three-meter segments of CNT wires were used as-received, soaked in 20 mL deionized water for 1 hour, or soaked in 20 mL of 5 mM potassium tetrabromaurate (III) hydrate (KAuBr_4 , Sigma-Aldrich, 99.9%) aqueous solution for 1 hour. The soaked CNT wires were densified at room temperature, without additional lubricant, using single-cut diamond radial drawing dies from Fort Wayne Wire Die with sequentially smaller diameters of 200, 166, 133, 120 and 100 μm . The densified CNT wires were pulled through each drawing die twice and are referred to as H_2O -densified or KAuBr_4 -densified, depending on the treatment solution in which they were soaked. The densified CNT wires were dried in a vacuum oven for 1 hour at 100 $^\circ\text{C}$ prior to characterization.

5.3.2 Physical Characterization

Five CNT wire segments with lengths of 15 cm were randomly sampled from the 3 meter length of wire from each of the three treatments: (1) As-Received, (2) H_2O -densified, and (3) KAuBr_4 -densified. An AmScope optical microscope was used to collect nine diameter measurements along the length of each sample segment, resulting in 45 total measurements per treatment.

The CNT wires were cross-sectioned using a VersaLaser VLS2.30 laser cutter from Universal Laser Systems to minimize physical deformation of the wires prior to imaging of the CNT wire cross-sectional geometry. A Hitachi S4000 scanning electron microscope

(SEM) with a 2-5 kV accelerating voltage range was used to capture images of the cross-sectioned samples and images along the length of the CNT wires.

Thermogravimetric analysis (TA Instruments TGA Q5000, Balance Purge: N₂(g) 20 mL/min, Sample Purge: Air 20 mL/min, Ramp Rate: 10 °C/min) was performed on KAuBr₄-doped and densified CNT wires, as-received CNT wires, and as-received pure KAuBr₄ solids.

5.3.3 Electrical Characterization

Four-terminal wire resistance measurements were collected at room temperature using a National Instruments NI PXI-5652 source/measure unit and an NI PXI-4071 digital multimeter for each of the five samples from each treatment. The failure current density was measured using an Arbin BT-2000 power supply in a four-terminal configuration, with a 2.5 cm separation between voltage sensing probes and <1 cm between source and sense probes. Current was applied in increasing 10 mA steps and maintained for 30 seconds at each step until wire failure to determine the failure current density in air. The current density at failure was determined for each sample dependent upon the average diameter specific to the sample.

The Arbin BT-2000 power supply was also used to obtain the initial, resting, and working conductivities as a function of increasing applied current density. The test includes an initial 1 to 10 mA current-voltage sweep, followed by a repeating sequence of three steps: (1) an “on” step, which exposes the wire to a single current for a specific time (e.g., 1 second, 30 seconds, 1 minute, 5 minutes), that increases by 10 mA each increment until failure; (2) a 30 second “rest” step; (3) a 1 to 10 mA I-V sweep. An example of the procedure to determine the electrical conductivity retention of the CNT wires as a function

of increasing applied current for the first few cycles in the case of the 30 second “on” step is shown in Figure 12. The first I-V sweep is used to determine the initial conductivity (σ_0) of the CNT wire sample at room temperature. The resting conductivity (σ_{Rest}) is calculated from the I-V sweep after each current “on” step. During the “on” step, the voltage and current are measured every second, allowing for the instantaneous conductivity to be calculated. The working conductivity (σ_{Work}) is calculated as the average of the last 5 instantaneous conductivity measurements for each “on” step.

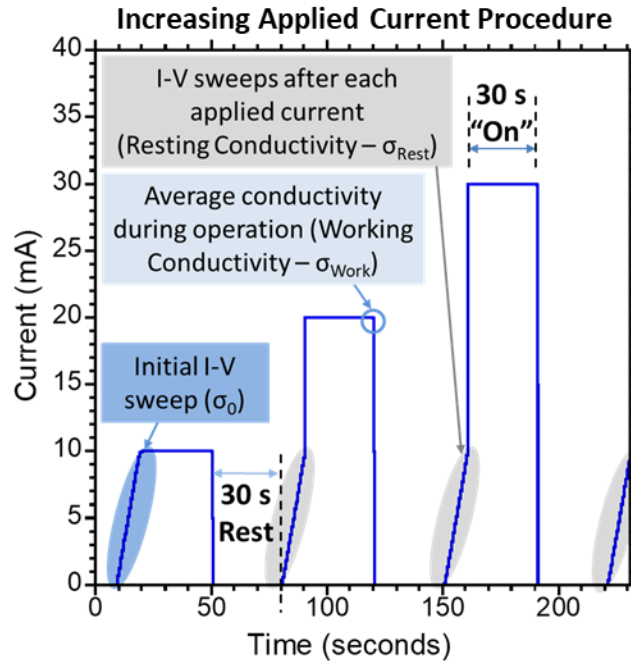


Figure 12. Overview of the representative procedure to determine the electrical conductivity retention of the CNT wires as a function of the applied current vs. time for the first few cycles using 30 second “on” and “rest” steps, detailing how the initial conductivity (σ_0), resting conductivities (σ_{Rest}), and working conductivities (σ_{Work}) are obtained.

The Arbin BT-2000 was used to determine the resting resistance of the CNT wires as a function of cycle number to constant applied current densities corresponding to 50% and 75% of the average current density at failure for each treatment. The test includes an initial

1 to 10 mA current-voltage sweep, followed by a repeating sequence of three steps: (1) an “on” step, which exposes the wire to the applied current density for 1 hour; (2) a 30 second “rest” step; and (3) a 1 to 10 mA I-V sweep. An example of the first I-V sweep and first cycle of the applied constant current density procedure is demonstrated by the schematic in Figure 2. The schematic is not to scale as to highlight the rest and I-V sweep steps. The first I-V sweep is used to determine the initial conductivity (σ_0) of the CNT wire sample at room temperature. The I-V sweep after each applied current step is used to determine the resting conductivity (σ_{Rest}) as a function of cycle number.

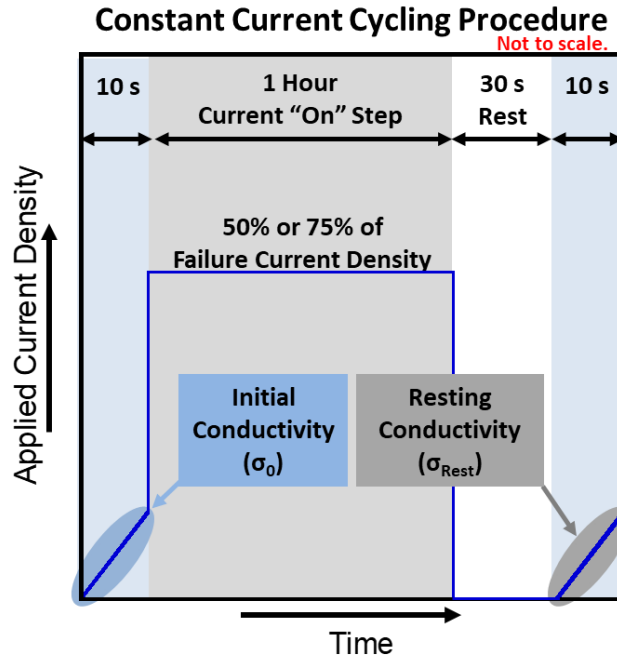


Figure 13: Overview of the initial I-V sweep and first cycle of the constant applied current procedure, detailing how the initial conductivity (σ_0) and resting conductivities (σ_{Rest}) are obtained.

5.3.4 CNT Wire Preparation for Thermal Stability Study

CNT wires were processed from the as-received CNT wire with various thermal oxidation and KAuBr_4 doping procedures, presented in Figure 14. A thermal oxidation step was

performed in a quartz tube furnace with a ramp-stop at 10 °C/min to 400 °C in air, which are equivalent conditions to the TGA procedure. The densification was performed as described in Section 1.1, except the final drawing die was 110 μm instead of 100 μm to prevent mechanical failure of the thermally oxidized samples.

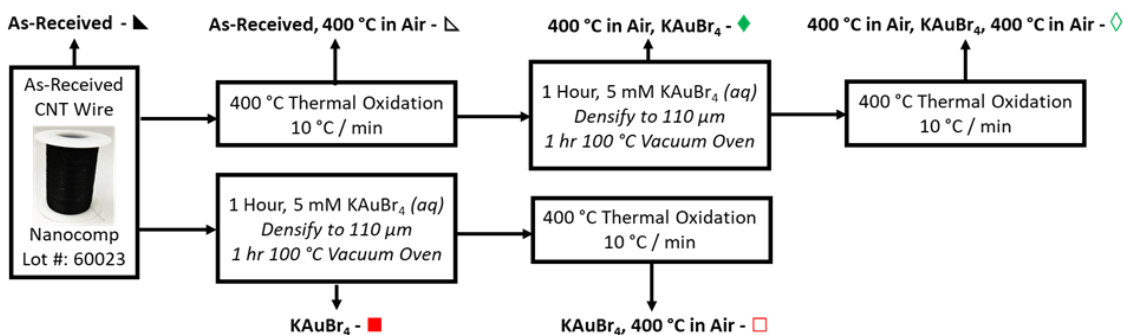


Figure 14: A schematic demonstrating the thermal oxidation and KAuBr₄ doping processes used to create the CNT wire samples for the thermal stability study.

5.3.5 Elemental Analysis of KAuBr₄-Doped CNT Wires

A Tescan Mira3 SEM equipped with a Bruker energy dispersive X-ray (EDX) spectrometer was used to determine the elemental composition of KAuBr₄-doped CNT wires before and after thermal oxidation to 400 °C.

5.4 Results

5.4.1 Physical Characterization

SEM images were used to investigate the surface morphology of the as-received, H₂O-densified, and KAuBr₄-densified CNT wires, shown in Figure 15a-c. The as-received CNT wires have evident axial striations (e.g. variations, gaps, and/or void spaces), which vary along the length of the wire, due to twisting of the material during wire production. The H₂O-densified CNT wires have less visible gaps and void spaces than the as-received CNT wire, but some visible striations still exist. The KAuBr₄-densified CNT wires show

minimal visible gaps or void spaces, indicating that the surface morphology of the KAuBr₄-densified wires is improved by this treatment.

Diameter measurements collected from optical microscope images determined that the as-received CNT wires have a diameter of $152 \pm 18 \mu\text{m}$, while the diameters of the H₂O-densified and KAuBr₄-densified wires are reduced to $139 \pm 6 \mu\text{m}$ and $128 \pm 7 \mu\text{m}$, respectively. Although the H₂O-densified and KAuBr₄-densified wires were densified with a final drawing die diameter of $100 \mu\text{m}$, both samples exhibit relaxation after densification, resulting in final average diameters greater than $100 \mu\text{m}$. The relaxation effect is less pronounced in the KAuBr₄-densified CNT wires than the H₂O-densified CNT wires. The variation in relaxation is consistent with previous work that demonstrated interhalogen compounds, IBr and ICl, dissolved in an organic solvent improve the capillary-induced densification of CNT fibers compared to samples exposed to the organic solvent without interhalogen compounds.³³ The coefficient of variance is reduced from 12% to 5% for the KAuBr₄-densified sample compared to the as-received CNT wires. Thus, demonstrating that radial densification with KAuBr₄ doping is a useful approach to increase physical uniformity while reducing the diameter along a CNT wire.

The cross-sectional area of each CNT wire was calculated using the average value of nine diameter measurements specific to each of the 5 samples from each of the three different treatments and assuming a cylindrical geometry. SEM image analysis of the cross-sectioned wires confirms the assumption of a circular cross-section when calculating cross-sectional area (see Figure 16a-c). The SEM images also show how densification and doping increases density via reduction of void space and improves the cross-sectional circularity of the CNT wires.

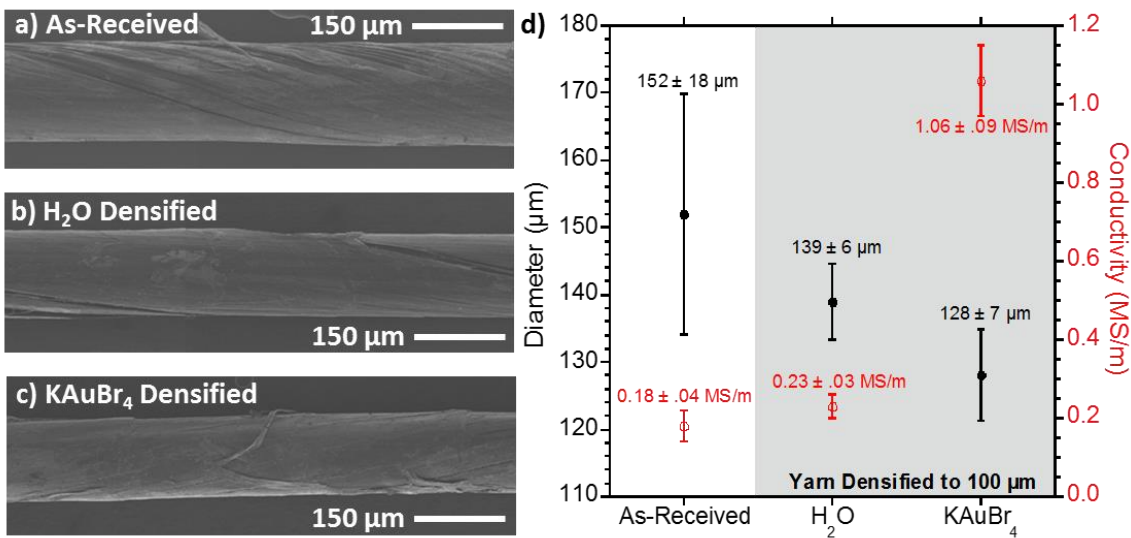


Figure 15. (a-c) SEM images of (a) as-received, (b) H₂O-densified, and (c) KAuBr₄-densified CNT wires. (d) Average diameter and electrical conductivity of five samples for each treatment. Error bars represent the standard deviation from the five measurements obtained via optical microscopy.

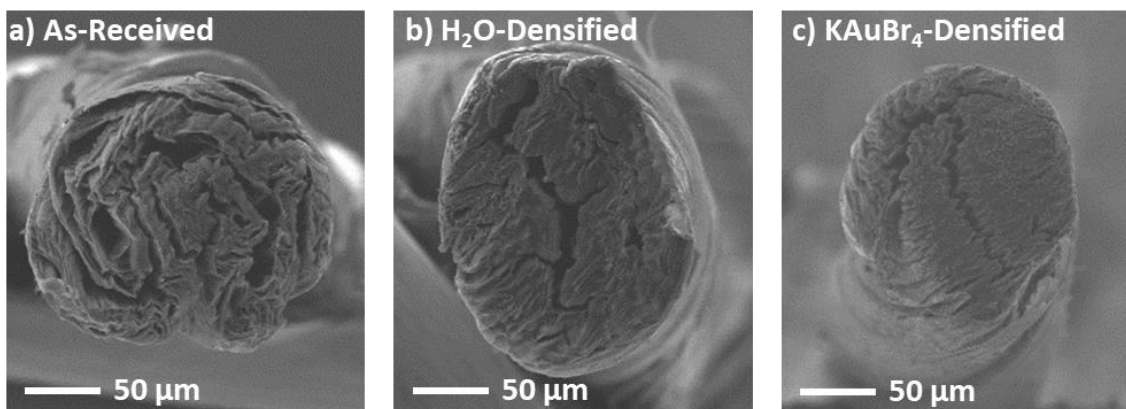


Figure 16: Cross-section SEMs of as-received, H₂O-densified, and KAuBr₄-densified CNT yarns.

5.4.2 Electrical Conductivity

The room temperature electrical conductivity of each CNT wire is calculated based on the resistance per length, determined via four-terminal resistance measurements, and the cross-sectional area specific to each wire. The measured electrical conductivities of five samples

from each treatment were used to determine the average electrical conductivity. The bulk electrical conductivity depends on the geometry of each CNT sample and is intrinsically linked to changes in cross-sectional area. The diameter and electrical conductivity of the as-received, H₂O-densified, and KAuBr₄-densified wires are shown in Figure 15d. The electrical conductivity of the as-received CNT wires is 0.18 ± 0.04 MS/m, whereas the H₂O-densified CNT wires have an average electrical conductivity of 0.23 ± 0.03 MS/m, demonstrating a 28% increase in electrical conductivity due to densification. The electrical conductivity increase is due to two factors: (1) the cross-sectional area is reduced and (2) the resistance per length is reduced (see Figure 17). The resistance per length of the H₂O-densified wires is less than that of the as-received CNT wires due to better electrical contact and physical proximity between CNTs and CNT bundles. The improved proximity and contact due to densification has been correlated to a reduced tunneling barrier between the CNTs and corresponding bundles.⁴⁹ Figure 17 also demonstrates that KAuBr₄-densified CNT wires have a resistance per length 77% less than the as-received CNT wires. The standard deviation in resistance per length for the KAuBr₄-densified CNT wires is 3 Ω /m, compared to values of 12 and 19 Ω /m for the as-received and H₂O-densified, respectively. The lower standard deviation in resistance per length for the KAuBr₄-densified CNT wires indicates that KAuBr₄-doping is a uniform process and reduces variation in the electrical transport. The combined effects of reducing the resistance per length and lowering the cross-sectional area through densification results in an average electrical conductivity for the KAuBr₄-densified CNT wires equal to 1.06 ± 0.09 MS/m, approximately six times greater than that of the as-received CNT wires. The slightly higher standard deviation in electrical conductivity for the KAuBr₄-densified CNT wires was the result of one of the

five KAuBr₄-densified yarns relaxing to a final average diameter of ~ 140 μm. Since the electrical conductivity is inversely related to area, the measured variation in diameter increases the standard deviation for the electrical conductivity of the KAuBr₄-densified CNT wires. Overall, the improvement in electrical conductivity includes the reduction of cross-sectional area and improved electrical transport due to enhanced CNT and CNT bundle contact, and the addition of charge carriers from KAuBr₄ doping.⁴⁹

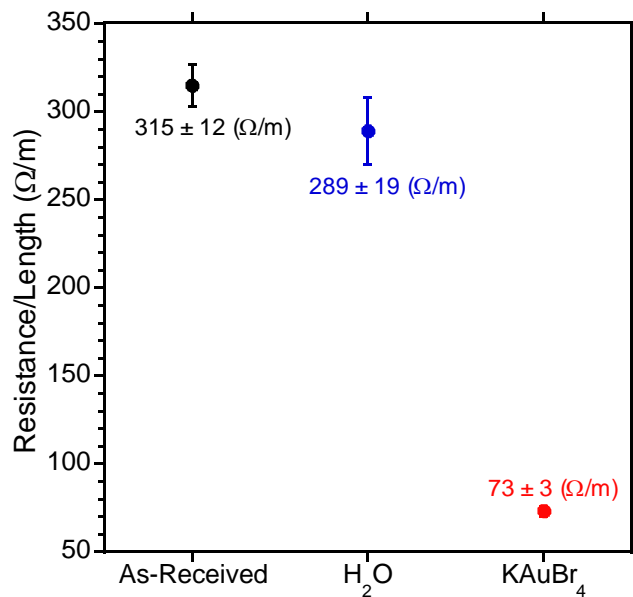


Figure 17: Resistance per length measurements taken at room temperature indicating the different charge transport properties of the CNT yarns, independent of changes in diameter.

5.4.3 Failure Current Density

In the present work, the failure current density for CNT conductors is determined by measuring the voltage while applying current in 30 second steps, increasing by 10 mA with each step, until the conductor fractures. The resulting voltage profiles as a function of applied current density for a representative sample from the five measurements for each treatment are shown in Figure 18. The slope of each voltage profile in its linear regime is a function of the resistance multiplied by the cross-sectional area. Thus, increased electrical

conductivity and reduced diameters result in a decreased slope and higher current density at failure. The average failure current density in air for five as-received CNT wires is 21 ± 5 MA/m². The reduction in cross-sectional area and slight reduction in resistance of the H₂O-densified CNT wires results in a slightly higher failure current density for five samples of 25 ± 2 MA/m². The KAuBr₄-densified CNT wires achieve an average failure current density for five samples of 35 ± 3 MA/m², which is an approximately 67% improvement over that of the as-received wires. The improved electrical conductivity from KAuBr₄ chemical doping directly results in improved failure current density of CNT wires. Using the fuse law relationship established for KAuBr₄-densified CNT sheet material by Cress et al., it is predicted that the failure current density for an equivalent 128 μm diameter conductor would be 11 MA/m². In contrast, the KAuBr₄-densified CNT wires achieve a failure current density more than three times greater than the predicted average value, demonstrating the improved quality of the CNT wire materials over previous commercial CNT sheets.

SEM images of the as-received, H₂O-densified, and KAuBr₄-densified CNT wires after failure current density experiments are shown in Figure 18b-d. The dashed lines indicate the average diameter, specific to the three different treatments, prior to failure. All of the samples have tapered at the point of failure, and this is most pronounced in the as-received sample. The SEM images show that metal catalyst particles accumulate near the failure point on all of the samples. Energy-dispersive X-ray spectroscopy of a similar Nanocomp Technologies Inc. CNT material indicates the presence of iron, suggesting that the accumulated metal is iron catalyst used during production of the CNT materials.⁵²

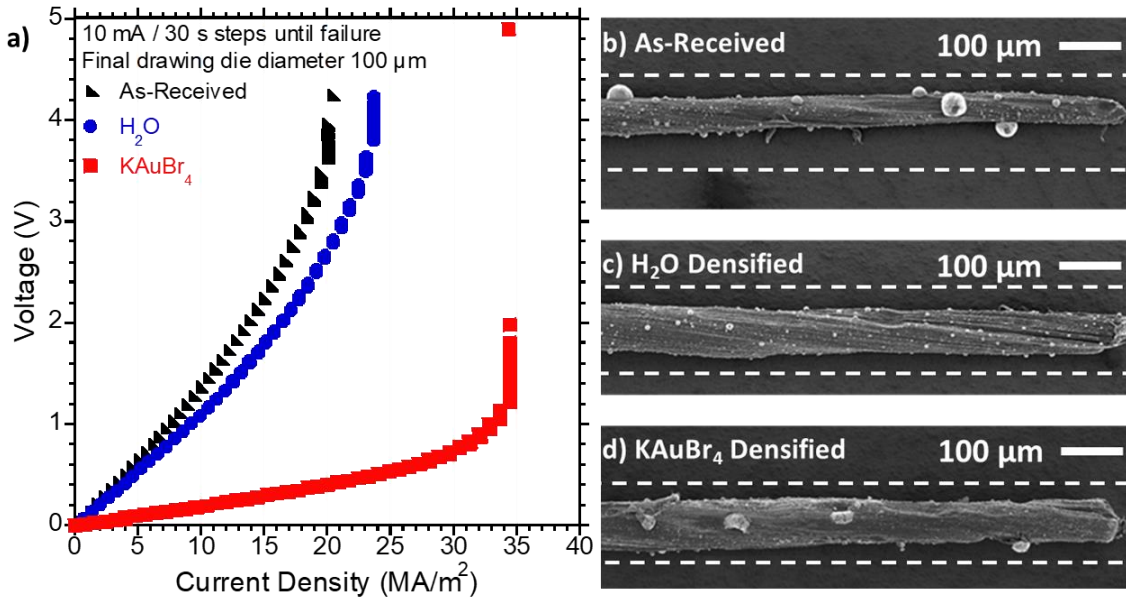


Figure 18. (a) The voltage and current density profiles of the as-received, H₂O-densified, and KAuBr₄-densified CNT wires from Figure 15, obtained by increasing the current by 10 mA steps, then maintained a constant current for 30 seconds. (b-d) SEM images of the CNT wires after failure.

5.4.4 Electrical Conductivity Retention

The electrical conductivity retention was quantified via measuring the resting and working conductivities as a function of applied current density. The resting conductivity (σ_{Rest}) is measured after an applied current step, followed by a fixed 30 second cooling time allowing for the material to cool to room temperature. During operation at high current, Joule heating occurs which can cause changes in the material (e.g., material degradation, defect formation, etc.), which are still present after current is no longer applied and the temperature of the conductor has returned to room temperature. The resting conductivity (σ_{Rest}) is used to define these changes that remain after current exposure. The working conductivity (σ_{Work}) accounts for the degradative changes of σ_{Rest} along with any real-time Joule heating induced changes in electrical conductivity during operation.

The effect of time for the applied current “on” steps was compared for times ranging from 1 second to 5 minutes, shown in Figure 19. The results, normalized to the initial conductivity, indicate that time steps of 30 s or greater result in similar failure current densities and similar trends in resting and working conductivity, independent of whether the materials were as-received or densified and doped. The CNT wire samples exposed to current “on” steps of 1 second most likely do not have time to reach a steady-state temperature, resulting in the material having lesser changes in conductivity, compared to the CNT wires exposed to 30 s or greater current “on” steps, at equivalent applied current densities. The densified CNT wires show a slight increase, up to 3.5%, in resting conductivity for the 5 minute step. This is repeatedly observed and may result from current annealing at the lower current densities prior to high current density exposure. Overall, the 30 second “on” step was selected given the consistency with longer step times while minimizing the total test time.

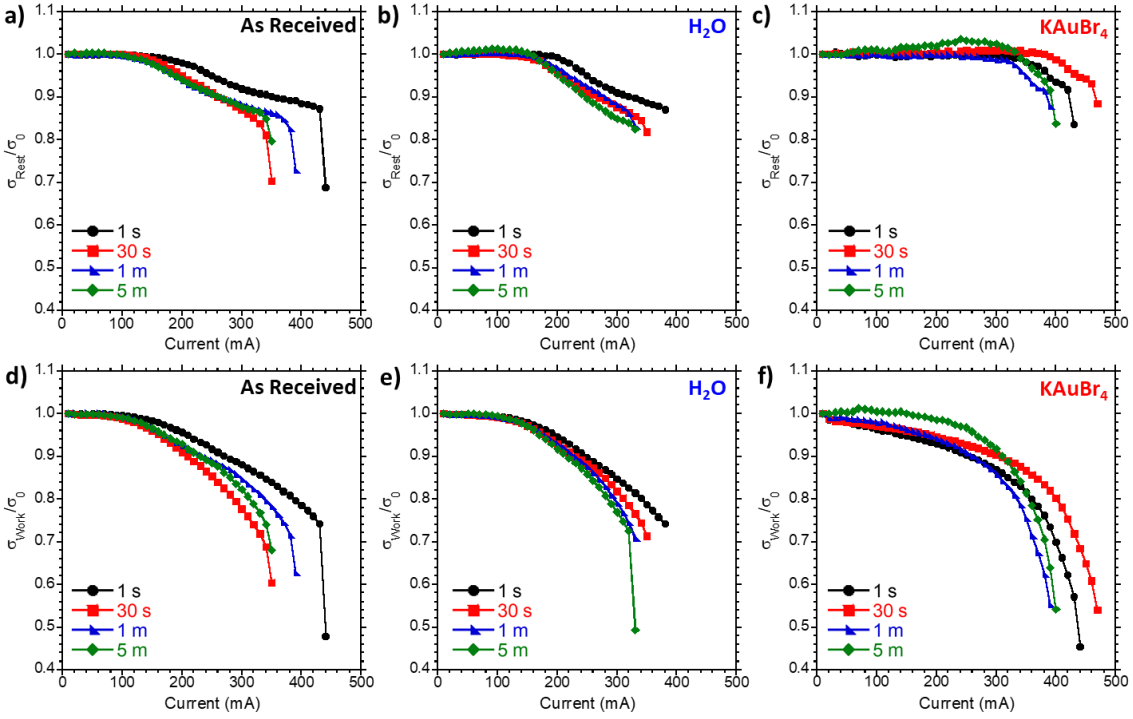


Figure 19: Relative change in resting and working conductivities for as-received, H_2O -densified, and $KAuBr_4$ -densified CNT yarns with varying current “on” step times.

The results of the resting and working conductivity tests for the as-received, H_2O -densified, and $KAuBr_4$ -densified samples with 30 second current “on” steps are presented in Figure 20. Overlaying the data (as in Figure 20) demonstrates the difference between working and resting conductivities. A 2% difference between these values for a given current density is considered a point of divergence where Joule heating during operation begins to affect the conductivity. For the as-received CNT wires, the working conductivity starts to deviate from the resting conductivity at about 7 MA/m^2 , indicating that Joule heating during operation results in a change in the working conductivity of the material due to the temperature-dependent resistance of CNTs. For the H_2O -densified and $KAuBr_4$ -densified CNT wire samples, the 2% difference between σ_{Work} and σ_{Rest} begins at about 9 MA/m^2 .

The difference between the resting and working conductivities increases for all samples as the current density approaches failure.

A 2% change in the resting conductivity compared to the initial conductivity was considered to signify the onset of material degradation in the CNT wires. Both the as-received and H₂O-densified CNT wires have no appreciable change (<2%) in σ_{Rest} until the current density reaches approximately 8 and 11 MA/m², respectively. The KAuBr₄-densified CNT wires exhibit even greater stability, with no appreciable change when exposed to a current density up to approximately 32 MA/m². A comparison of the as-received, H₂O-densified, and KAuBr₄-densified CNT wires show a less than 2% change in σ_{Rest} at current densities of 39%, 45%, and 91% of their failure current densities, respectively. The results reported by Wang et al. exhibit an ~30% decrease in resting electrical conductivity at ~25% of the failure current density for CSA-doped CNT wires.⁴⁴ The decrease in electrical conductivity was reported as an irreversible de-doping process, limiting the current density range in which the sample can retain its initial electrical performance.⁴⁴ In contrast, the KAuBr₄-densified CNT wires shown in Figure 20 retain electrical conductivity up to ~86% of the current density at failure, demonstrating that KAuBr₄ results in a more stable dopant than CSA.

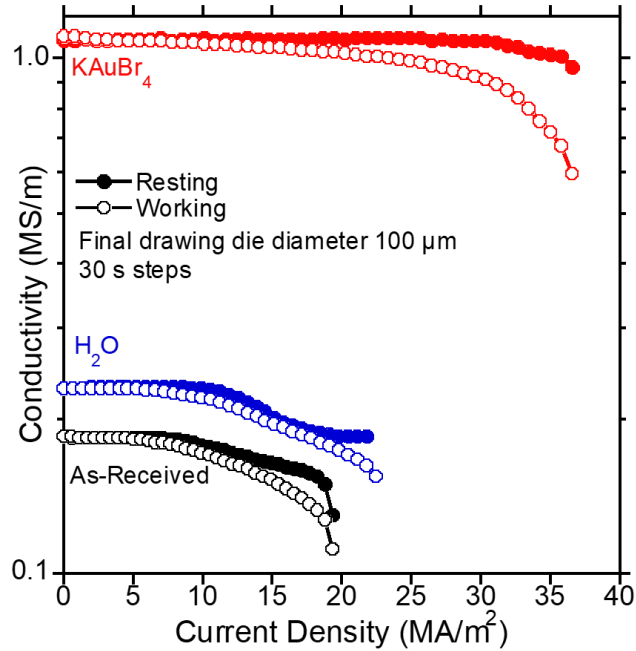


Figure 20. The resting and working conductivities for the as-received, H₂O-densified, and KAuBr₄-densified CNT wires measured with 30 s, 10 mA steps until failure.

The electrical conductivity retention of CNT conductors during operation was analyzed via a 24 hour, cyclic procedure at current densities equal to 50% and 75% of the current density at failure for the as-received, H₂O-densified, and KAuBr₄-densified CNT wires. An initial 1-10 mA I-V sweep, prior to current application, was applied in order to determine an initial conductivity (σ_0). During constant current application, the applied current density was held for one hour. After each hour, the CNT wire was brought to rest for 30 seconds, allowing the conductor to cool. Afterwards, a 1-10 mA I-V sweep was obtained in order to determine the resting conductivity (σ_{Rest}) after current application as a function of cycle number. The resting conductivities as a function of cycle number are presented in Figure 21.

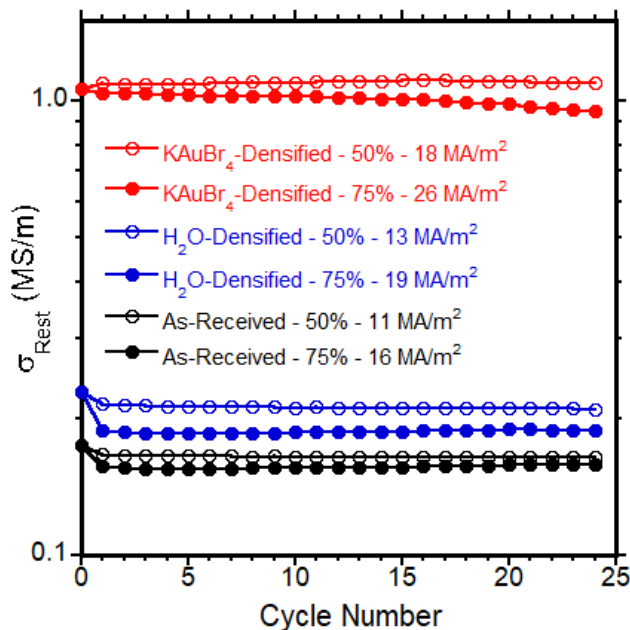


Figure 21: The resting conductivities of the as-received, H₂O-densified, and KAuBr₄-densified CNT wires after each 1 hour cycle at 50% or 75% of the current density at failure for a total of 24 cycles.

The as-received and H₂O-densified CNT wires exhibit a decrease in resting conductivity after the first cycle corresponding to the similar reduction in resting conductivity at comparable current densities observed during the increasing applied current procedure (Figure 6). After the first cycle, the as-received and H₂O-densified CNT wires were relatively stable over 24 cycles at current densities equal to 50% and 75% of their respective current density at failure, thus demonstrating that the electrical conductivity retention is stable during repeated current application.

For the KAuBr₄-densified wires, 50% of the current density at failure is ~18 MA/m², approximately the applied current density used for the as-received and H₂O-densified CNT wires operating at a current density equal to 75% of their current densities at failure. The KAuBr₄-densified CNT wire carrying a current equal to 50% of the current density at failure exhibited relatively no change in resting electrical conductivity over the entirety of

the test, including after the first cycle. The KAuBr₄-densified CNT wire operating at 75% of its current density at failure (i.e. 26 MA/m²) exhibits a subtle fade in resting electrical conductivity within the 24 cycles of the constant current cycling procedure. However, the resting electrical conductivity retention exceeds 89% for the KAuBr₄-doped CNT wires operating at a current density equivalent to 75% of the current density at failure.

5.4.5 Thermal Stability and Enhancement

Thermogravimetric analysis (TGA) was used to compare the thermal stability of KAuBr₄-densified CNT wires to neat KAuBr₄ and as-received CNT wires. The TGA results shown in Figure 22 demonstrate that the KAuBr₄-densified CNT wire exhibits a ~10% decrease in mass below 400 °C, unlike the as-received wire, which shows minimal change. The derivative weight changes of the as-received and KAuBr₄-doped CNT materials indicates the onset of carbon-based material degradation to be after 400 °C, while doping degradation occurs prior to 400 °C. Therefore, thermal oxidation was performed to 400 °C for the as-received and doped CNT wires, as described in Figure 14, to understand how CNT conductors are affected when thermally brought to conditions similar to those before failure via applied current.

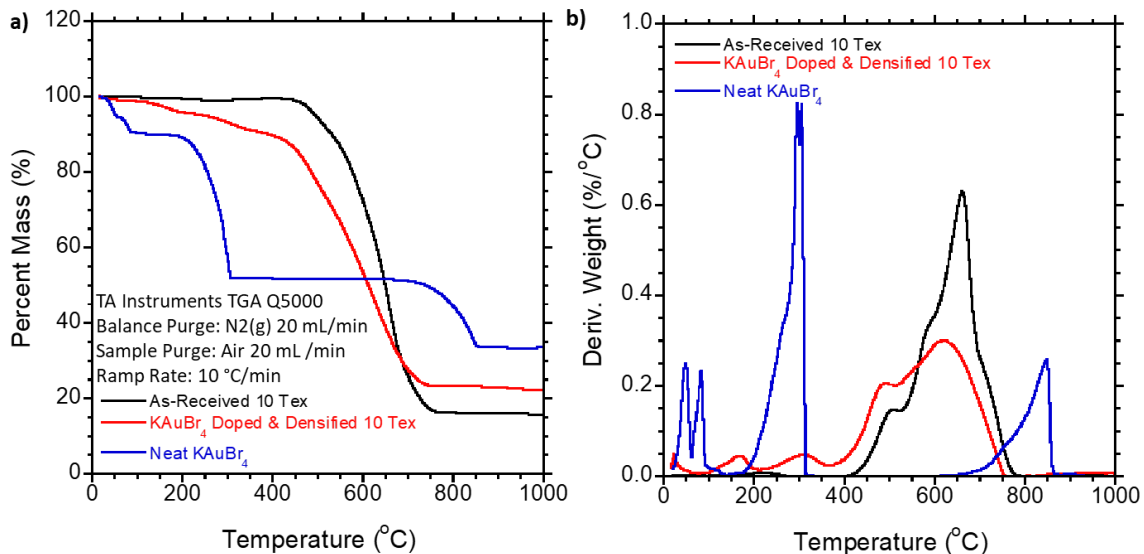


Figure 22: Thermogravimetric analysis of as-received and KAuBr₄-densified CNT yarns compared to neat KAuBr₄ solids.

The effects of thermal oxidation on the electrical properties (resistance per length) are displayed in Figure 23. The resistance per length increases for CNT wire samples that are exposed to a final thermal oxidation step, compared to the similar CNT wires, which did not undergo a final thermal oxidation. The increase in absolute resistance per length after thermal oxidation is similar across all CNT treatments indicating that the CNT materials exhibit a degradation in electrical properties during thermal oxidation to 400 °C. Thermal oxidation to 400 °C results in degradation of KAuBr₄-doping, but the resistance per length remains improved with a value of 181 Ω/m, compared to the thermally oxidized as-received sample with a resistance per length of 413 Ω/m. The electrical property degradation is less substantial for the samples that have been doped prior to thermal oxidation, indicating that the KAuBr₄-doping results in electrical conductivity retention after thermal oxidation to 400 °C. The thermally oxidized then KAuBr₄-doped CNT wires (400 °C in Air, KAuBr₄ – ♦) exhibit a 16% reduction in resistance per length after doping, which indicates that the

materials can be more effectively doped after removal of amorphous carbon¹⁵ because the dopant can interact more favorably with the CNTs.

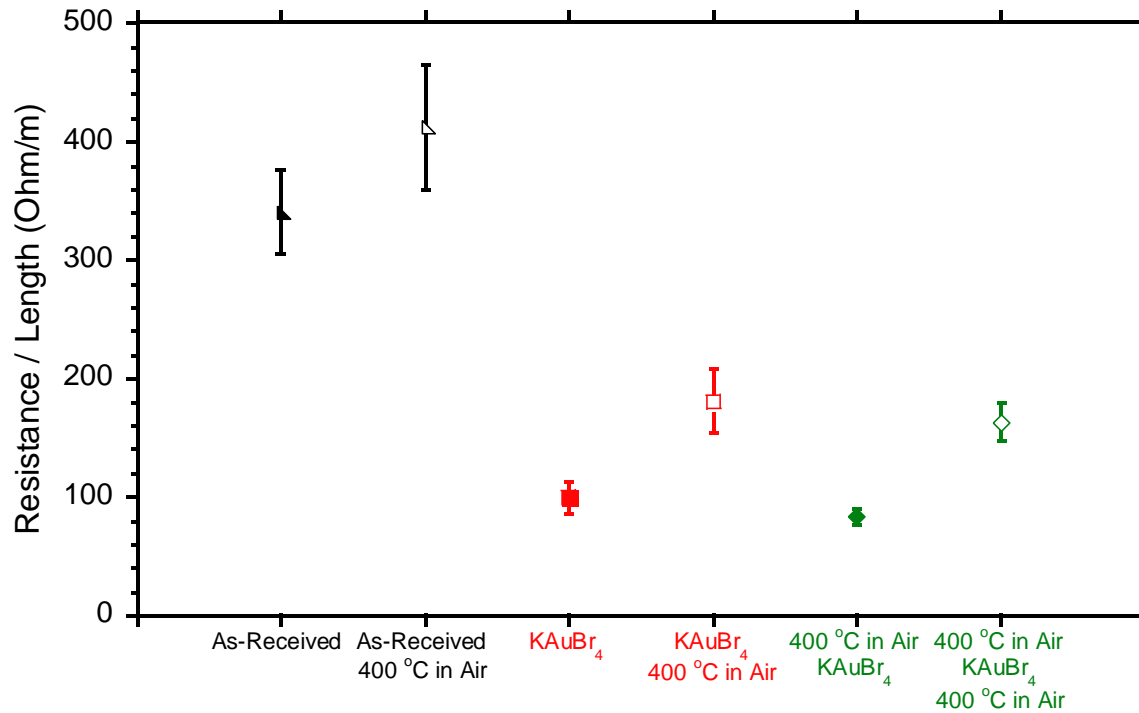


Figure 23: Resistance per length of CNT yarn samples for thermal stability study taken at room temperature.

Figure 24 summarizes the measured resting and working conductivities, normalized with respect to the initial conductivity (σ_0), as a function of increasing current density for the CNT wires exposed to various thermal oxidation and KAuBr₄ doping procedures. The CNT wires that were processed with a final thermal oxidation step exhibit significant deviation in the normalized σ_{Work} compared to σ_{Rest} at increasing current densities. Specifically, in the case of the as-received CNT wire (\blacktriangle), there is no appreciable difference between σ_{Rest} and σ_{Work} until $\sim 7 \text{ MA/m}^2$, compared to the thermally oxidized as-received sample (As-Received, 400 °C in air – \blacktriangle), which undergoes a deviation between σ_{Rest} and σ_{Work} at just $\sim 1 \text{ MA/m}^2$. Both KAuBr₄-doped samples that received a final oxidation (KAuBr₄, 400 °C

in air – □; and 400 °C in air, KAuBr₄, 400 °C in air – ◇) have a deviation in σ_{Work} from σ_{Rest} at ~5 MA/m², while this variation does not occur in the KAuBr₄-doped sample (■) until ~12 MA/m² and ~16 MA/m² for the thermally oxidized sample followed by doping (400 °C in air, KAuBr₄ – ◆). The CNT wire which was thermally oxidized after KAuBr₄-doping (KAuBr₄, 400 °C in air – □) exhibits a decrease in normalized σ_{Work} by ~20% at a current density of ~10 MA/m². In contrast, the samples which were prepared with KAuBr₄ doping as the final step show current density values in excess of 25 MA/m² for a similar ~20% decrease in the normalized σ_{Work} . Therefore, the thermal oxidation of KAuBr₄-doped CNT wires results in improved electrical conductivity compared to as-received CNT wires, but does not result in improved electrical conductivity retention during operation.

A final KAuBr₄ doping step for CNT wires also allows for greater applied current densities prior to σ_{Rest} reduction (i.e., material and/or dopant degradation). The KAuBr₄-doped samples that have a final thermal oxidation step (KAuBr₄, 400 °C in air – □) exhibit a 2% change in σ_{Rest} after ~8 MA/m², similar to the as-received CNT samples. The failure current density of the sample doped and thermally oxidized (KAuBr₄, 400 °C in air – □) is 30 MA/m², compared to 18 MA/m² for the as-received sample (▲), even though changes in σ_{Rest} occur at a similar current density. The failure current density is lower than that reported in the previous section due to the final drawing die diameter being 110 μm rather than 100 μm. The 7 μm increase in diameter for the KAuBr₄-doped samples densified to 110 μm results in the ~5 MA/m² decrease in failure current density. The CNT wire sample that was processed with a thermal oxidation step before chemical doping (400 °C in air, KAuBr₄ – ◆) exhibits behavior similar to the KAuBr₄-doped CNT wires (■), except for a slight decrease in σ_{Rest} at ~33% of the material's failure current density. The KAuBr₄-doped

CNT wire (■) maintains σ_{Rest} at current densities up to 26 MA/m² and fail at a current density of ~30 MA/m², while the sample that was processed with a thermal oxidation step before chemical doping (400 °C in air, KAuBr₄ – ◆) maintains σ_{Rest} until ~28 MA/m² and has a failure current density of ~34 MA/m². The improved electrical conductivity retention and failure current density of the CNT wire thermally oxidized before chemical doping (400 °C in air, KAuBr₄ – ◆) compared to the KAuBr₄-doped CNT wire (■) is attributed to the reduced resistance per length reported in Figure 23, demonstrating the advantage removing amorphous carbon prior to doping has on doping efficacy.

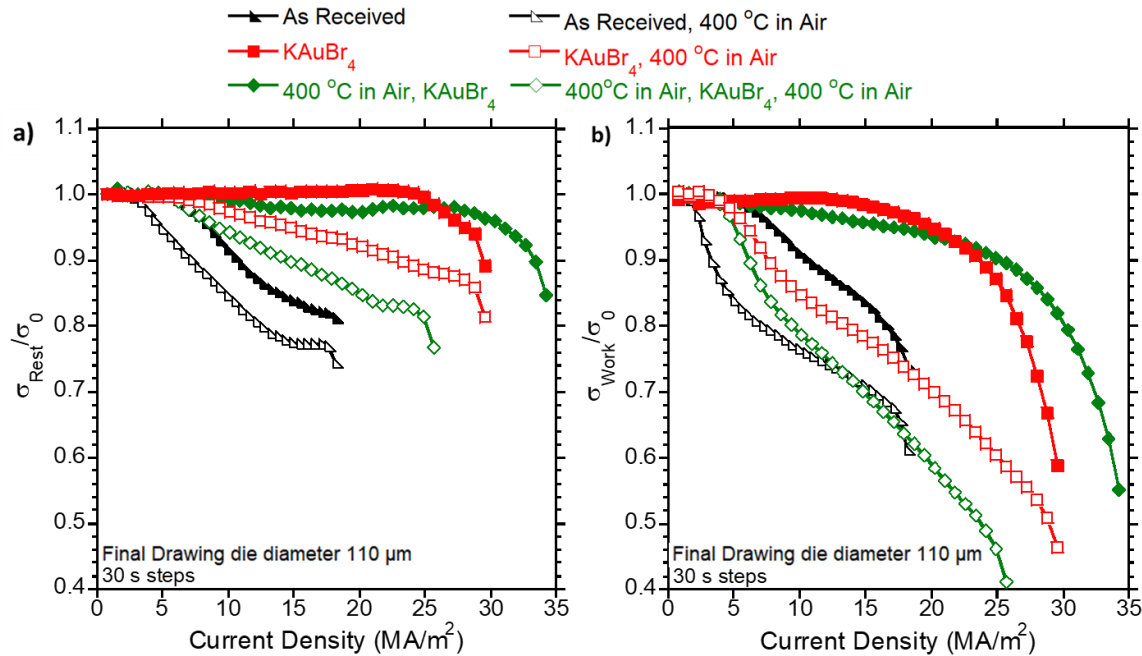


Figure 24. The (a) resting and (b) working conductivities normalized with respect to the initial conductivity of each CNT wire as a function of applied current density.

5.4.6 Elemental Analysis of KAuBr₄-Doped CNT Wires

Energy dispersive X-ray (EDX) spectroscopy was used to analyze the elemental composition of the surface of KAuBr₄-doped CNT wires before (KAuBr₄ - ■) and after

thermal oxidation (KAuBr_4 , 400 °C in air – □). Figure 9a shows the as-doped (KAuBr_4 - ■) CNT sample via SEM along with the elemental spatial analysis of bromine and gold. Presence of bromine and gold is uniformly distributed across the CNT surface, demonstrating the ability of aqueous KAuBr_4 -doping to effectively dope the CNT wire materials. Figure 9b shows the KAuBr_4 -doped and thermally oxidized CNT sample (KAuBr_4 , 400 °C in air – □) via SEM along with the elemental spatial analysis of bromine and gold. The SEM image of the KAuBr_4 -doped and thermally oxidized CNT sample shows accumulation of particles on the surface of the CNTs. The elemental spatial analysis of gold and bromine demonstrates that the particles which have accumulated on the surface of the CNTs are predominantly gold particles with trace bromine. The remaining chemical composition analysis of potassium, carbon, iron, and oxygen is presented in Figure 26.

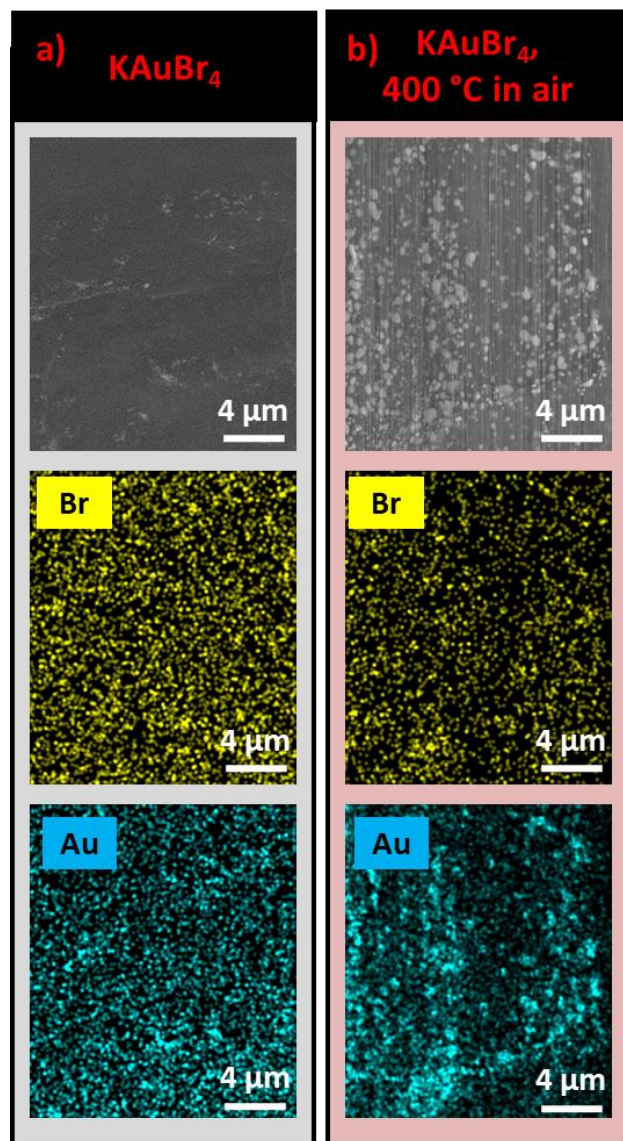


Figure 25: SEMs of the CNT wires samples along with bromine and gold elemental analysis from EDX spectroscopy for KAuBr₄-doped CNT samples a) before (KAuBr₄ - ■) and b) after thermal oxidation to 400 °C (KAuBr₄, 400 °C in air - □).

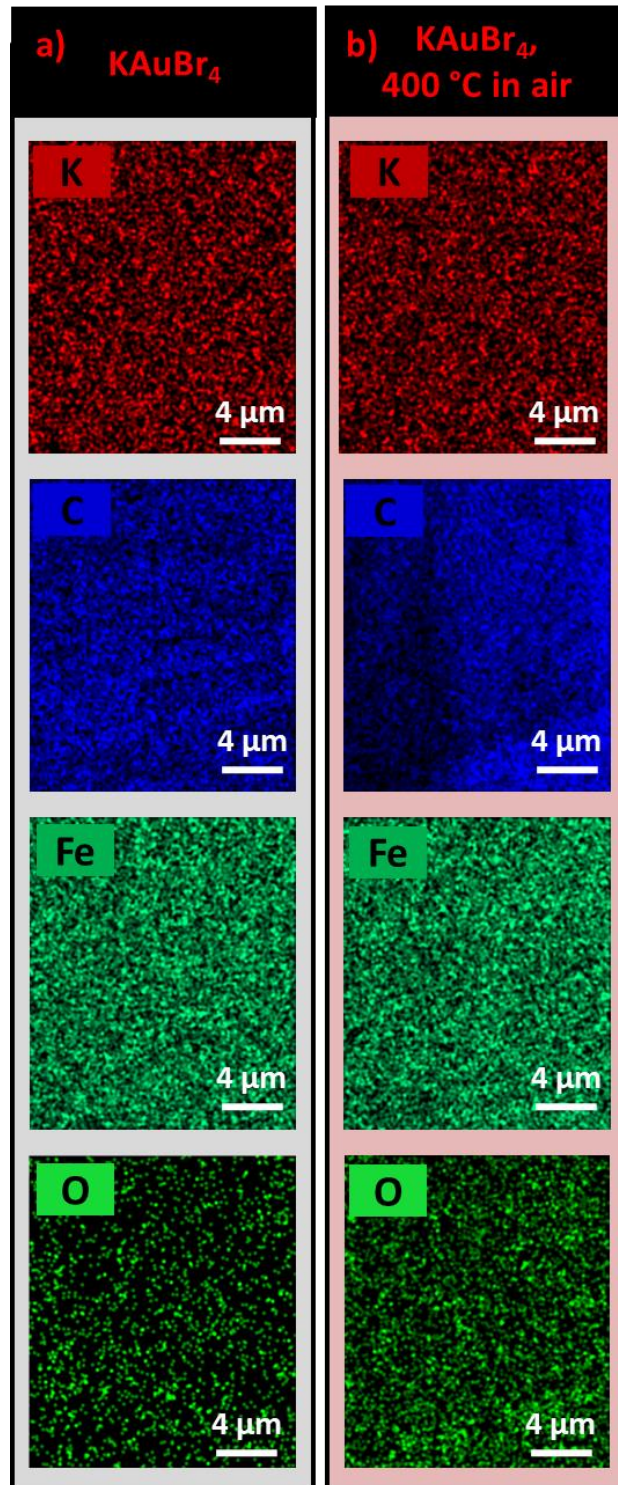


Figure 26: Elemental spatial analysis from EDX spectroscopy of potassium, carbon, iron, and oxygen for KAuBr₄-doped CNT samples a) before (KAuBr₄ - ■) and b) after thermal oxidation to 400 °C (KAuBr₄, 400 °C in air - □).

The weight percent composition of the KAuBr₄-doped CNT wires before (KAuBr₄ - ■) and after thermal oxidation to 400 °C (KAuBr₄, 400 °C in air – □) are displayed in Table 2. The bromine weight percentage for a KAuBr₄-doped CNT sample decreases from 12% after KAuBr₄-doping to 1% after subsequent thermal oxidation to 400 °C. The weight percent of gold present increases from 24% after KAuBr₄-doping to 43% after subsequent thermal oxidation to 400 °C. The increase in gold weight percent results from the accumulation of gold particles after thermal oxidation. Therefore, the residual doping is attributed to trace bromine that is present from the EDX data as well as Au nanoparticles that can provide additional nanoscale transport.⁵³ The effects of the residual doping are demonstrated in the resistance per length of the KAuBr₄-doped and thermally oxidized samples (KAuBr₄, 400 °C in air – □) presented in Figure 23, which maintain a resistance per length approximately 47% less than the as-received CNT wires. Thus, EDX analysis has demonstrated that thermal oxidation to 400 °C results in degradation of the dopant through bromine removal, but maintains lower resistance per length. Therefore, KAuBr₄-doped CNT wire samples that are brought to near failure conditions (400 °C) are able to maintain lower resistance per length and enhanced current density at failure due to the thermal stability of KAuBr₄-doping compared to as-received CNT wires.

Table 2: The weight percent composition of the KAuBr_4 -doped CNT wires before (KAuBr_4 - ■) and after thermal oxidation to 400 °C (KAuBr_4 , 400 °C in air – □).

Element	KAuBr_4 (wt. %)	KAuBr_4 , 400 °C in air (wt. %)
C	53	46
Au	24	43
Br	12	1
Fe	8	8
O	2	2
K	1	0

5.5 Discussion

The improved failure current density of KAuBr_4 -doped CNT conductors at high current densities is attributed to the improved electrical conductivity from chemical doping and densification. The improved electrical conductivity of KAuBr_4 -doped CNT conductors lowers the Joule heating at comparable current densities,⁴³ thereby maintaining a temperature below the threshold of the onset of material degradation. The result of this enhanced property is a greater failure current density for KAuBr_4 -doped samples compared to the as-received CNT wires.

The physical origin of the electrical conductivity retention achieved for KAuBr_4 -doped CNT wires at high current density is attributed to its decomposition into other CNT chemical dopants and its thermal stability as an ionic species. The decomposition of KAuBr_4 -doped CNT wires at increasing temperatures can be assumed to be similar to that which occurs with thermal decomposition of HAuCl_4 . Otto et al. used x-ray diffraction to

analyze the residual decomposition products of HAuCl_4 after distinct decomposition steps determined via TGA and mass spectrometry.⁵⁴ It was determined that HAuCl_4 decomposes to AuCl_3 at 190 °C, with subsequent release of Cl_2 to form AuCl at 240 °C, ultimately resulting in Au at 520 °C. The thermal decomposition for KAuBr_4 -doped CNTs is likely similar to HAuCl_4 , with the exception being the evolution of bromine gas. From the TGA thermogram (Figure 22), the mass loss of the KAuBr_4 -densified CNT wires prior to 100 °C is attributed to excess H_2O evaporating. The mass loss at ~300 °C is assigned to the production of Br_2 gas during the decomposition of AuBr_3 to AuBr . The resistance per length for the KAuBr_4 -doped samples thermally oxidized to 400 °C is still less than the as-received CNT wire (see Figure 23). Therefore, the residual doping is attributed to trace bromine that is present from the EDX data as well as gold nanoparticles that can provide additional nanoscale transport.⁵³ Therefore, the cascade of decomposition products elucidates a potentially critical characteristic of gold halide dopants, whereby the dopant efficacy is maintained when the doped-CNT conductors reach higher temperatures because the products are effective CNT dopants.^{16,55}

The electrical conductivity retention of KAuBr_4 -doped CNT conductors is superior to other high efficacy dopants because of the thermal stability of the dopant. The work performed by Wang et al. using CSA-doped CNT wires did not exhibit a similar retention of electrical conductivity due to a distinct de-doping of the CSA due to its boiling point at 150 °C.⁴⁴ Similarly, pure halogen dopants such as Br_2 and I_2 which result in high CNT conductivity values^{34,56,57} are not likely to exhibit sustained retention of electrical conductivity at elevated applied current due to relatively low boiling temperatures of 59 °C and 184 °C, respectively.⁵⁸ Although acid and halogen dopants have resulted in promising

enhancements in room temperature electrical conductivity, these CNT dopants are not preferable to high current applications due to their low thermal stability. Therefore, KAuBr₄ has emerged as the premier CNT dopant for high current density applications because of the thermal stability of KAuBr₄ and its decomposition cascade into other CNT dopants resulting in enhanced electrical conductivity retention.

5.6 Conclusion

Densification and chemical doping with KAuBr₄ of commercially available CNT wires successfully increases the electrical conductivity by ~6x and the current-carrying capacity by ~1.7x, compared to the as-received materials. Electrical conductivity retention as a function of increasing applied current was quantified via resting and working conductivity measurements taken at room temperature. KAuBr₄-doped samples were determined to have minimal changes in resting conductivity at current densities up to 32 MA/m², resulting in a CNT conductor with both improved conductivity and the ability to maintain this conductivity at high applied current densities. Thermal oxidation and doping studies were used to understand the exceptional electrical conductivity retention of the KAuBr₄-doped CNT wire materials and demonstrated that the electrical conductivity retention is a direct result of the thermal stability of KAuBr₄ and the decomposition cascade of KAuBr₄ into other thermally stable dopants.

6 Halogen Doped CNT Wires: Doping Efficacy, Electrical Performance Retention, and Dopant Degradation

This chapter summarizes the direct comparison of I₂, IBr, and KAuBr₄ doped CNT wires in regards to their electrical conductivity and electrical performance retention. The work concludes with the development of a dopant degradation mechanism derived from the findings of controlled thermal oxidation procedures coupled with elemental analysis via energy dispersive X-ray spectroscopy.

6.1 Abstract

A direct comparison of the doping efficacy, electrical performance retention, and dopant degradation are performed on commercially available CNT wires doped with I₂, IBr, and KAuBr₄. The chemical doping procedures result in a greater than 4X improvement in electrical conductivity, to $\sim 7-8 \times 10^5$ MS/m, with no statistically significant difference between the I₂, IBr, or KAuBr₄ dopants. The electrical performance retention as a function of current density is quantified via measuring the resting electrical conductivity after exposure to increasing applied current densities. The resting conductivity of the I₂ and IBr doped CNT wires decreases with increasing applied current densities, approaching the conductivity values of the as-received CNT material that have not been doped, while the KAuBr₄ doped CNT wires do not have a reduction in resting resistance until near failure and maintain a resting conductivity 3.8X greater than the as-received. The electrical performance retention as a function of current cycling is quantified via measuring the resting electrical conductivity after repeated exposure to specific applied current densities. With repeated cycling at 25% of its failure current density, KAuBr₄ was identified as the only dopant able to maintain its initial electrical conductivity for 24 one-hour cycles.

Elemental spatial analysis from energy dispersive X-ray spectroscopy, coupled with measuring the changes in electrical conductivity of doped samples thermally oxidized to various temperatures determined that the low thermal stability of I₂ and IBr causes these halogen doped CNT wires to undergo dopant desorption, while KAuBr₄ doped CNT wires result in KAuBr₄ degradation into other viable dopants. The thermal stability of KAuBr₄, along with its degradation cascade, allow for KAuBr₄ doped CNT wires to maintain their improved electrical conductivity during increasing applied currents and repeated low current cycles, while I₂ and IBr doped conductors are not stable. Thus, motivating the future adoption of stable KAuBr₄ doped CNT wires in a variety of space and power transmission applications.

6.2 Introduction

Carbon nanotube (CNT) conductors have emerged as a viable lightweight and strong alternative to traditional metal wires. Replacement of conventional metals in coaxial cables with CNTs produces coaxial cables with 80% less mass per length, allowing for greater payloads, reduced fuel consumption, and reduced transportation costs benefitting the next generation of space and defense technologies.⁴⁷ CNT wires are also advantageous compared to metal conductors due to their ability to withstand greater mechanical load, improved flexure tolerance, and corrosion resistance.^{46,59}

Chemical doping is used to improve the electrical conductivity of bulk CNT conductors by decreasing the junction resistance between CNTs and improving the charge transfer along CNTs.⁴⁹ Recent work compared the doping efficacy of 43 dopants and identified chlorosulfonic acid (CSA), iodine (I₂), iodine monobromide (IBr), and potassium tetrabromoaurate (KAuBr₄) as the superior dopants for increasing the electrical

conductivity of single-walled carbon nanotubes.¹⁶ Chlorosulfonic acid is commonly used in the processing of CNT wires and thin-films resulting in residual doping and a ~3X improvement in electrical conductivity.^{3,4,16,22,24} The first doped CNT wires to have specific electrical conductivity greater than copper used iodine vapor deposition.³⁴ Solution based IBr doping has been optimized to increase the electrical conductivity of CNT wires by approximately 8X,³² while aqueous KAuBr₄ doping coupled with densification has also demonstrated an order-of-magnitude improvement in electrical conductivity.^{43,49,60} While the improvements to the electrical conductivity of doped CNT wires is promising, the current carrying capacity and stability of these doped CNT conductors have been largely unexplored.

In air, CNT wire failure at high applied current densities is the result of Joule heating increasing the temperature of the CNT conductors until eventual thermal oxidation.⁴³ Therefore, improving the electrical conductivity of a CNT conductor should result in lower temperature at a given current, allowing for higher current densities prior to CNT wire failure. For doped CNT wires the degradation of the dopant must also be considered. If dopants are stable at elevated temperatures and current densities, they maintain the improved electrical conductivity of the CNT conductor as it is self-heated, and therefore reduce Joule heating and allow for higher current densities to be achieved prior to failure. However, it has been demonstrated that certain dopants like CSA exhibit a de-doping mechanism which manifests as an irreversible decrease in conductivity at current densities much lower (~40%) than the failure current density.⁴⁴ Thus at higher current densities, conductivity improvements are lost and the failure current density is not improved. In contrast, a similar study probing the degradation of KAuBr₄ doped CNT wires found

that the KAuBr_4 dopant degrades into other viable dopants (referred to as a dopant cascade) resulting in improved stability over a larger range of applied current densities.⁶⁰ Presently, there is no direct comparison between the emerging halogen and gold halide dopants regarding their stability during applied currents and their resulting usefulness for high current applications.

The present work directly analyzes the doping efficacy, electrical performance retention, and dopant degradation of IBr , KAuBr_4 , and I_2 doped CNT wires. Comparisons are made between the doping efficacy and resulting maximum current density before wire failure. Further analysis probes the electrical conductivity retention of the doped CNT wires as a function of increasing applied current densities and repeated low current cycling. Thermogravimetric analysis demonstrates the difference in thermal stability between the various doped CNT wires and indicates that changes after thermal oxidation to 200 and 400 °C are points of interest. Energy dispersive x-ray spectroscopy is used to analyze the elemental composition of the as-doped samples with and without thermal oxidation, allowing for the development of dopant degradation mechanisms. A discussion of the relationship between dopant thermal stability and the resulting effects on electrical performance retention provides a framework for selection of stable chemical dopants for high current applications.

6.3 Results and Discussions

CNT yarns purchased from Nanocomp Technologies Inc. (8-12 Tex, Lot # 60023) were evaluated as-received or doped with iodine vapor (I_2)¹⁶, iodine monobromide in hexanes (IBr)³², or aqueous potassium tetrabromoaurate (III) hydrate (KAuBr_4)⁶⁰. The I_2 vapor process started with a previously published doping procedure coupled with static

vacuum.^{16,52} After 15 minutes of dopant exposure the measured voltage across the CNT conductors reached a constant with surplus purple I₂ vapor still visible, indicating saturation had been reached. The chosen doping time was 30 minutes to ensure saturation. The IBr in hexanes procedure was the direct result of previously published work which optimized the concentration, time, and doping solvent for doping these CNT yarns with IBr.³² The KAuBr₄ procedure used was based on a previous optimization of KAuCl₄ doping of similar CNT materials.⁴⁶ Optimized conditions were used for all doping procedures to ensure saturation of the dopant adsorbed to the CNT wires.

The average diameter and standard deviation resulting from each CNT treatment is obtained from nine measurements taken from five randomly selected samples for each CNT treatment (see Figure 27). The average diameter of the as-received CNT wires was $152 \pm 24 \mu\text{m}$. For the I₂, IBr, and KAuBr₄ doped samples the average diameters were $146 \pm 20 \mu\text{m}$, $172 \pm 11 \mu\text{m}$, and $144 \pm 21 \mu\text{m}$, respectively. These values are all relatively similar except the IBr doped CNT samples exhibited some swelling as a result of exposure to IBr in hexanes. Based on previous work demonstrating the cylindrical nature of these CNT wires⁶⁰, the diameter was used to calculate the cross-sectional area. The cross-sectional area is used to determine the electrical conductivity and applied current densities for the CNT wire samples.

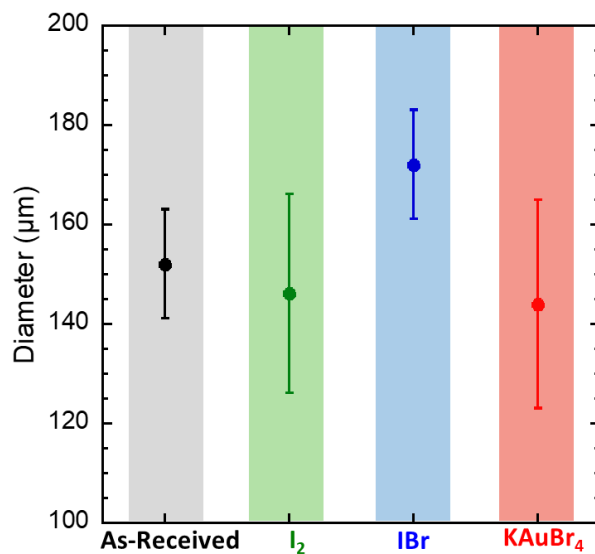


Figure 27: Diameter measurements of as-received and doped CNT wires.

The conductance measurements quantify the electrical conductance independent of diameter effects (see Figure 28a). The average room temperature conductance for 2.5 cm lengths of the as-received CNT wires was 127 ± 3 mS. The I₂, IBr, and KAuBr₄ doped samples had average room temperature conductances for 2.5 cm lengths of 487 ± 18 mS, 784 ± 46 mS, 506 ± 38 mS, respectively. The corresponding increase in conductance for the I₂, IBr, and KAuBr₄ doped CNT wires compared to the as-received were 3.8X, 6.2X, and 4.0X, respectively.

The electrical conductivity is calculated using the average cross-sectional area and resistance per length from each CNT treatment (see Figure 28b). The average room temperature electrical conductivity of the as-received CNT wires was $(1.7 \pm 0.4) \times 10^5$ S/m. The I₂, IBr, and KAuBr₄ doped samples had average room temperature electrical conductivities of $(7.3 \pm 1.4) \times 10^5$ S/m, $(8.4 \pm 0.9) \times 10^5$ S/m, and $(7.8 \pm 1.7) \times 10^5$ S/m, respectively. The corresponding increase in electrical conductivity for the I₂, IBr, and KAuBr₄ doped CNT wires compared to the as-received wires was a factor of 4.2, 4.8, and

4.4X, respectively. IBr doping results in the greatest increase in conductance, but swelling caused by exposure to IBr in hexanes results in room temperature electrical conductivity similar to that of the KAuBr_4 and I_2 doped CNT wires. Each dopant realizes similar electrical conductivities for the CNT wires, indicating that dopant saturation has been achieved and direct comparisons between the doped CNT wires can be made.

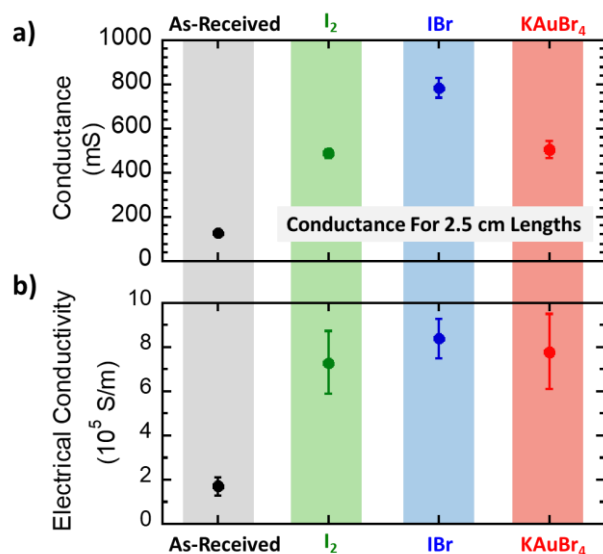


Figure 28: (a) Conductance for 2.5 cm CNT wire lengths and (b) electrical conductivity of as-received and doped CNT wires.

The room temperature current carrying capacity was quantified as the maximum current achieved prior to CNT wire failure. Wire failure is the result of Joule heating at greater applied currents, this heating continues until thermal oxidation occurs resulting in degradation of the wire and eventual breakage, as previously imaged for these CNT wires.⁶⁰ A representative current-voltage profile for one of the five samples from each of the CNT wire treatments is shown in Figure 29a. The as-received CNT wires have lesser electrical conductance than the doped CNT wires resulting in greater voltage at low applied currents compared to the doped CNT wires. The IBr and KAuBr_4 doped CNT wires have similar

current-voltage profiles; the slope of the KAuBr₄ doped CNT wires is greater than the IBr doped CNT wires due to the greater electrical conductance of the IBr doped CNT wires. The I₂ doped CNT wires have a similar current-voltage profile to the IBr and KAuBr₄ doped CNT wires until ~ 250 mA. At applied currents greater than 250 mA, the voltage of the I₂ doped CNT wires begins to increase and steadily approaches the voltage of the as-received CNT wires at similar applied currents. This increase in voltage is attributed to the de-doping of I₂ resulting in decreased conductance of the I₂ doped CNT wires, similar to the de-doping that has been observed for chlorosulfonic acid doped CNT wires.⁴⁴

The average current at failure of five samples for the as-received and doped CNT wires are presented in Figure 29b. The as-received CNT wires have an average current at failure of 358 ± 11 mA. The I₂, IBr, and KAuBr₄ doped samples had average current at failures of 348 ± 18 mA, 394 ± 17 mA, and 398 ± 16 mA, respectively. The average current at failure of the I₂ doped CNT wire samples was 3% less than that of the as-received CNT wires. The reduction in current at failure for the I₂ doped CNT wires is likely due to the intercalation of I₂ between the CNTs and its subsequent reversal during de-doping, which has been demonstrated to disturb the stacking of CNTs thus resulting in decreased electrical conductivity.⁴⁵ The corresponding increase in failure current for the IBr and KAuBr₄ doped CNT wires compared to the as-received were 10% and 11%, respectively. Improvements in failure current for IBr and KAuBr₄ doped CNT wires indicates that the dopant continues to reduce Joule heating at increasing applied currents allowing for the CNT wires to achieve greater currents at failure.

The failure current density normalizes the average current at failure to the cross-sectional area of each CNT sample, the results are displayed in Figure 29c. The as-received CNT

wires have an average failure current density of $20 \pm 4 \text{ MA/m}^2$. The I_2 , IBr, and KAuBr_4 doped samples had average failure current densities of $21 \pm 4 \text{ MA/m}^2$, $17 \pm 2 \text{ MA/m}^2$, $24 \pm 5 \text{ MA/m}^2$, respectively. There is no statistical difference between the failure current densities of the as-received and doped CNT wires.

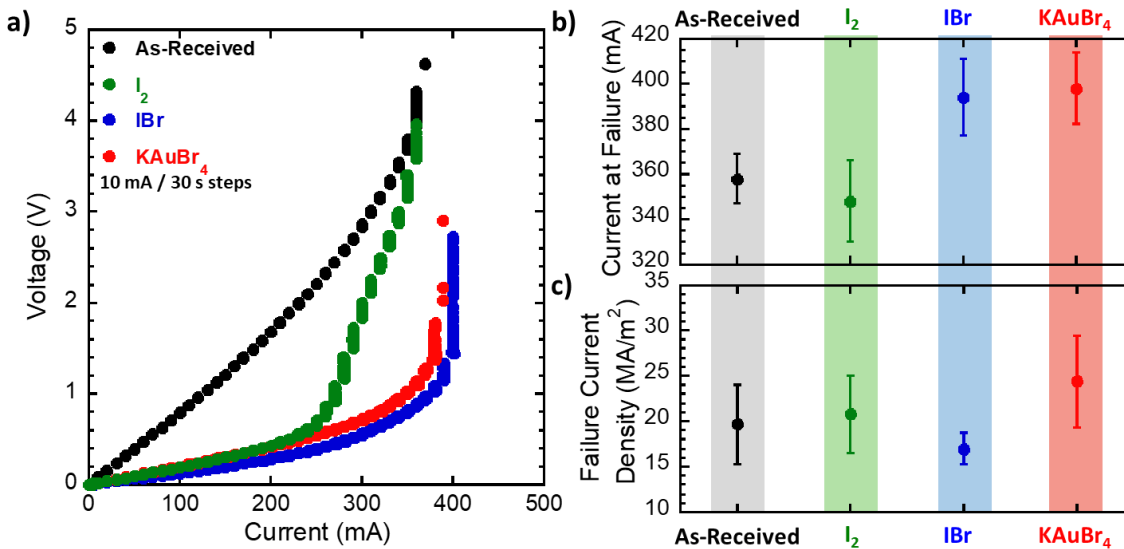


Figure 29: (a) The current-voltage profiles of as-received and doped CNT wires brought to failure using 10 mA, 30 s applied current steps. The average (b) current at failure and (c) failure current density of the as-received and doped CNT wires.

An increasing applied current procedure was used to determine the electrical performance retention as a function of applied current density, the resulting resting conductivities for the as-received and doped CNT wires are presented in Figure 30a. The as-received CNT wires exhibit no change in resting conductivity until $\sim 8 \text{ MA/m}^2$, followed by a linear decrease in resting conductivity until near failure, similar to previously reported electrical performance retention testing on these CNT wires.⁶⁰ The resting conductivities of the I_2 and IBr doped CNT wires decrease with increasing applied current densities, approaching similar values to the as-received CNT wires. The reduction in resting conductivity of I_2 and IBr doped CNT wires to near that of the CNT wires not exposed to chemical dopants

indicates that IBr and I₂ doping are not stable when Joule heating raises the temperature of the CNT wires. The KAuBr₄ doped CNT wires exhibit no changes in resting conductivity until ~ 18 MA/m² and at failure maintain a resting conductivity 3.8X greater than the as-received materials, indicating that improvements in electrical conductivity are retained despite Joule heating at greater applied current densities. Although IBr doped CNT wires have a greater initial conductivity than KAuBr₄ doped CNT wires, degradation of the IBr doped CNT wires results in KAuBr₄ doped CNT wires having a greater resting conductivity at current densities greater than 11 MA/m², indicating that KAuBr₄ doped CNTs are better suited for high current applications.

A constant current cycling procedure was used to determine the electrical performance retention as a function of repeated applied current; the resulting resting conductivities for the as-received and doped CNT wires are presented in Figure 30b. The applied current densities were 25% of the failure current density of the as-received, IBr, KAuBr₄, and I₂ doped CNT wires (5 MA/m², 4 MA/m², 6 MA/m², and 5 MA/m², respectively). The constant applied current density was selected to be 25% of the failure current density because it corresponds to an applied current less than the onset of degradation in electrical performance retention as a function of increasing applied current density for the as-received and doped CNT wires. The as-received and KAuBr₄ doped CNT wires exhibit no significant change in resting resistance over the full 24 cycles. During the 24 cycles, the resting conductivity of the IBr and I₂ doped CNT wires, compared to their initial conductivities, decreases by 30% and 38%, respectively. Although IBr doped CNT wires have a higher starting electrical conductivity than the KAuBr₄ doped CNT wires, the instability of the dopant results in IBr doped CNT wires having a lower electrical

conductivity within one hour of low current exposure. IBr and I₂ doped CNT wires are not stable over time when operating at 25% of their failure current densities, while KAuBr₄ doped CNT wires maintain the initial conductivity over time.

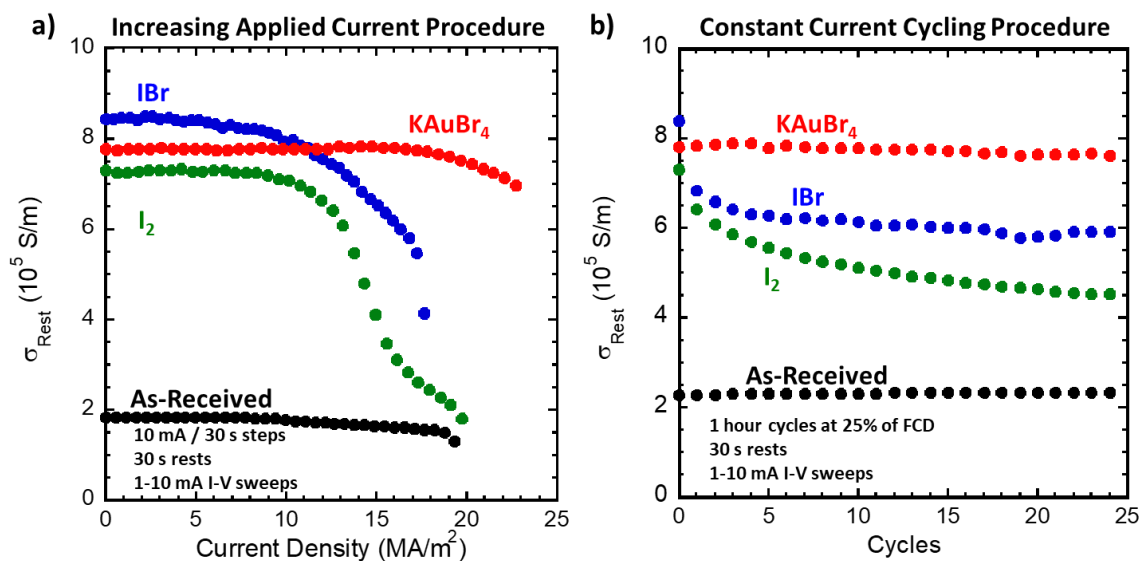


Figure 30: (a) The resting conductivity as a function of applied current density for the as-received and doped CNT wires. (b) The resting conductivity as a function of cycles performed at 25% of the failure current density for the as-received and doped CNT wires.

Thermogravimetric analysis (TGA) for each of the as-received and doped CNT wires compared to the pure doping solids provides information about the thermal stability of the dopants and how that stability differs when adsorbed to the CNT wires. The normalized derivative weight percent as a function of temperature for the as-received and doped CNT wires along with the pure doping solids are presented in Figure 31a. The weight percents as a function of temperature are presented in Figure 31b. The peak temperature of the I₂ doping solids is at 128 °C while the I₂ doped CNT wires see a wider degradation peak at 114 °C. The peak temperature of the IBr doping solids is at 111 °C while the IBr doped CNT wires sees a wider degradation peak at 123 °C. Prior to 400 °C, the KAuBr₄ solids exhibit an initial peak at 237 °C followed by a more substantial peak at 304 °C, whereas

the KAuBr_4 doped CNT wires show two wider less intense peaks at 192 °C and 334 °C. 200 °C and 400 °C were determined to be points of interest where the effects after dopant desorption could be analyzed.

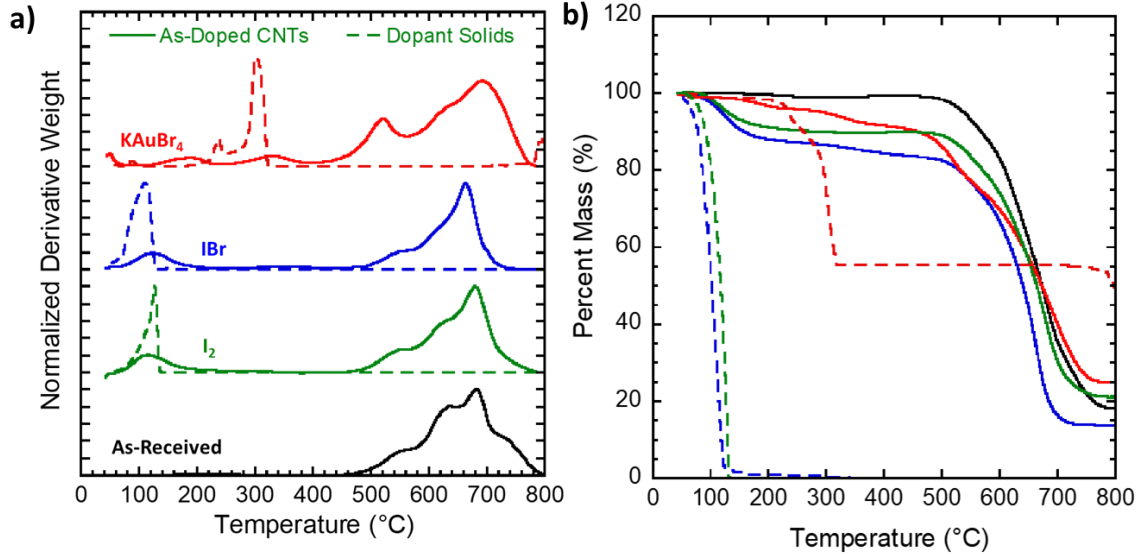


Figure 31: (a) Normalized derivative weight as a function of increasing temperature of the as-received and doped CNT wires and the pure doping solids. (b) Thermogravimetric analysis of as-received and doped CNT wires along with the pure doping solids.

As-received and doped samples were treated with 200 and 400 °C thermal oxidations conducted in a tube furnace with similar conditions to that of the TGA. The average electrical conductivity of the five as-received CNT wires was $(1.7 \pm 0.4) \times 10^5$ S/m; there was no significant change after a 200 °C thermal oxidation and a reduction to $(1.4 \pm 0.2) \times 10^5$ S/m after a 400 °C thermal oxidation, corresponding to an 18% reduction in electrical conductivity. The electrical conductivity of the I_2 doped CNT wires decreased from $(7.2 \pm 1.4) \times 10^5$ S/m to $(2.7 \pm 0.4) \times 10^5$ S/m after a 200 °C thermal oxidation and $(1.7 \pm 0.2) \times 10^5$ S/m after a 400 °C thermal oxidation, corresponding to reductions in electrical conductivity of 62% and 76%, respectively. The I_2 doped CNT wires after thermal oxidation to 400 °C exhibit no improvement in electrical conductivity compared to the as-

received CNT wires indicating that there is no longer any benefit of doping present. The electrical conductivity of the IBr doped CNT wires reduced from $(8.4 \pm 0.9) \times 10^5$ MS/m to $(5.7 \pm 0.6) \times 10^5$ S/m after a 200 °C thermal oxidation and $(2.3 \pm 0.2) \times 10^5$ S/m after a 400 °C thermal oxidation, corresponding to reductions in electrical conductivity of 32% and 73%, respectively. The electrical conductivity of the KAuBr₄ doped CNT wires reduced from $(7.7 \pm 1.7) \times 10^5$ S/m to $(7.0 \pm 0.9) \times 10^5$ S/m after a 200 °C thermal oxidation and $(3.8 \pm 0.4) \times 10^5$ S/m after a 400 °C thermal oxidation, corresponding to reductions in electrical conductivity of 11% and 51%, respectively. The IBr and KAuBr₄ doped CNT wires thermally oxidized to 400 °C maintain electrical conductivities 1.3X and 2.2X, respectively, greater than the as-received CNT wires, indicating that there is still residual dopant remaining resulting in improved electrical conductivity.

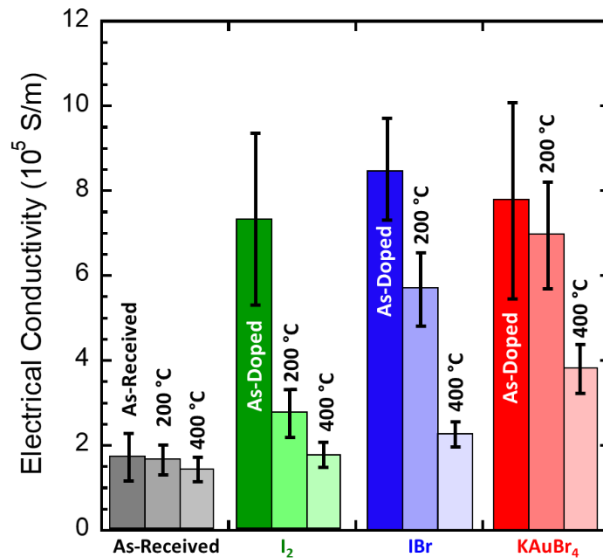


Figure 32: The average room temperature electrical conductivity of as-received and doped CNT wires with and without thermal oxidations to 200 and 400 °C calculated by 5 samples per treatment.

Energy dispersive X-ray (EDX) spectroscopy was used to analyze the elemental composition of as-received and doped CNT wires with and without thermal oxidations to

200 °C and 400 °C; the weight percent analysis is presented in Table 3. The scanning electron microscopy (SEM) images and elemental spatial analysis of the doped CNT wires and their corresponding dopants are presented in Figure 33-35. The as-received CNT wires show no significant change in carbon, iron, or oxygen content as a result of thermal oxidation to 200 °C or 400 °C, which is consistent with the TGA results that show no degradation in the as-received CNT wires prior to 400 °C. The I₂ doped CNT wires exhibit near total removal of iodine with thermal oxidation to 400 °C which corresponds to the 400 °C thermally oxidized I₂ doped CNTs having no improvement in electrical conductivity compared to the as-received CNTs. Analysis of the as-doped IBr doped CNT wires indicates that the samples contain equal weight percents of iodine and bromine. Considering that iodine weighs approximately 80% more than bromine, equal weight percentages indicate that there is preferential adsorption of bromine to the CNTs compared to iodine. Thermal oxidation to 200 °C and 400 °C causes desorption of iodine and bromine resulting in partially IBr doped CNT samples with bromine remaining preferentially adsorbed to the CNTs compared to iodine. This preferential adsorption of bromine is attributed to its greater electronegativity compared to iodine. The KAuBr₄ doped CNT wires exhibit a slight decrease in bromine during thermal oxidation to 200 °C and further removal of bromine with thermal oxidation to 400 °C. The reduction in bromine is similar to that of previous work indicating the decomposition of AuBr₃ to AuBr at temperatures ~300 °C.^{55,60} Thermal oxidation to 400 °C also results in accumulation of gold particles at the surface seen in the elemental spatial analysis in Figure 35. The improved electrical conductivity of KAuBr₄ doped CNT wires after thermal oxidation to 400 °C is attributed

to the gold nanoparticles, which provides for improved nanoscale transport,⁵³ and trace bromine remaining.

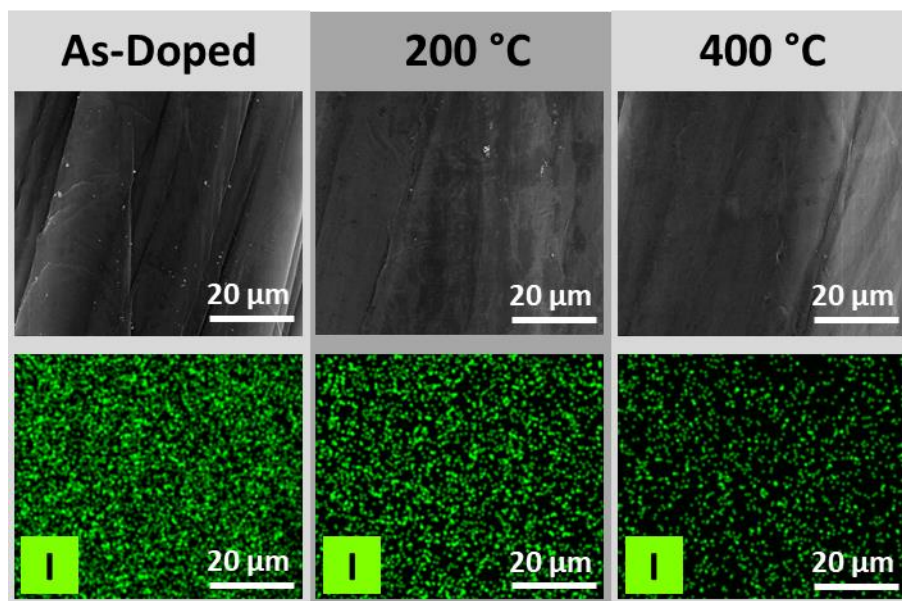


Figure 33: SEM images of the as-doped and thermally oxidized I₂ doped CNT wires along with the iodine elemental analysis from EDX spectroscopy.

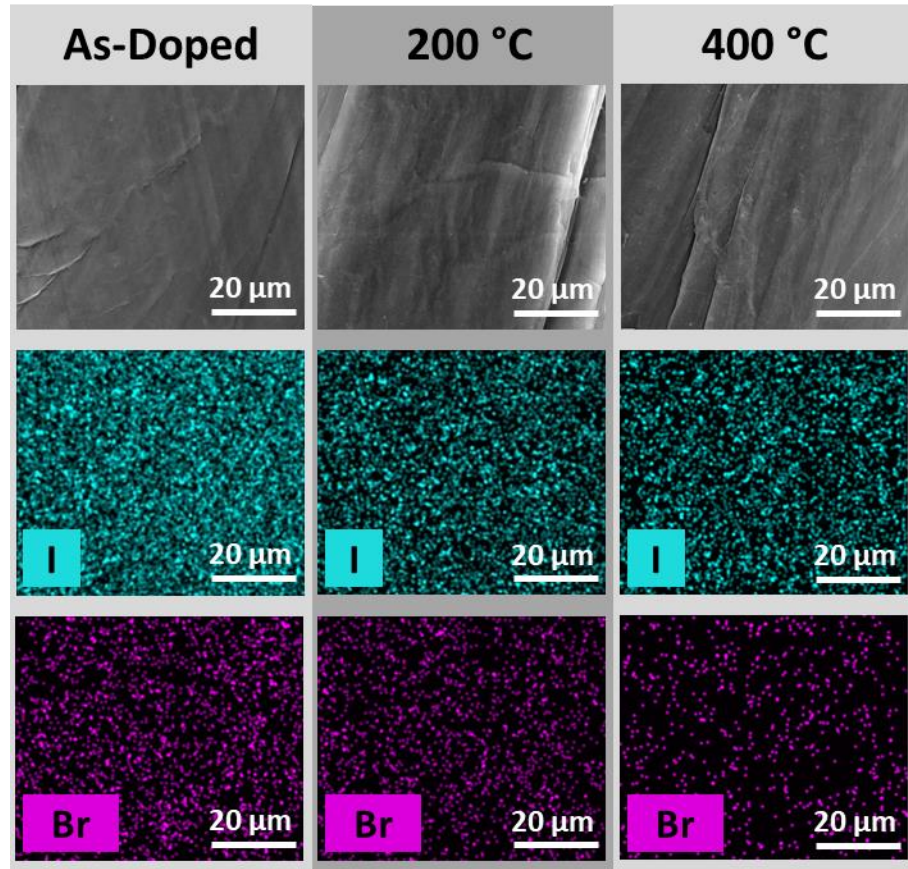


Figure 34: SEM images of the as-doped and thermally oxidized IBr doped CNT wires along with the iodine and bromine elemental analysis from EDX spectroscopy.

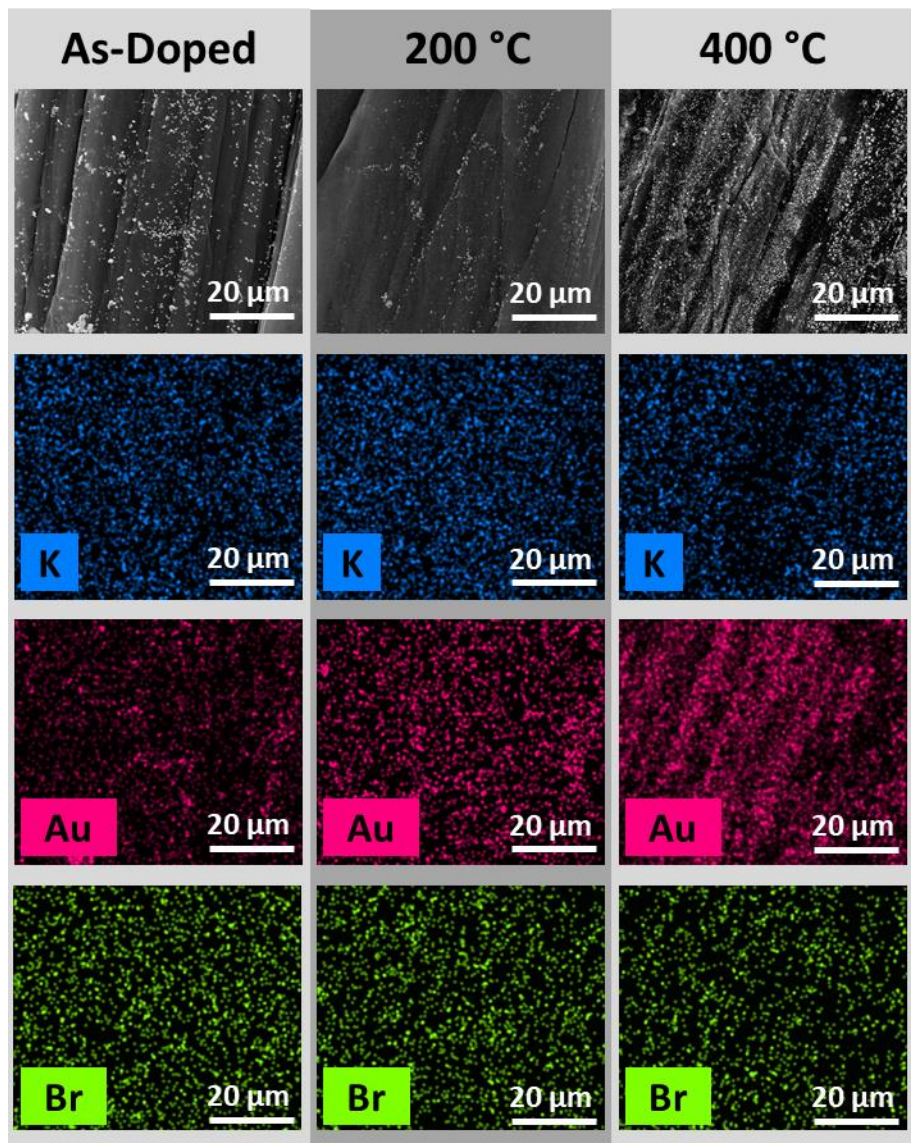


Figure 35: SEM images of the as-doped and thermally oxidized KAuBr_4 doped CNT wires along with the potassium, gold, and bromine elemental analysis from EDX spectroscopy.

Table 3: Weight percent composition based on energy dispersive X-ray spectroscopy of the as-received and doped CNT wires with and without 200 and 400 °C thermal oxidations.

	As-Received CNTs (Weight %)			I ₂ Doped CNTs (Weight %)			IBr Doped CNTs (Weight %)			KAuBr ₄ Doped CNTs (Weight %)		
		200 °C	400 °C		200 °C	400 °C		200 °C	400 °C		200 °C	400 °C
C	69	66	67	60	59	50	35	53	52	47	50	27
Fe	28	32	29	26	36	48	17	20	33	12	16	9
O	3	2	4	1	1	1	0	1	0	2	0	1
K	--	--	--	--	--	--	--	--	--	1	1	1
Au	--	--	--	--	--	--	--	--	--	19	17	60
Br	--	--	--	--	--	--	24	18	8	19	16	2
I	--	--	--	13	4	1	24	8	7	--	--	--

The amounts of remaining halogen present after thermal oxidations to 200 and 400 °C were directly compared to the electrical conductivity retention in Figure 36. Assuming for a 1 mg sample, the mass of halogen per sample was normalized to the mass of iron content for each sample. Iron is used as an internal standard due to its strong and consistent signal that is not affected by thermal oxidations. The mass percents of halogen remaining after the 200 and 400 °C thermal oxidations were compared to that of the as-doped CNT samples. The electrical conductivity retention was considered as the percent of electrical conductivity remaining compared to the as-doped CNT wires and the thermally oxidized as-received CNT wires. For the I₂ doped CNT wires there was a direct correlation between the amount of remaining iodine and the conductivity retention after both the 200 and 400 °C thermal oxidations. For IBr doped CNT wires the analysis was performed relating conductivity retention to the mass percent remaining of iodine and total halogen content, presented in Figure 37. The electrical conductivity retention did not directly correlate with the remaining mass percents of iodine or total halogens present in the IBr doped CNT wires. The conductivity retention did directly correlate to the mass percent of bromine

remaining in the thermally oxidized samples, indicating that when iodine and bromine are adsorbed, it is bromine content that directly affects electrical conductivity. The KAuBr_4 doped CNT wires have greater conductivity retention compared to the percent bromine remaining after both thermal oxidations to 200 °C and 400 °C; this is attributed to the presence of Au nanoparticles (observed in Figure 35) providing additional improvements in electrical conductivity,⁵³ in addition to the remaining bromine.

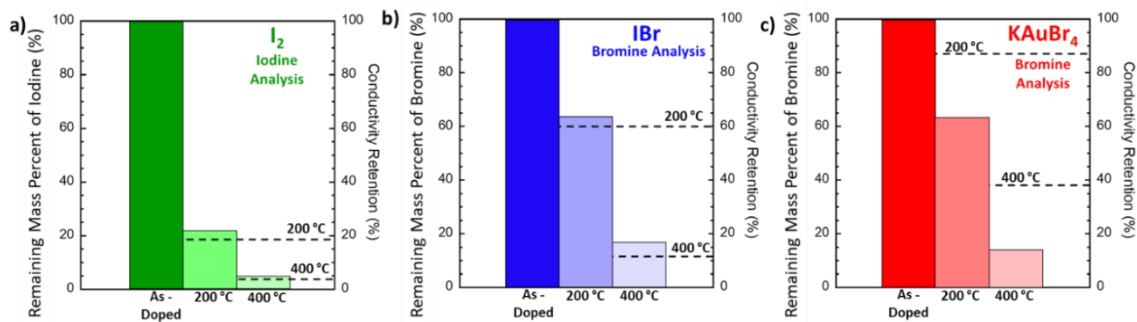


Figure 36: The mass percentage of halogen remaining compared to the conductivity retention of the (a) I_2 , (b) IBr , and (c) KAuBr_4 , doped CNT wires with and without thermal oxidation to 200 and 400 °C.

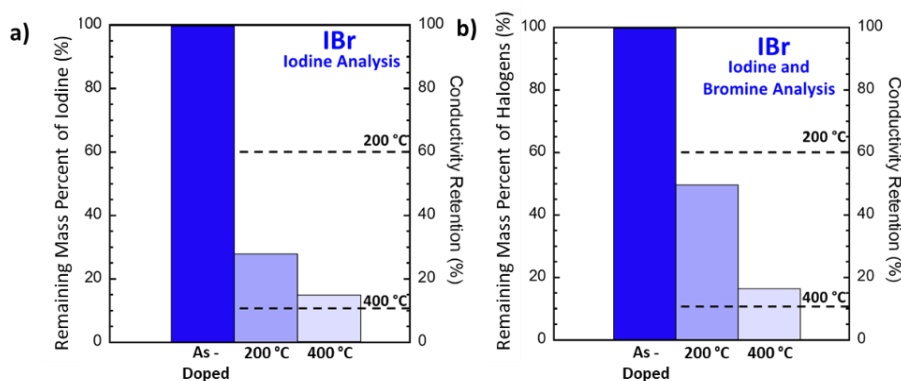


Figure 37: The remaining mass percent of (a) iodine and (b) iodine and bromine present compared to the electrical conductivity retention for the IBr doped CNT wires with and without thermal oxidation to 200 and 400 °C.

A direct relationship can be made between the dopant degradation mechanism and the resulting electrical performance retention. Figure 38 shows qualitatively how the

desorption of halogens and decomposition of KAuBr_4 from CNT wires at increasing temperatures results in changes in the electrical conductivity. The I_2 and IBr dopants desorb from the CNT wires resulting in decreasing dopant content with increased temperature, which directly relates to the electrical conductivity of the halogen doped CNT wires. The desorption of the halogens results in the electrical conductivity approaching that of the as-received materials which have not been doped. Based on the TGA spectra and previous work performed with gold halide dopants, KAuBr_4 decomposes into AuBr_3 and AuBr , which are also viable dopants.^{16,54,55,60} Based on the TGA spectra the decomposition of KAuBr_4 occurs at 192 °C and 334 °C and releases bromine leaving the gold particles and trace bromine that continue to improve the electrical conductivity.⁵³ KAuBr_4 doping of CNT wires has demonstrated that high thermal stability dopants or those capable of degrading into other viable dopants are advantageous for high current CNT applications due to their electrical performance retention.

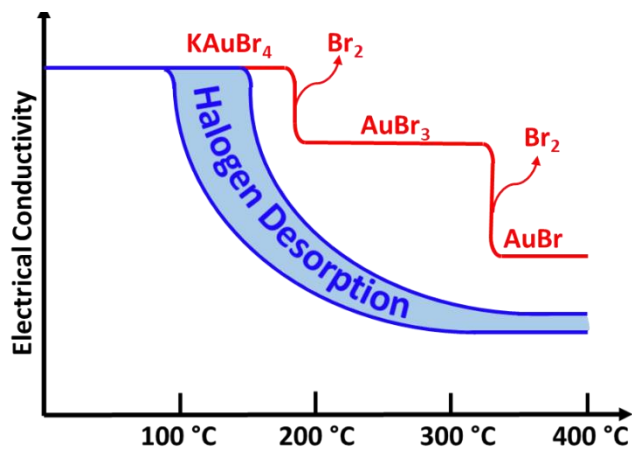


Figure 38: Representative graph relating temperature and electrical conductivity of halogen and KAuBr_4 doped CNT wires demonstrating the relationship between dopant degradation and electrical conductivity.

6.4 Experimental Section

Doping Procedures

CNT yarns were purchased from Nanocomp Technologies Inc. (8-12 Tex, Lot # 60023). The IBr doped CNT samples were soaked in a 20.7 g/L solution of IBr in hexanes for 1 hour based on the previous work performed by the research group.³² The KAuBr₄ doped CNT samples were doped for 1 hour in 5 mM KAuBr₄ aqueous solution, then dried in a vacuum oven for 1 hour at 100 °C.^{46,60} The iodine vapor doping was performed on three CNT wire segments with lengths of 12 cm for 30 minutes under static vacuum of ~300 mbar with 50 mg of I₂ solids using a 100 °C mantle temperature.^{16,52}

Diameter, Electrical Conductivity, and Current Carrying Capacity Measurements

Five CNT wire segments with lengths of 6 cm were randomly sampled from each of the treatments. An AmScope optical microscope was used to collect nine diameter measurements along the length of each sample segment.

Resistance per length measurements were collected at room temperature using a National Instruments NI PXI-5652 source/measure unit and an NI PXI-4071 digital multimeter with a four-point probe configuration for five samples from each treatment.

An Arbin BT-2000 power supply was used to measure the failure current density of 5 samples per treatment by applying current in increasing 10 mA steps held for 30 s each until ultimate wire failure in air. The failure current density Arbin testing utilized a four-terminal configuration with <1 cm between source and sense probes and 2.5 cm between the voltage sensing probes.

Electrical Performance Retention - Increasing Applied Current Procedure

An increasing applied current procedure was used to determine the electrical performance retention as a function of applied current density. The procedure starts with an initial 1-10 mA current-voltage sweep used to determine the initial conductivity (σ_0). The procedure then repeats a sequence of three steps: 1) a 30 s current “on” step which increases each cycle by 10 mA until ultimate wire failure, 2) a rest step which allows the CNT wire to cool to room temperature, and 3) a 1-10 mA current-voltage sweep used to determine the resting conductivity (σ_{Rest}) as a function of the previously applied current density.⁶⁰

Electrical Performance Retention – Constant Current Cycling Procedure

A constant current cycling procedure was used to determine the electrical performance retention as a function of low-current cycles. The procedure starts with an initial 1-10 mA current-voltage sweep used to determine the initial conductivity (σ_0). The procedure then repeats a sequence of three steps: 1) a 1 h current “on” step at an applied current density equivalent to 25% of the failure current density specific to the CNT treatment, 2) a rest step which allows the CNT wire to cool to room temperature, and 3) a 1-10 mA current-voltage sweep used to determine the resting conductivity (σ_{Rest}) as a function of cycle number.⁶⁰

Thermogravimetric Analysis, Thermal Oxidation Procedures, and Energy Dispersive X-ray Spectroscopy

Thermogravimetric analysis (TGA) (TA Instruments TGA Q5000; balance purge: N₂(g) 20 mL/min; sample purge: air 20 mL/min; ramp rate: 10 °C/min) was performed on the as-received and doped CNT wire samples as well as the as-received pure doping solids.

The thermal oxidation treatments of the as-received and doped CNT wires used a tube furnace with 5 SCFH of flowing air with a ramp rate of 10 °C/min to 200 or 400 °C.

A Tescan Mira3 SEM equipped with a Bruker Quantax energy-dispersive X-ray (EDX) spectrometer was used to determine the elemental composition of the as-received and doped CNT samples with and without the varying thermal oxidation procedures.

6.5 Conclusions

The resulting electrical properties of commercially available CNT wires doped with I₂, IBr, and KAuBr₄ were directly compared. Saturation of the CNT wires with each dopant resulted in electrical conductivities ~4X greater than that of the as-received CNTs. Electrical performance retention studies demonstrated that the KAuBr₄ doped CNT wires can maintain resting conductivity until near wire failure, while the I₂ and IBr doped CNT wires exhibit degradation of the electrical conductivity to values approaching that of the as-received CNT materials. With repeated low current cycling, KAuBr₄ was identified as the only dopant able to maintain its initial electrical conductivity over time. Thermal stability analysis determined that I₂ and IBr doped CNT wires undergo dopant desorption, while KAuBr₄ doped CNT wires result in dopant degradation into other viable dopants, thus maintaining improved electrical conductivity over greater applied current densities. KAuBr₄ doped CNT wires have emerged as lightweight conductors capable of retaining their improved electrical properties during long-term, high current applications. Thus, motivating the future adoption of stable KAuBr₄ doped CNT wires in a variety of space and defense technologies.

7 Additional Considerations

The present work has focused on chemical doping of commercially scaled CNT wires available in kilometer lengths as these materials are better suited for immediate production and adoption in applications requiring low weight and high strength. In order to

demonstrate the possibilities of these chemical dopants to produce high electrical conductivity CNT wires, this chapter begins with applying the previously determined doping procedures to in-house extruded CNT wires and commercially available CNT wires from DexMat, with starting conductivities of ~ 2 and 6 MS/m, respectively. Recent work has demonstrated that current-induced heating of the CNT wires during deposition of copper produces favorable results,⁵² so similar hot filament deposition of iodine was performed to explore if improved vapor deposition could be achieved. Beyond demonstrating improvements in electrical conductivity, further work was performed to quantify the effect doping conditions have on electrical performance retention. The electrical conductivity, failure current density and electrical performance retention as a function of increasing applied current was compared for IBr and KAuBr_4 doped CNT wires exposed to their doping solutions for 1 or 3 hours. This body of work demonstrates the upper electrical conductivity possibilities of these dopants and further explores the relationship between the dopants and their electrical performance retention.

During the continuous current cycling tests performed on the as-received CNT wires, low current application (25% of the failure current density) occasionally resulted in improvements in the resting conductivity. 25% of the failure current density corresponds to just below the onset of material degradation observed during the electrical performance retention as a function of increasing applied current tests. Over the course of 15 days of low current exposure the as-received CNT wires would exhibit a $\sim 45\%$ increase in electrical conductivity. Further testing determined that this improvement only occurs in ambient air environments and not in dry, inert environments. This was the first demonstration of low current application resulting in ambient doping of CNTs.

The electrical performance retention was not previously related to the temperature of the CNT wires due to their small diameter (150 μm) preventing accurate temperature measurements. In order to relate the changes in electrical performance retention with the temperature of the conductors, large diameter CNT wires were prepared from densified CNT sheet materials, allowing for direct measurement of temperature during increasing applied current testing. This work found that the changes in the working resistance of the conductors are directly related to the temperature during operation. Further elucidating the degradation of these CNT conductors at increasing applied currents via relating the degradation to the temperature of the conductor.

Forced cooling via the use of a fan has previously been demonstrated to increase the failure current density of CNT conductors, in order to expand upon this work, CNT wires were exposed to cooled baths of propylene glycol. This work demonstrates how convective cooling in 0 $^{\circ}\text{C}$ environments can allow for improvements in current density at failure by factors of 13x. Understanding how cooled environments improve the current carrying capacity of CNT conductors demonstrates that usefulness of CNT conductors in cooled marine and space applications.

Lastly this chapter considers the power dissipated by various CNT wires compared to copper. The power dissipated is the I^2R loss of energy via heat and is related to the inefficiency of the materials as a conductor. This analysis provides an understanding of which CNT materials dissipate the least power and allows for comparisons between various doped and undoped CNT wires.

The goal of this chapter is to expand upon the ability of the dopants to improve electrical conductivity, further probe electrical performance retention, consider the effects of various

environments on electrical performance, and compare the power dissipated by these CNT conductors. Record breaking electrical conductivity and current carrying capacity will be discussed and electrical performance retention is related to doping conditions and to the resulting temperature caused by increasing applied current exposure. This chapter will provide insights into a variety of not previously discussed factors that affect the practical operation of CNT conductors.

7.1 Chemical Doping of Extruded CNT Wires

In-house extruded CNT wires were chemically doped with I_2 , $KAuBr_4$, and IBr to demonstrate the ability to improve the electrical conductivity of CSA doped CNT wires. The wires used were produced via co-axial extrusion from a SWCNT/CSA dispersion (22/12 Gauge, Outer flow rate = 7,000 mL/hr) and contain excess CSA. The $KAuBr_4$ doping procedure involved soaking the wires in 5 mM aqueous $KAuBr_4$ solution for 1 hour then drying in a vacuum oven at 100 °C for 1 hour to remove excess moisture. I_2 doping was performed by exposing CNT wires for 30 minutes to 50 mg of I_2 under static vacuum with a mantle temperature of 100 °C. The IBr doping procedure involved soaking the wire in 20.7 g/L IBr in hexanes for 1 hour. These conditions were based on current best practices to serve as an initial survey of chemically doping extruded CNT wires. The resistance per length measurements are presented in Figure 39. The resistance per length was used to analyze the doping efficacy independent of possible changes in diameter due to solvent effects.

I_2 and IBr doping resulted in 10 and 30% reductions in resistance per length, respectively. The aqueous $KAuBr_4$ doping resulted in an increase in resistance per length of 24%. The extruded wires contain residual CSA which chemically dopes the CNT wires. This increase

in resistance is likely the unfavorable degradation of CSA due to the use of aqueous solvent. After 10 days of exposure to ambient conditions, the resistance of the CNT wire increased by ~12% due to the instability of CSA-doping. This wire was then doped with 5 mM KAuBr_4 dissolved in methanol resulting in a decrease in resistance of ~ 7%. This study demonstrates that the solvent used for doping CSA-extruded CNT conductors must be compatible with CSA or will have an overall negative impact on electrical properties. KAuBr_4 doping of CSA extruded wires requires the use of an organic solvent.

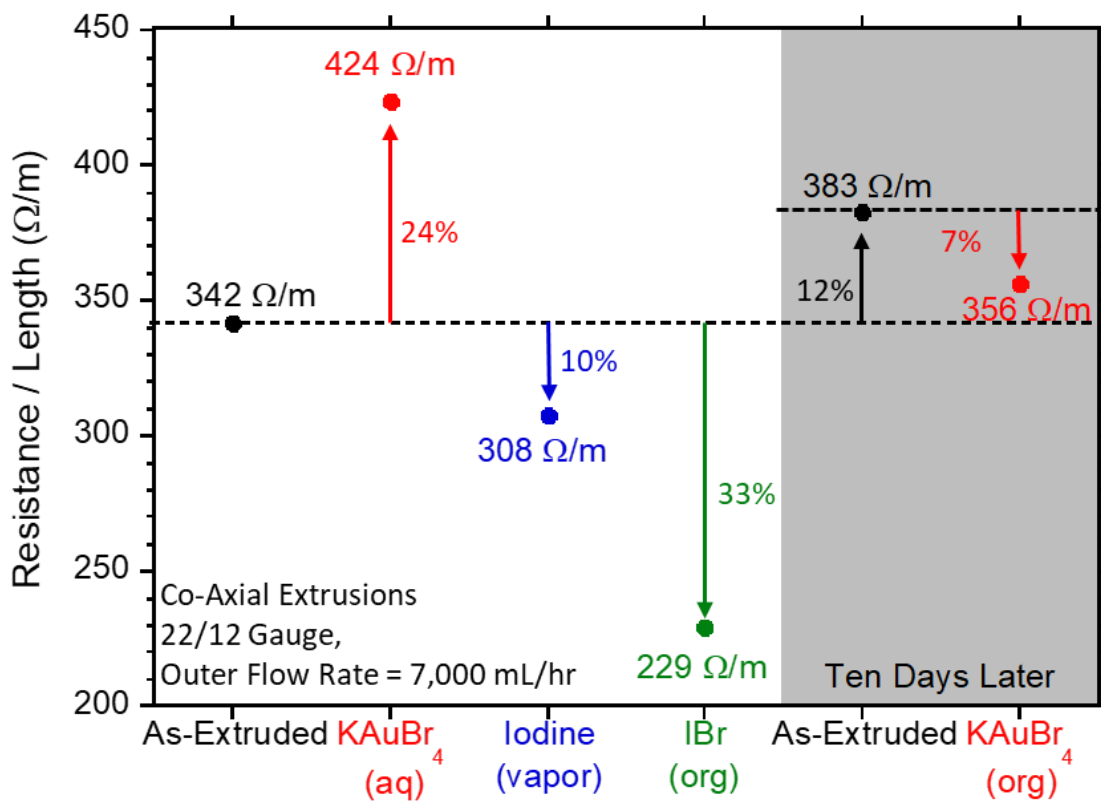


Figure 39: Resistance per length measurements of an extruded wire doped with KAuBr_4 , I_2 , and IBr . After 10 days of storage in ambient conditions, the resistance per length of the as-extruded wire was measured again and then doped with KAuBr_4 in organic solution.

7.2 Chemical Doping of DexMat CNT Wires

Recently high-quality CNT wires and ribbons have become commercially available via DexMat, a start-up company from Rice University. The 20 μm CNT wire has a resistance per length of 392 Ω/m corresponding to an electrical conductivity of $\sim 6 \text{ MS}/\text{m}$, while the 3-ply CNT wire has a resistance per length of 18.6 Ω/m corresponding to an electrical conductivity of $\sim 2 \text{ MS}/\text{m}$. SEM images are presented in Figure 40.

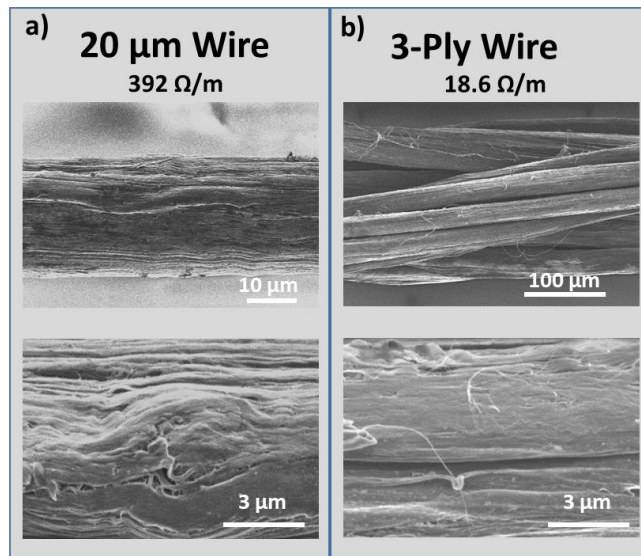


Figure 40: Scanning electron microscope images of (a) 20 μm DexMat wire and (b) 3-ply DexMat wire.

The as-received 20 μm DexMat wires were exposed to either a vacuum environment or IBr doping solution in order to determine the stability of the CNT material and its ability to be doped, the resulting effects on resistance per length as a function of time are presented in Figure 41. DexMat claims that the CNT wire has been purified of CSA which is used during the manufacturing of the material. Exposure to a 100 $^{\circ}\text{C}$ vacuum oven for 1 hour results in a 25% increase in resistance per length. 11 days after vacuum exposure the initial resistance per length is not recovered, indicating that a dopant has been desorbed from the DexMat

material. The 20 μm DexMat CNT wires were also exposed to 20.7 g/L IBr in hexanes for 1 hour resulting in a resistance per length of 209 Ω/m , corresponding to a maximum electrical conductivity of ~ 12 MS/m, greater than the literature values for doped CNT conductors. 11 days of ambient exposure result in an $\sim 30\%$ increase in resistance per length.

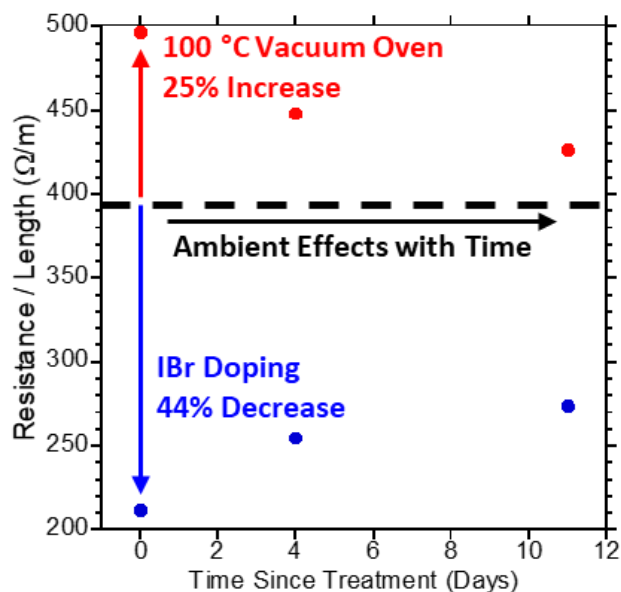


Figure 41: Resistance per length of 20 μm DexMat CNT wire after exposure to a vacuum oven or IBr doping solution and the resulting change as a function of time.

7.3 Chemical Doping of Commercial CNT Wires with I_2 Vapor

An analysis on the effect of heating the 10 tex NCTI CNT wires during I_2 vapor deposition was performed to determine if improved doping could be achieved. The CNT wires were exposed to 50 mg of I_2 under static vacuum for 30 minutes with a mantle temperature of 100 $^\circ\text{C}$. The CNT wire was either at room temperature or Joule heated by an applied current load of 200 mA. A control was exposed to the 200 mA applied current load under static vacuum without the presence of I_2 in order to understand the effects of Joule heating without I_2 doping. The results presented in

Table 4 were compared to the starting CNT wires and KAuBr₄-doped CNT wires. The results show no significant change in chemical doping with heating of the CNT wire during I₂ doping. The CNT wires doped with I₂ have a ~78% reduction in resistance per length compared to the as-received material, the reduction in resistance per length is similar to the KAuBr₄ doped CNT wires. The resistance per length of the control sample increased most likely due to degradation caused by Joule heating. Cool filament I₂ vapor doping for 30 minutes is sufficient to produce I₂ doped CNT wires with electrical conductivities comparable to the standard KAuBr₄ doped CNT wires.

Table 4: Resistance per length measurements of NCTI CNT wires exposed to I₂ vapor with and without Joule heating the CNT wires.

Samples	Current (mA)	Iodine Present	Resistance / Length (Ω/m)
As-Received	---	---	315
Control	200	No	344
Hot Filament	200	Yes	74
Cold Filament	0	Yes	67
KAuBr ₄	---	---	73

7.4 Stability as a Function of Doping Conditions

10 tex CNT wires were doped with IBr and KAuBr₄ for varying lengths of time in order to determine the effects doping conditions have on the electrical properties and electrical performance retention. The IBr doped CNT samples were exposed to 20.7 g/L IBr in hexanes for 1 or 3 hours. The KAuBr₄ doped CNT samples were doped in 5 mM aqueous KAuBr₄ for 1 or 3 hours then dried in a vacuum oven for 1 hour. 5 samples for each treatment were used to determine the average electrical conductivity and failure current density. The electrical conductivities are presented in Figure 42. The improvement in electrical conductivity of the IBr and KAuBr₄ doped CNT wires, independent of doping

time, were statistically similar and resulting in a greater than 4x improvement compared to the as-received CNT wires.

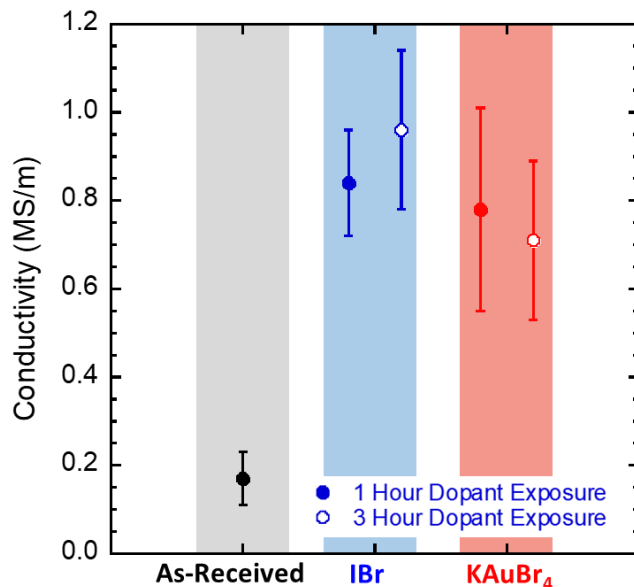


Figure 42: The average room temperature electrical conductivity for as-received, IBr, and KAuBr₄ doped CNT wires. The doped CNT wires were exposed to the doping solutions for 1 or 3 hours.

The failure current density of the as-received and doped CNT wires was measured using an Arbin BT-2000 which applied increasing 10 mA steps held for 30 seconds until ultimate wire failure in air. The current-voltage profiles presented in Figure 43a demonstrate the increased electrical conductivities of the doped CNT samples resulting in the ability to maintain lower voltages at equivalent applied current densities. The average failure current densities are presented in Figure 43b. There is no statistical difference in failure current density for the as-received and doped CNT wire samples.

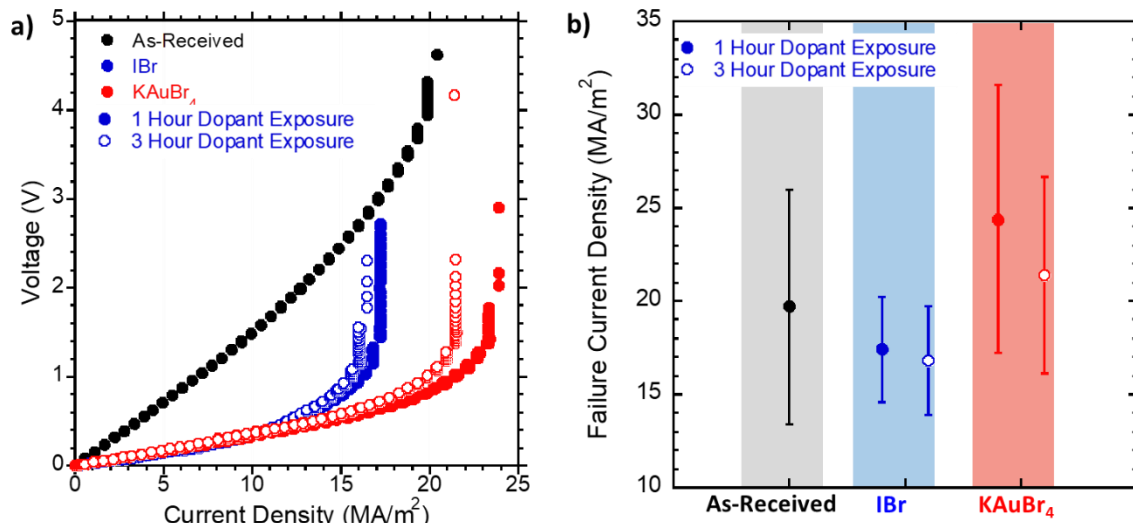


Figure 43: (a) The current-voltage profiles of as-received, IBr, and KAuBr₄ doped CNT wires during increasing 10 mA current steps held for 30 seconds until ultimate wire failure. The doped CNT wires were exposed to the doping solutions of 1 or 3 hours. (b) The resulting failure current densities for the as-received and doped CNT wires.

Electrical performance retention as a function of increasing applied current density was used to determine the resting conductivity of the as-received, IBr, and KAuBr₄ doped CNT wires, the results are presented in Figure 44. The IBr sample doped for 3 hours has rapidly decreasing resting conductivity at low current densities, this is likely due to lesser stability of the additionally adsorbed IBr, compared to the 1 hour doped IBr samples. The KAuBr₄ doped samples have similar changes in resting conductivity independent of the duration of chemical doping. KAuBr₄ doped CNTs are more stable with increasing applied current density.

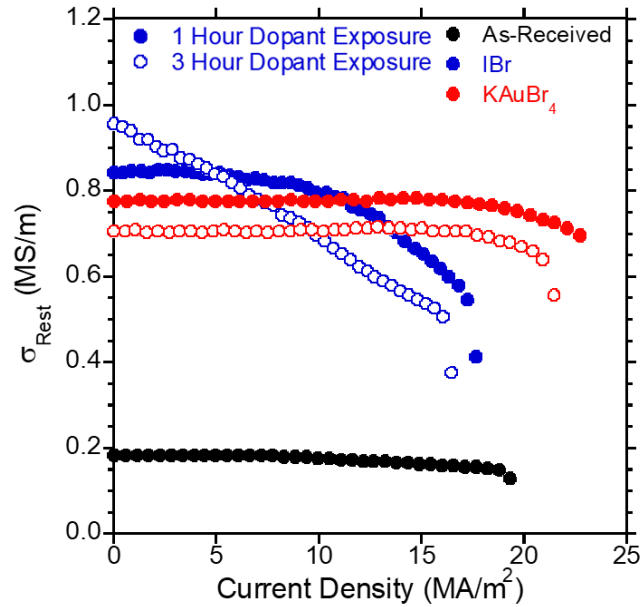


Figure 44: Resting conductivity as a function of increasing applied current density for as-received, IBr, and KAuBr₄ doped CNT wires. The doped CNT wires were exposed to the doping solutions for 1 or 3 hours.

7.5 Low Current Stability: Ambient Doping

Electrical performance retention as a function of constant applied current cycling was performed on as-received 10 tex CNT wires. The applied current “on” steps corresponded to 25, 50, and 75% of the failure current density of the CNT wires. The current and voltage profiles are presented in Figure 45. The voltage profile of the CNT wire exposed to 25% of the failure current density decreases throughout the 24 hours of applied current. The voltage profile of the CNT wire exposed to 50% of the failure current density initially increases then begins to plateau throughout the 24 hours of applied current. The voltage profile of the CNT wire exposed to 75% of the failure current density continues to increase throughout the 24 hours of applied current. The voltage profiles trends correspond to the working conductivity of the as-received CNT wires as they are measured during the “on” current steps.

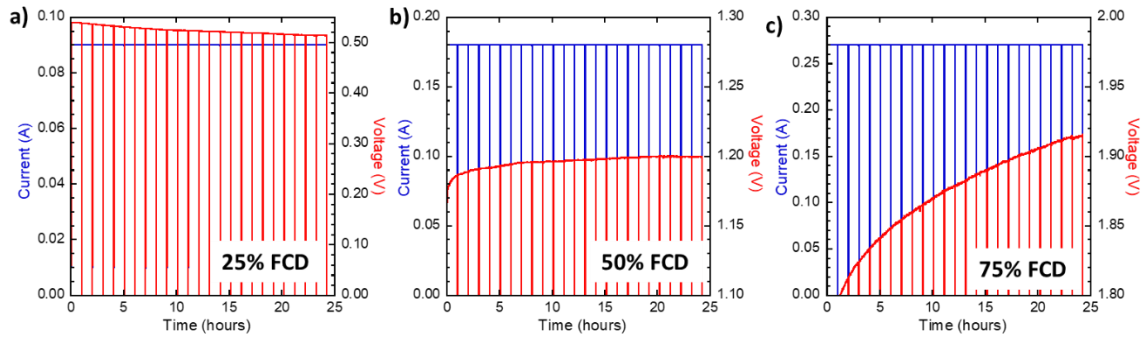


Figure 45: The current and voltage profiles of as-received CNT wires exposed to constant applied current cycles corresponding to a) 25, (b) 50, and (c) 75% of the failure current density (FCD) with intermittent rest and I-V sweeps.

The relative resting and working electrical conductivities are presented in Figure 46. The resting conductivity of the wires exposed to 50 and 75% of the failure current density decreases during the first 1 hour cycle by 5 and 10%, respectively. Throughout the 24 cycles, the CNT wire exposed to 25% of the failure current density exhibits a steady increase in resting conductivity corresponding to a 5% increase in electrical conductivity after 24 cycles. The increase in electrical conductivity as a result of low current exposure has not previously been observed in the literature.

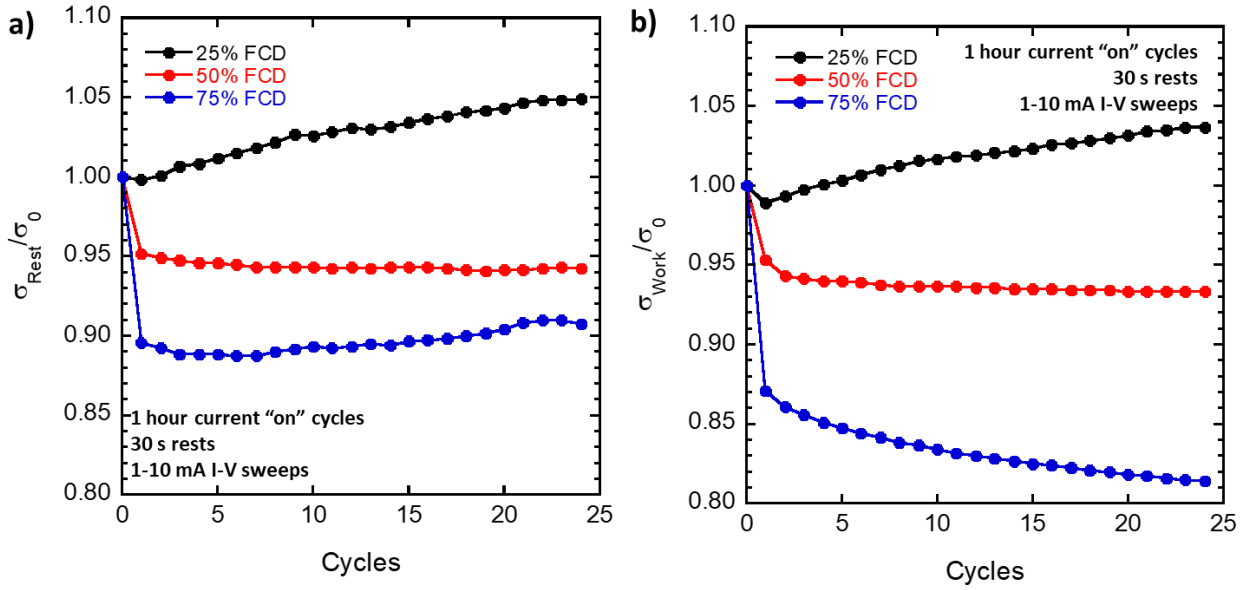


Figure 46: The relative (a) resting and (b) working electrical conductivities of the as-received CNT wires exposed to 25, 50, and 75% of the failure current density (FCD).

Three as-received CNT wire samples were exposed to 25% of their failure current density for 15 days. Current-voltage sweeps to 10 mA were applied every hour in order to determine the resting resistance of the CNT wires, the results are presented in Figure 47. The abrupt increases in resting conductivity are the result of power failure. The average increase in resting conductivity after 15 days was 45%. Independent electrical conductivity measurements were collected on the CNT wire samples after the 15 days of low current exposure to ensure that the increase in electrical conductivity was not an artifact of how the measurement was taken. The independent electrical conductivity measurements found that the CNT wires exposed to 25% of their failure current density had an average electrical conductivity of 0.29 MS/m, corresponding to a 42% increase in electrical conductivity.

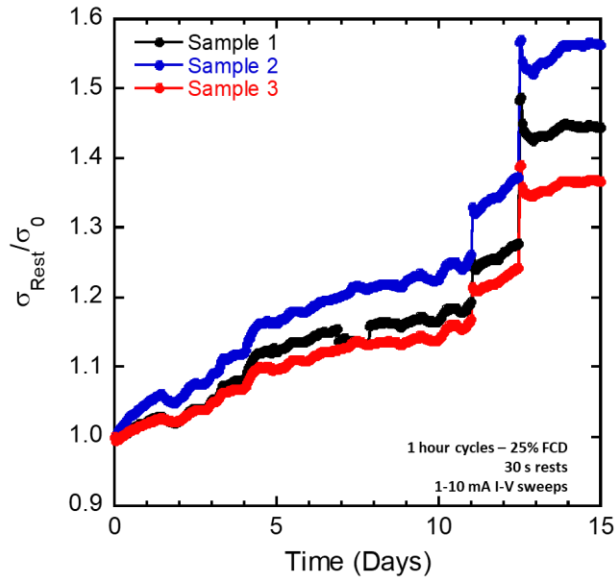


Figure 47: The resting conductivity as a function of time for constant current cycling of as-received CNT wires at an applied current density corresponding to 25% of the failure current density.

As-received CNT wires were exposed to 25% of their failure current density for 3 days in air or argon environments. The argon environment was used as an inert gas without the presence of water and oxygen. 10 mA current-voltage sweeps were applied every hour in order to determine the resting resistance of the CNT wires, the results are presented in Figure 48. Within 3 days, the CNT wire in air experiences an increase in resting electrical conductivity of 9%. The CNT sample exposed to argon has a 5% decrease in resting electrical conductivity within 5 days. The increase in resting electrical conductivity of the as-received CNT wires in air during low current exposure is likely due the adsorption of H₂O and oxygen, which both p-dope CNT materials.^{61,62}

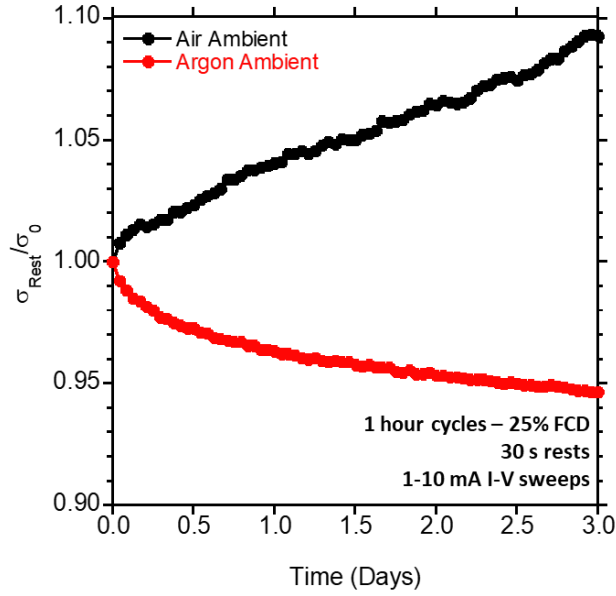


Figure 48: The resting conductivity of as-received CNT wires exposed to 25% of their failure current density in air or argon environments.

7.6 Temperature and Electrical Performance Retention

Electrical performance retention as a function of increasing applied current was performed on large diameter CNT wires in order to determine the temperature related to increases in relative resting and working resistance. CNT wires were prepared from Nanocomp CNT sheet materials, soaked in either H₂O or 5 mM KAuBr₄ aqueous solutions for 1 hour prior to densification to a final wire diameter of 1 mm and then dried in a vacuum oven at 100 °C for 1 hour. The magnitude of the current “on” steps and I-V sweeps was 100 mA to account for the greater currents at failure for the large diameter CNT wires. A thermocouple was used to measure the temperature at the center of the CNT wires. The resulting changes in resting and working resistances and the corresponding temperature measurements are presented in Figure 49. For both the H₂O-densified and KAuBr₄-densified CNT wires, increases in the relative resting resistance directly correspond to temperature increases. The temperature of the H₂O-densified CNT wires steadily increases to ~320 °C prior to eventual

wire failure at 458 °C. The temperature of the KAuBr₄-densified CNT wires remains below ~120 °C until near ultimate wire failure. The electrical stability of the KAuBr₄-densified CNT wires is maintained at greater applied currents due to reduced Joule heating which prevents the onset of increased temperatures and the resulting material degradation.

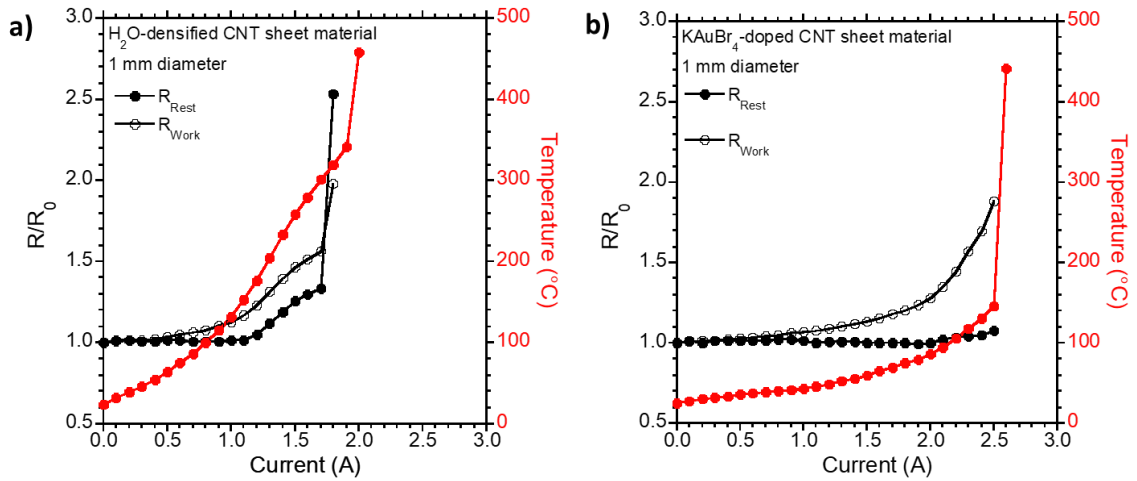


Figure 49: The relative changes in resting and working resistances for 1mm diameter (a) H₂O-densified and (b) KAuBr₄-densified CNT wires as a function of increasing applied current and the corresponding temperature measurements.

7.7 Forced Cooling to Demonstrate Current Carrying Capacity Possibilities

Presently, the maximum current density at failure for bulk CNT conductors is 4 orders of magnitude less than that reported of a single MWCNT. The present work explored cooling during current-carrying capacity testing in order to demonstrate the upper limits of failure current density for bulk CNT conductors when oxidation and vaporization are prevented.

A high voltage direct current power supply was used to perform failure current density testing of commercially available CNT wires in a 0 °C 3:1 propylene glycol:water recirculating bath. The procedure used a four-point terminal and applied increasing 1 V steps held for 30 s each. The length between the voltage sense probes for the 10 tex and 3-Ply CNT wires was 5 cm and for the 20 μm diameter DexMat wire was 2 cm, due to

material constraints. The resulting current densities as a function of voltage are presented in Figure 50a. For all of the CNT materials, there is a linear relationship between current density and voltage until failure, indicating no change in resistance prior to failure and that failure is likely due to thermal runaway at a localized defect. The current densities at failure for the 10 tex, 3-ply DexMat, and 20 μm DexMat CNT wires in 0 $^{\circ}\text{C}$ polypropylene were 158, 601, and 2,067 MA/m^2 , respectively (see Figure 50b). Previously, the highest reported current density at failure was 455 MA/m^2 for a 20.5 μm diameter CSA extruded wire in a room temperature nitrogen environment.⁴⁴ The liquid cooled 20 μm DexMat material has demonstrated a 2,067 MA/m^2 current density at failure, 4x greater than any reported values in the literature. The ability of the 20 μm DexMat material to maintain its electrical properties at current densities up to 2,067 MA/m^2 in cooled environments demonstrates the potential of these conductors for space and sea environments.

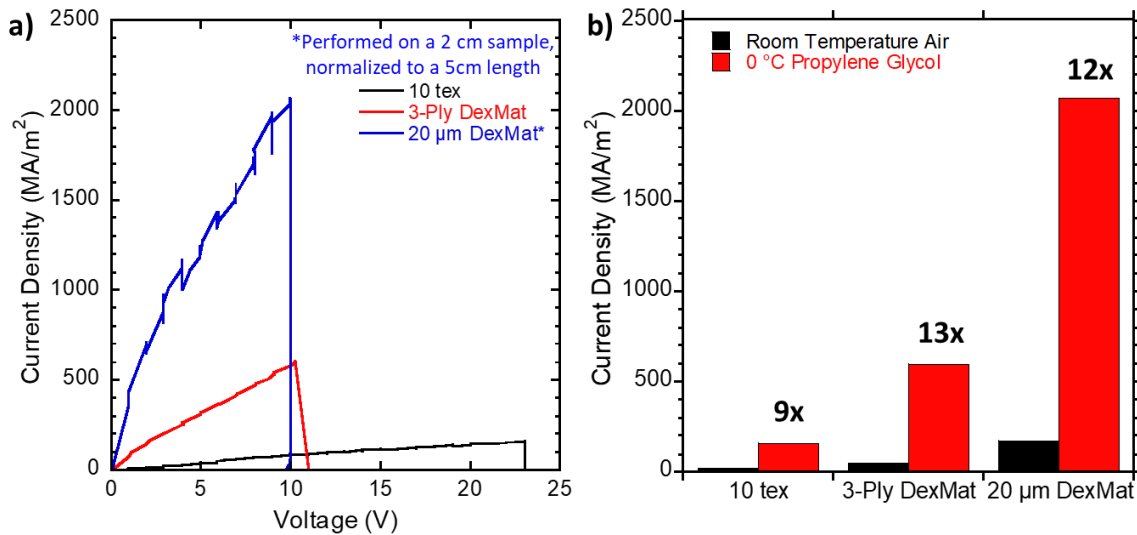


Figure 50: (a) Resulting current densities as a function of applied voltage for 10 tex, 3-ply DexMat, and 20 μm DexMat CNT wires in 0 $^{\circ}\text{C}$ polypropylene. (b) The current density at failure for the 10 tex, 3-ply DexMat, and 20 μm DexMat CNT wires in room temperature air and 0 $^{\circ}\text{C}$ polypropylene. The improvement in current density at failure for the samples in 0 $^{\circ}\text{C}$ propylene glycol compared to the samples tested in air are listed.

7.8 Power Analysis

The power dissipated by as-received and KAuBr_4 doped 10 tex wires were directly compared to that of 20 μm diameter DexMat wires and 127 μm diameter copper. The power dissipated was calculated as the I^2R losses obtained during failure current density testing and are presented in Figure 51. The power dissipated is considered to be a loss in energy via heat. The observed maximum power that a particular conductor can handle is determined by how hot the wire can get before it fails. The expected failure mechanism for copper is melting and for CNTs is thermal oxidization. The melting temperature of copper (1085 °C) is much higher than the thermal oxidation temperature of CNTs (~500 °C), and one would expect copper outperforming CNTs. How hot the conductor will get, as a function of the applied power, depends on the dimensions of the wire, and its thermal conductivity. When different wire geometries are used, the power dissipation can be normalized to the power density (by dividing power by the cross-sectional area of the wire), and the maximum power density will then only depend on the temperature of the wire. A 127 μm diameter copper wire has a maximum power density of 241 MW/m^2 , which is similar to the 152 μm diameter as-received CNT wires that have a maximum power density of 214 MW/m^2 . This is significant and it indicates that both wires can carry a similar amount of energy before failure but that the CNT wires will remain much cooler than the copper wires, which indicates that the thermal conductivity of the CNT is much higher than that of copper. The KAuBr_4 doped CNT wires have a maximum power density of 89 MW/m^2 , relating to approximately 58% less power dissipated than the as-received. This could be an indication of a lower thermal conductivity as well as a rapid desorption of the conduction-enhancing dopants, which leads to rapid thermal runaway condition and an

abrupt increase in resistance and temperature. The 20 μm diameter DexMat CNT wire had a maximum power density of 455 MW/m^2 , this is a more than 2x greater power carrying capabilities than the 10 tex wires, which indicates improved thermal conductivity as the wires remain below the decomposition temperature. The copper and KAuBr_4 doped CNT wires had greater increases in normalized resistance at equivalent power densities than the as-received 10 tex and DexMat CNT wires. The greater changes in normalized resistance of the copper and KAuBr_4 doped CNT wires is likely due to the metallic nature of the conductors resulting in greater temperature coefficients of resistance.³¹

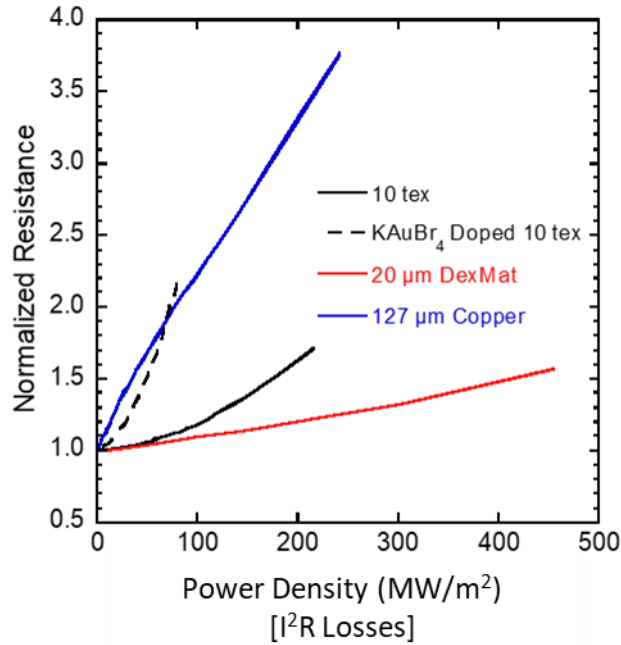


Figure 51: Power dissipation and resulting normalized resistances of as-received and KAuBr_4 doped 10 tex CNT wires, 20 μm DexMat CNT wires, and 127 μm copper wires.

7.9 Conclusions

Chemical doping was applied to CSA extruded CNT wires and novel, high quality CNT wires to demonstrate the upper bounds of electrical conductivity by the previously studied chemical dopants. Chemical doping of CSA extruded CNTs demonstrated the importance

of using an appropriate solvent for chemical doping and realized a 33% reduction in resistance with IBr doping in hexanes. Chemical doping of high quality DexMat CNT wires with IBr allowed for record breaking electrical conductivity of ~12 MS/m.

Varied doping procedures were performed in order to ensure optimal electrical conductivities were achieved and to allow for the effects of doping procedure on electrical performance retention to be understood. Hot filament I₂ vapor deposition was deemed unnecessary and did not yield improved electrical conductivity compared to cool filament deposition. Varying the doping exposure duration for IBr and KAuBr₄ from 1 hour to 3 hours provided no change in electrical conductivity but demonstrated that the additionally adsorbed IBr is not stable at low applied current densities. This work supported the conclusion that 1 hour doping exposure was suitable for the solution based doping IBr and KAuBr₄ of CNT wires.

Low current operation of CNT conductors resulting in improved electrical conductivity had not been previously observed in the literature. Performing electrical performance retention testing of the CNT wires in a dry argon environment allowed for the determination that this phenomena of improved electrical conductivity during low current operation is the result of ambient doping from oxygen and moisture in the air.

Forced cooling of the CNT wires allowed for efficient heat transfer from the CNT wires, thus preventing the onset of thermal degradation and allowing for record breaking failure current densities to be achieved. For the various CNT wires tested, forced cooling via a 0 °C propylene glycol circulating bath increased the failure current density by ~ 10x. The 20 μm DexMat CNT wires had a failure current density of 2,067 MA/m², exceeding previously reported literature values by a factor of ~4x. Forced cooling demonstrates the

ability of CNT wires to carry high applied current densities in cool environments, benefiting space and marine applications.

Finally, an analysis of power dissipation of various CNT conductors demonstrates the loss of energy during operation of these CNT wires. The KAuBr_4 doped 10 tex CNT wires dissipate 63% less power than copper wires with a 127 μm diameter. The power dissipation is critical in understanding the efficiency of these CNT wire conductors.

Chapter 7 addressed a variety of not previously discussed factors that affect the practical operation of CNT conductors. Record breaking electrical conductivity was demonstrated via IBr doping of DexMat CNT wires. Doping conditions were shown to affect the electrical performance retention of IBr doped CNT wires, but not KAuBr_4 doped CNT wires. Low current application resulting in reduced electrical conductivity was demonstrated for the first time and determined to be the result of ambient doping. Failure current densities $\sim 4\text{x}$ greater than previously reported were achieved via exposure to 0 °C propylene glycol. These advances demonstrate the possibilities of improving the electrical properties of commercially available CNT wires while elucidating the mechanisms behind these improvements. The work presented in this chapter will serve the field via understanding of the importance of dopant and dopant solvent selection, testing as a function of varied doping conditions and ambient environments, and the determination of how CNT wires vary in their power dissipation.

8 Dissertation Conclusions

The work in this dissertation has demonstrated the capabilities of three emerging CNT dopants to improve the electrical properties of commercial CNT wires and developed the basis by which to understand how doped CNT conductors will behave during applied current operation. The primary contributions of this dissertation include: (1) directly comparing the effects of I_2 , $I\text{Br}$, and KAuBr_4 chemical doping on the electrical conductivity and current carrying capacity of commercial CNT wires, (2) measuring the electrical performance retention as a function of increasing applied current density and constant current cycling for doped CNT conductors, (3) demonstrating improved electrical performance retention of doped CNT conductors is the result of greater thermal stability of the dopant, (4) demonstrating that dopant degradation via desorption results in reduced electrical performance retention compared to dopants which decompose into other viable dopants, referred to as a dopant cascade, and (5) the demonstration of KAuBr_4 as the most promising chemical dopant to date for CNTs, capable of producing improved electrical conductivity conductors that are stable over greater applied current densities and repeated low current cycling. Overall, it is shown that a combined analysis of the electrical performance retention at increasing applied current, along with thermal oxidation characterization of the doped conductors, and elemental analysis after thermal degradation, provides the requisite data to understand the stability of chemically-doped CNT conductors.

Throughout the literature, the prominent chemical dopants for improving the electrical conductivity and current carrying capacity of CNT wires have been I_2 , $I\text{Br}$, and KAuBr_4 , aside from chlorosulfonic acid used during extrusion, which has previously been

demonstrated as unstable during increasing applied current. Although the ability of these dopants to improve electrical conductivity has been well understood, the use of various starting materials and discrepancies in testing conditions have prevented the direct comparison of the current carrying capacity and stability of these dopants. In this work, a cost-effective, commercially available CNT material produced in kilometer lengths was used as the common starting material from which comparisons in electrical performance and stability could be made. The scaled nature of the material was attractive as it is widely available and suitable for immediate implementation in various power transmission applications. Optimized doping of these CNT wires with I₂, IBr, and KAuBr₄ demonstrated similar ~4x improvements in electrical conductivity to 7-8 x 10⁵ MS/m and minimal change in failure current density, compared to the as-received. Further work showed that doping with IBr of high quality DexMat CNT wires results in record breaking electrical conductivities of 12 MS/m, demonstrating the present upper bounds of these chemical dopants to improve electrical conductivity in commercial CNTs.

The electrical performance retention, defined as the room temperature electrical conductivity after exposure to increasing applied current or constant current cycling, was established as a metric for doped CNT stability. The electrical performance retention method serves as a means by which to select chemical dopants suitable for high current and sustained current applications. The method works due to Joule heating during applied current, which is a function of the resistance of the CNT materials. The change in electrical conductivity for the doped CNT wires is directly related to chemical dopant desorption and/or decomposition, and eventually the degradation of the CNT wires. The room temperature electrical conductivities of the I₂ and IBr doped CNT wires were found to

degrade after exposure to increasing applied currents, approaching the electrical conductivity of the starting materials, while KAuBr_4 doped CNT wires exhibited minimal degradation in resting conductivity until near wire failure. The electrical conductivity of KAuBr_4 doped CNT wires are stable with increasing applied current densities, the underlying mechanism of this stability compared to the halogen dopants has not previously been understood.

The mechanism behind the electrical performance retention of the halogen doped CNTs was probed via thermal stability analysis coupled with an analysis of the elemental composition of the doped CNT conductors after exposure to increased temperature. Thermogravimetric analysis (TGA) was used to probe the thermal stability of the doped CNT conductors and the pure dopants. TGA demonstrates that the halogen dopants exhibit distinct degradation peaks prior to 150 °C, while KAuBr_4 doped CNTs have degradation peaks at 192 °C and 334 °C. Doped samples were prepared and thermally oxidized to 200 °C and 400 °C in order to probe the electrical properties and elemental composition as a result of thermal degradation. Elemental analysis of the thermally oxidized, doped CNT conductors, coupled with the thermal stability analysis, demonstrated that the I_2 and IBr desorb from the CNTs, while KAuBr_4 can degrade into AuBr_3 , AuBr and Au . The dopant cascade of KAuBr_4 was determined to be favorable as it results in the sustained presence of CNT chemical dopants and residual gold nanoparticles which serve as interconnections between CNTs, providing sustained improvements in electrical conductivity.

The body of work in this dissertation outlines a systematic approach by which to relate the electrical performance retention to the thermal stability of a chemical dopant by quantifying the elemental composition of the dopant after exposure to elevated

temperatures. The approach mimics the thermal degradation observed via Joule heating during applied current application. A major finding in the work was that the dopant degradation mechanism could result in dopant cascades where the dopant decomposes into other thermally stable CNT dopants with favorable electrochemical potentials, allowing for continued improvements in electrical conductivity after initial dopant degradation. This work can be extended to identify thermally stable or cascading chemical dopants for high current applications and supports the implementation of these doped CNT conductors in power transmission applications requiring improved electrical conductivity that is sustained throughout application.

Additional studies presented in Chapter 7 serve to further understand the possibilities of CNT wire electrical properties, the electrical performance retention, and practical engineering considerations. The results in this dissertation were based upon bare CNT conductors, but several power transmission applications will require the use of insulation, which will likely prevent any effects from ambient doping. For practical adoption, insulation will limit the CNT conductors to operate at temperatures suitable to the specific insulator materials used. A relevant example supporting the need for insulation showed how application of a continuous low current through CNT wires resulted in an increased electrical conductivity with time, and was identified to be an effect of ambient doping occurring during operation. Additional work presented in Section 7.6 demonstrated how the temperature of the conductors can be measured as a function of applied current, allowing for specific operating currents to be determined based on the temperature requirements of the insulator. The large diameter CNT wires prepared in Section 7.6 demonstrated that the KAuBr_4 -densified CNT wires can operate at ~75% of their failure

current density while maintaining a temperature less than 90 °C, which would be within the operating temperatures for many conventional insulating materials like cross-linked polyethylene and teflon. Section 7.7 demonstrated unprecedented failure current densities of greater than 2 GA/m² for CNT materials when operating in a 0 °C propylene glycol environment, representing a 12x improvement over room temperature measurements in air. Thus, the potential to dramatically increase the current carrying capacity of CNT wires was shown for naturally cooled environments or when liquid cooling can be used within the wire insulation. As these CNT materials are adopted into practical operation, the additional considerations of Chapter 7 will serve to understand how doped CNT conductors behave as a function of temperature and to elucidate the phenomena of low current application resulting in reduced electrical conductivity.

The future holds the possibility of improved dopants, techniques to prevent dopant desorption, and passivation layers that could prevent thermal oxidation. The electrical performance retention will serve as a metric by which to benchmark these advances in electrical conductivity and the resulting stability during operation. As electrical conductivity of CNT conductors continues to improve towards that of conventional metals, the method of relating the electrical performance retention to the thermal stability and degradation mechanisms will allow for the stability during operation to be well understood. The understanding of the electrical performance retention of the doped CNT conductors will directly allow for their facile adoption into next generation, lighter, and more robust power transmission technologies.

9 References

- (1) Sumlo Iijima. Helical Microtubules of Graphitic Carbon. *Nature* **1991**, 354 (354), 56–58.
- (2) Golnabi, H. Carbon Nanotube Research Developments in Terms of Published Papers and Patents , Synthesis and Production. *Sci. Iran.* **2012**, 19 (6), 2012–2022. <https://doi.org/10.1016/j.scient.2012.10.036>.
- (3) Tsentalovich, D. E.; Headrick, R. J.; Mirri, F.; Hao, J.; Behabtu, N.; Young, C. C.; Pasquali, M. Influence of Carbon Nanotube Characteristics on Macroscopic Fiber Properties. *ACS Appl. Mater. Interfaces* **2017**, 9, 36189–36198. <https://doi.org/10.1021/acsami.7b10968>.
- (4) Behabtu, N.; Young, C. C.; Tsentalovich, D. E.; Kleinerman, O.; Wang, X.; Ma, A. W. K.; Bengio, E. A.; ter Waarbeek, R. F.; de Jong, J. J.; Hoogerwerf, R. E.; et al. Strong, Light, Multifunctional Fibers of Carbon Nanotubes with Ultrahigh Conductivity. *Science* (80-.). **2013**, 339 (6116), 182–186. <https://doi.org/10.1126/science.1228061>.
- (5) Landi, B. J.; Ganter, M. J.; Cress, C. D.; DiLeo, R. A.; Raffaele, R. P. Carbon Nanotubes for Lithium Ion Batteries. *Energy Environ. Sci.* **2009**, 2 (6), 638–654. <https://doi.org/10.1039/b904116h>.
- (6) Venema, L. C.; Wildo, J. W. G.; Dekker, C. Electronic Structure of Atomically Resolved Carbon Nanotubes “. **1998**, 584 (10), 1996–1999.
- (7) S. Reich, C. T. and J. M. *Carbon Nanotubes: Basic Concepts and Physical Properties.*; Wiley-VCH Verlag GmbH: Berlin, Germany, 2004.

- (8) Landi, B. J. High Energy Density Lithium-Ion Batteries with Carbon Nanotube Anodes. **2010**. <https://doi.org/10.1557/JMR.2010.0209>.
- (9) Liu, W.; Chai, S.; Rahman, A.; Hashim, U. Journal of Industrial and Engineering Chemistry Synthesis and Characterization of Graphene and Carbon Nanotubes : A Review on the Past and Recent Developments. *J. Ind. Eng. Chem.* **2014**, *20* (4), 1171–1185. <https://doi.org/10.1016/j.jiec.2013.08.028>.
- (10) Prasek, J.; Drbohlavova, J.; Chomoucka, J.; Hubalek, J.; Jasek, O.; Kizek, R. Methods for Carbon Nanotubes Synthesis — Review. **2011**, 15872–15884. <https://doi.org/10.1039/c1jm12254a>.
- (11) Eatemadi, A.; Daraee, H.; Karimkhanloo, H.; Kouhi, M.; Zarghami, N. Carbon Nanotubes : Properties , Synthesis , Purification , and Medical Applications. *Nanoscale Res. Lett.* **2014**, *9* (1), 1–13.
- (12) Guo, T.; Nikolaev, P.; Thess, A.; Colbert, D. T.; Smalley, R. E. Catalytic Growth of Single-Walled Nanotubes by Laser Vaporization. **1995**, *2614* (September).
- (13) Jose Yacaman, M.; Mikoyoshido, M.; Rendon, L.; Santiesbeng J G. Catalytic Growth of Carbon Microtubules with Fullerene Structure. *Applied Physics Letters*. AMER INST PHYSICS: WOODBURY 1993, pp 657–659.
- (14) Landi, B. J.; Cress, C. D.; Evans, C. M.; Raffaele, R. P.; York, N. Thermal Oxidation Profiling of Single-Walled Carbon Nanotubes. **2005**, No. 8, 6819–6834. <https://doi.org/10.1021/cm052002u>.
- (15) Schauerman, C. M.; Alvarenga, J.; Staub, J.; Forney, M. W.; Foringer, R.; Landi, B.

- J. Ultrasonic Welding of Bulk Carbon Nanotube Conductors. *Adv. Eng. Mater.* **2015**, *17* (1), 76–83. <https://doi.org/10.1002/adem.201400117>.
- (16) Puchades, I.; Lawlor, C. C.; Schauerman, C. M.; Bucossi, A. R.; Rossi, J. E.; Cox, N. D.; Landi, B. J. Mechanism of Chemical Doping in Electronic-Type-Separated Single Wall Carbon Nanotubes towards High Electrical Conductivity. *J. Mater. Chem. C* **2015**, *3* (39), 10256–10266. <https://doi.org/10.1039/C5TC02053K>.
- (17) Tulevski, G. S.; Franklin, A. D.; Afzali, A. High Purity Isolation and Quantification of Semiconducting Carbon Nanotubes via Column Chromatography. *ACS Nano* **2013**, No. 4, 2971–2976. <https://doi.org/10.1021/nn400053k>.
- (18) Green, A. A.; Hersam, M. C. Nearly Single-Chirality Single-Walled Carbon Nanotubes Produced via Orthogonal Iterative Density Gradient Ultracentrifugation. **2011**, 2185–2190. <https://doi.org/10.1002/adma.201100034>.
- (19) Tanaka, T.; Jin, H.; Miyata, Y.; Kataura, H. High-Yield Separation of Metallic and Semiconducting Single-Wall Carbon Nanotubes by Agarose Gel Electrophoresis. **2008**. <https://doi.org/10.1143/APEX.1.114001>.
- (20) NanoIntegris. *NanoIntegris Promotional Brochure*.
- (21) Ramesh, S.; Ericson, L. M.; Davis, V. A.; Saini, R. K.; Kittrell, C.; Pasquali, M.; Billups, W. E.; Adams, W. W.; Hauge, R. H.; Smalley, R. E. Dissolution of Pristine Single Walled Carbon Nanotubes in Superacids by Direct. **2004**, 8794–8798. <https://doi.org/10.1021/jp036971t>.
- (22) Davis, V. A.; Parra-vasquez, A. N. G.; Green, M. J.; Rai, P. K.; Behabtu, N.; Prieto,

- V.; Booker, R. D.; Schmidt, J.; Kesselman, E.; Talmon, Y.; et al. True Solutions of Single-Walled Carbon Nanotubes for Assembly into Macroscopic Materials. *Nat. Nanotechnol.* **2009**, *4* (May 2014), 830–834. <https://doi.org/10.1038/nnano.2009.302>.
- (23) Parra-vasquez, A. N. G.; Behabtu, N.; Green, K. M. J.; Pint, C. L.; Young, K. C. C.; Schmidt, J.; Kesselman, E.; Goyal, A.; Ajayan, P. M.; Cohen, Y.; et al. Spontaneous Dissolution of Ultralong Single- and Multiwalled Carbon Nanotubes. *ACS Nano* **2010**, *4* (7), 3969–3978.
- (24) Bucossi, A. R.; Cress, C. D.; Schauerman, C. M.; Rossi, J. E.; Puchades, I.; Landi, B. J. Enhanced Electrical Conductivity in Extruded Single-Wall Carbon Nanotube Wires from Modified Coagulation Parameters and Mechanical Processing. *ACS Appl. Mater. Interfaces* **2015**, *7* (49), 27299–27305. <https://doi.org/10.1021/acsami.5b08668>.
- (25) Zhang, M. Zhang, M., Atkinson, K. R. & Baughman, R. H. Multifunctional Carbon Nanotube Multifunctional Carbon Nanotube Yarns by Downsizing an Ancient Technology. **2015**, No. December 2004, 1358–1361. <https://doi.org/10.1126/science.1104276>.
- (26) Kaili Jiang, Qunqing Li, S. F. Spinning Continuous Carbon Nanotube Yarns. *Nature* **2002**, *419* (1999), 1274014.
- (27) Zhu, H. W.; Xu, C. L.; Wu, D. H.; Wei, B. Q.; Vajtai, R.; Ajayan, P. M. Direct Synthesis of Long Single-Walled Carbon Nanotube Strands. **2002**, *296* (May), 884–886.

- (28) Chem, J. M.; Wu, A. S.; Chou, T.; Gillespie, J. W.; Rioux, J. Electromechanical Response and Failure Behaviour of Aerogel-Spun Carbon Nanotube Fibres under Tensile Loading. **2012**, 6792–6798. <https://doi.org/10.1039/c2jm15869h>.
- (29) Ian, A.; Alan, H. Direct Spinning of Carbon Nanotube Fibers from Chemical Vapor Deposition Synthesis. *Science (80-.)*. **2004**, 304, 276–278.
- (30) Koziol, K. High-Performance Carbon Nanotube Fiber. *Science (80-.)*. **2007**, 1892. <https://doi.org/10.1126/science.1147635>.
- (31) Alvarenga, J.; Jarosz, P. R.; Schauerman, C. M.; Moses, B. T.; Landi, B. J.; Cress, C. D.; Raffaele, R. P. High Conductivity Carbon Nanotube Wires from Radial Densification and Ionic Doping. *Appl. Phys. Lett.* **2010**, 97 (18), 95–98. <https://doi.org/10.1063/1.3506703>.
- (32) Bucossi, A.; Frink, Q.; Rossi, J. E.; Landi, B. Effects of Solution Properties on Iodine Monobromide Doping for Enhanced Bulk Carbon Nanotube Electrical Conductivity. *ACS Appl. Nano Mater.* **2018**, 1 (5), 2088–2094. <https://doi.org/10.1021/acsanm.8b00041>.
- (33) Janas, D.; Milowska, K. Z.; Bristowe, P. D.; Koziol, K. K. Improving the Electrical Properties of Carbon Nanotubes with Interhalogen Compounds. *Nanoscale* **2017**, 9 (9), 3212–3221. <https://doi.org/10.1039/C7NR00224F>.
- (34) Zhao, Y.; Wei, J.; Vajtai, R.; Ajayan, P. M.; Barrera, E. V. Iodine Doped Carbon Nanotube Cables Exceeding Specific Electrical Conductivity of Metals. *Sci. Rep.* **2011**, 1 (83), 10.1038/srep00083. <https://doi.org/10.1038/srep00083>.

- (35) Zhang, S.; Park, J. G.; Nguyen, N.; Jolowsky, C.; Hao, A.; Liang, R. Ultra-High Conductivity and Metallic Conduction Mechanism of Scale-up Continuous Carbon Nanotube Sheets by Mechanical Stretching and Stable Chemical Doping. *Carbon N. Y.* **2017**, *125*, 649–658. <https://doi.org/10.1016/j.carbon.2017.09.089>.
- (36) Tsapenko, A. P.; Goldt, A. E.; Shulga, E.; Popov, Z. I.; Maslakov, K. I.; Anisimov, A. S.; Sorokin, P. B.; Nasibulin, A. G. Highly Conductive and Transparent Films of HAuCl₄-Doped Single-Walled Carbon Nanotubes for Flexible Applications. *Carbon N. Y.* **2018**, *130*, 448–457. <https://doi.org/10.1016/j.carbon.2018.01.016>.
- (37) Ghosh, S.; Yamijala, S. R. K. C. S.; Pati, S. K.; Rao, C. N. R. The Interaction of Halogen Molecules with SWNTs and Graphene. *RSC Adv.* **2012**, *2* (3), 1181–1188. <https://doi.org/10.1039/c1ra00295c>.
- (38) Anders, G. J. *Rating of Electric Cables: Ampacity Computations for Transmission, Distribution, and Industrial Applications*; Institute of Electrical and Electronics Engineers: New York, 1997.
- (39) H. W. Beaty and D. G. Fink. *Standard Handbook for Electrical Engineers.*, 15th ed.; McGraw-Hill: New York, 2007.
- (40) Wei, B. Q.; Vajtai, R.; Ajayan, P. M. Reliability and Current Carrying Capacity of Carbon Nanotubes. *Appl. Phys. Lett.* **2001**, *79* (8), 1172–1174. <https://doi.org/10.1063/1.1396632>.
- (41) Hauder, M.; Gstöttner, J.; Hansch, W.; Schmitt-Landsiedel, D. Scaling Properties and Electromigration Resistance of Sputtered Ag Metallization Lines. *Appl. Phys. Lett.* **2001**, *78* (6), 838–840. <https://doi.org/10.1063/1.1345801>.

- (42) Preece, W. H. II. On the Heating Effects of Electric Currents. *Proc. R. Soc. London* **1883**.
- (43) Cress, C. D.; Ganter, M. J.; Schauerman, C. M.; Soule, K.; Rossi, J. E.; Lawlor, C. C.; Puchades, I.; Ubnoske, S. M.; Bucossi, A. R.; Landi, B. J. Carbon Nanotube Wires with Continuous Current Rating Exceeding 20 Amperes. *J. Appl. Phys.* **2017**, *122* (2), 025101. <https://doi.org/10.1063/1.4990981>.
- (44) Wang, X.; Behabtu, N.; Young, C. C.; Tsentlovich, D. E.; Pasquali, M.; Kono, J. High-Ampacity Power Cables of Tightly-Packed and Aligned Carbon Nanotubes. *Adv. Funct. Mater.* **2014**, *24* (21), 3241–3249. <https://doi.org/10.1002/adfm.201303865>.
- (45) Grigorian, L.; Williams, K. A.; Fang, S.; Sumanasekera, G. U.; Loper, A. L.; Dickey, E. C.; Pennycook, S. J.; Eklund, P. C. Reversible Intercalation of Charged Iodine Chains into Carbon Nanotube Ropes. *Phys. Rev. Lett.* **1998**, *80* (25), 5560.
- (46) Jarosz, P.; Schauerman, C.; Alvarenga, J.; Moses, B.; Mastrangelo, T.; Raffaele, R.; Ridgley, R.; Landi, B. Carbon Nanotube Wires and Cables: Near-Term Applications and Future Perspectives. *Nanoscale* **2011**, *3* (11), 4542. <https://doi.org/10.1039/c1nr10814j>.
- (47) Jarosz, P. R.; Shaukat, A.; Schauerman, C. M.; Cress, C. D.; Kladitis, P. E.; Ridgley, R. D.; Landi, B. J. High-Performance, Lightweight Coaxial Cable from Carbon Nanotube Conductors. *ACS Appl. Mater. Interfaces* **2012**, *4* (2), 1103–1109. <https://doi.org/10.1021/am201729g>.
- (48) Janas, D.; Vilatela, A. C.; Koziol, K. K. Performance of Carbon Nanotube Wires

- in Extreme Conditions. *Carbon N. Y.* **2013**, 62, 438–446.
<https://doi.org/10.1016/j.carbon.2013.06.029>.
- (49) Alvarenga, J.; Jarosz, P. R.; Schauerman, C. M.; Moses, B. T.; Landi, B. J.; Cress, C. D.; Raffaele, R. P. High Conductivity Carbon Nanotube Wires from Radial Densification and Ionic Doping. *Appl. Phys. Lett.* **2010**, 97, 182106.
<https://doi.org/10.1063/1.3506703>.
- (50) Cress, C. D.; Schauerman, C. M.; Landi, B. J.; Messenger, S. R.; Raffaele, R. P.; Walters, R. J. Radiation Effects in Single-Walled Carbon Nanotube Papers. *J. Appl. Phys.* **2010**, 107 (1), 014316. <https://doi.org/10.1063/1.3268470>.
- (51) Chin, K. Y. Molecular Doping of Carbon Nanotube Conductors, University of Texas at Austin, 2018.
- (52) Leggiero, A. P.; Trettner, K. J.; Ursino, H. L.; McIntyre, D. J.; Schauer, M.; Zeira, E.; Cress, C. D.; Landi, B. J. High Conductivity Copper–Carbon Nanotube Hybrids via Site-Specific Chemical Vapor Deposition. *ACS Appl. Nano Mater.* **2018**, 2 (1), 118–126. <https://doi.org/10.1021/acsanm.8b01740>.
- (53) Randeniya, L. K.; Bendavid, A.; Martin, P. J.; Tran, C. Composite Yarns of Multiwalled Carbon Nanotubes with Metallic Electrical Conductivity. *Small* **2010**, 6 (16), 1806–1811. <https://doi.org/10.1002/sml.201000493>.
- (54) Otto, K.; Oja Acik, I.; Krunks, M.; Tõnsuaadu, K.; Mere, A. Thermal Decomposition Study of $\text{HAuCl}_4 \cdot 3\text{H}_2\text{O}$ and AgNO_3 as Precursors for Plasmonic Metal Nanoparticles. *J. Therm. Anal. Calorim.* **2014**, 118 (2), 1065–1072.
<https://doi.org/10.1007/s10973-014-3814-3>.

- (55) Kim, S. M.; Kim, K. K.; Jo, Y. W.; Park, M. H.; Chae, S. J.; Duong, D. L.; Yang, C. W.; Kong, J.; Lee, Y. H. Role of Anions in the AuCl₃-Doping of Carbon Nanotubes. *ACS Nano* **2011**, 5 (2), 1236–1242. <https://doi.org/10.1021/nn1028532>.
- (56) Jhi, S.; Louie, S. G.; Cohen, M. L. Electronic Properties of Bromine-Doped Carbon Nanotubes. *Solid State Commun.* **2002**, 123, 495–499.
- (57) Zubair, A.; Tristant, D.; Nie, C.; Tsentalovich, D. E.; Headrick, R. J.; Pasquali, M.; Kono, J.; Meunier, V.; Flahaut, E.; Monthieux, M.; et al. Charged Iodide in Chains behind the Highly Efficient Iodine Doping in Carbon Nanotubes. *Phys. Rev. Mater.* **2017**, 064002, 1–7. <https://doi.org/10.1103/PhysRevMaterials.1.064002>.
- (58) Haynes, W. M. *CRC Handbook of Chemistry and Physics: A Ready-Reference Book of Chemical and Physical Data*; CRC Press: Boca Raton; London; New York, 2014.
- (59) Yu, M.; Lourie, O.; Dyer, M. J.; Moloni, K.; Kelly, T. F.; Ruoff, R. S. Strength and Breaking Mechanism of Multiwalled Carbon Nanotubes Under Tensile Load. *Science* (80-.). **2000**, 287 (5453), 637–640.
- (60) Soule, K. J.; Lawlor, C. C.; Bucossi, A. R.; Cress, C. D.; Puchades, I.; Landi, B. J. Sustaining Enhanced Electrical Conductivity in KAuBr₄-Doped Carbon Nanotube Wires at High Current Densities. *ACS Appl. Nano Mater.* **2019**, 2 (11), 7340–7349. <https://doi.org/10.1021/acsanm.9b01859>.
- (61) Nanotube, C. C.; Barnes, T. M.; Blackburn, J. L.; Lagemaat, J. Van De; Coutts, T. J.; Heben, M. J. Tunneling in the Temperature-. *ACS Nano* **2008**, 2 (9).
- (62) Zettl, A. Extreme Oxygen Sensitivity of Electronic Properties of Carbon Nanotubes.

Science (80-). **2000**, 287 (5459), 1801–1804.

<https://doi.org/10.1126/science.287.5459.1801>.